THE UNIVERSITY OF CALGARY

A COMPREHENSIVE STUDY ON GPS ASSISTED AERIAL TRIANGULATION

by

HAMID EBADI

A DISSERTATION

SUBMITTED TO THE FACULTY OF GRADUATE STUDIES

IN PARTIAL FULFILLMENT OF THE REQUIREMENTS FOR THE

DEGREE OF DOCTOR OF PHILOSOPHY

DEPARTMENT OF GEOMATICS ENGINEERING

CALGARY, ALBERTA

JUNE, 1997

ABSTRACT

Aerial Triangulation (AT) has been used for mapping purposes for a long time to provide 3D coordinates of object points on the ground. This technique uses series of overlapping photographs, and some control points, in order to establish the relationship between the image coordinate system and object coordinate system. In the process of bundle block adjustment, image coordinate observations and coordinates of the ground control points are simultaneously adjusted and the exterior orientation parameters, as well as the ground coordinates of all tie and pass points, are estimated. One of the biggest challenges in AT is to reduce the number of control points. One effective way is to directly measure the exterior orientation parameters of the camera at the time of exposure.

Airborne kinematic GPS (Global Positioning System) provides a means of determining the position of the aerial camera at each instant of exposure. The combined GPS-photogrammetric block adjustment takes advantage of weighted GPS observations, which significantly reduces the number of ground control points needed in a conventional block adjustment.

A comprehensive software package, GAP (General Adjustment Program), was developed in this research to effectively integrate and adjust GPS, geodetic, and photogrammetric observations. Optimization of the GPS-photogrammetric bundle block adjustments for both simulated large scale mapping and real medium scale mapping was carried out.

Aspects of reliability, and precision, as well as practical considerations, for an airborne GPS-photogrammetry system were also investigated.

GPS coordinates of the camera exposure stations do not permit recovery of the roll angle of the aircraft in a GPS single strip triangulation. Therefore, ground control points are still required in addition to the GPS coordinates of exposure stations to overcome this problem, and to eliminate singularity of the normal matrix in the least squares adjustment.

A new technique for GPS single strip triangulation using geometric constraints of man-made structures (e.g., high voltage towers) located along the flight line was proposed, and successfully implemented on real data. This new technique eliminates the need for multiple strips of photography, which has been adapted conventionally to recover the roll angle. The time and the cost of corridor mapping projects are significantly reduced by incorporating this technique.

ACKNOWLEDGMENTS

I would like to thank my supervisor, Dr. M. A. Chapman, for his continued support, encouragement, and guidance throughout the course of my Ph.D. program. I gained from him many academic and social values. I wish also to thank my supervisory committee, Dr. M. J. Collins and Dr. S. E. Franklin for providing valuable reading material.

I gratefully acknowledge the financial support provided by the Iranian Ministry of Culture and Higher Education and the Department of Geomatics Engineering. Trans Alta Utilities Ltd., and Measurement Science, Inc. are acknowledged for providing data for this project. Special thanks goes to Garth Wanamaker for measuring the image coordinates of tower structures.

I take this opportunity to thank my fellow graduate students in the Digital Photogrammetry Group: Darren Cosandier for allowing me the use of his GPS processing software package and Derek Lichti and Bruce Chaplin for proofreading this dissertation.

I also appreciate the secretaries, technicians, and computer specialists of the Department of Geomatics Engineering who, in one way or another, helped me to enjoy my graduate studies.

Finally, I would like to thank my wife, Nooshin, for her continuous encouragement and sacrifices. She and my daughter, Shadi, helped me to balance my academic and personal life.

TABLE OF CONTENTS

Page

LIST OF TABLES

LIST OF FIGURES

CHAPTER 1

INTRODUCTION

Aerial triangulation is a general term for photogrammetric methods of coordinating points on the ground using a series of overlapping aerial photographs (Faig, 1985). Although the major application of aerial triangulation is for mapping purposes, nowadays it has been used in a variety of approaches such as terrestrial photogrammetry, control densification, and cadastral surveying.

1. 1. History of Aerial Triangulation

Aerial triangulation has progressed through different stages in the past; namely, radial, strip, and block triangulation. Each of these methods had merit in their day but were eventually replaced by more advanced approaches as a result of technological changes.

1. 1. 1. Strip Triangulation

Strip triangulation, developed in the 1920's, used a Multiplex instrument to recreate the aerial photography mission. It is based on a dependent-pair relative orientation and scale transfer to ensure uniform scale along the strip. The sequential dependent-pair relative orientation plus scale transfer, starting from a controlled model is known as cantilever extension, and is equivalent to an open traverse in surveying. If ground control points are used at the end or in between, the method is called "bridging", and is similar to a controlled traverse in surveying.

Mechanical or graphical interpolation techniques were then used to fit the measured strip coordinates to the ground control. Numerical strip adjustments began in the 1960's when digital computers became available. A number of polynomial interpolation adjustment formulations were developed for this purpose (Schut, 1968).

The transition from analog aerial triangulation to analytical procedures was realized with the advent of computers (e.g., analytical relative orientation, absolute orientation, etc.). The input for fully analytical aerial triangulation is photo coordinates measured in mono or stereo mode using comparators.

1. 1. 2. Block Triangulation

Block triangulation (by bundles or independent models) provides the best internal geometric strength compared to strip triangulation (Ackermann, 1975). The available tie points in consecutive strips assists in the roll angle recovery, which is one of the weaknesses inherent in strip triangulation. In terms of the computational aspects, aerial triangulation methods are categorized as: analog, semi-analytical, analytical, and digital triangulation.

1. 1. 2. 1 Analog Aerial Triangulation

This method uses a "first order" stereo plotter to carry out relative and approximate absolute orientation of the first model and subsequent cantilever extension. The strip or block adjustment is then performed using the resulting strip coordinates.

1. 1. 2. 2 Semi-Analytical Aerial Triangulation

Relative orientation of each individual model is performed using a precision plotter (e.g., Wild A10). The resulting model coordinates are introduced in a rigorous simultaneous independent model block adjustment. Independent models can also be linked together analytically to form strips, which are then used for strip adjustment or block adjustment with strips.

1. 1. 2. 3. Analytical Aerial Triangulation

The input for analytical aerial triangulation are image coordinates measured by a comparator (in stereo mode or mono mode plus point transfer device). A bundle block adjustment is then performed, incorporating all image coordinates measured in all photographs. An analytical plotter in comparator mode can also be used to measure the image coordinates.

1. 1. 2. 4. Digital Aerial Triangulation

This method uses a photogrammetric workstation which can display digital images. Selection and transfer of tie points and measurement tasks that are performed manually in analytical triangulation are now automated using image matching techniques. The procedure is almost fully automatic, but allows interactive guidance and interference.

1. 1. 3. Control Requirements for Photogrammetric Blocks

Any block consisting of two or more overlapping photographs requires that it be absolutely oriented relative to the ground coordinate system. The 3D spatial similarity

transformation with 7 parameters (3 rotations, 3 translations, 1 scale) is usually employed for absolute orientation, and usually employs at least 2 horizontal and 3 vertical control points. Due to the influence of point transfer errors (e.g., image coordinate measurements of conjugate points), and extrapolation beyond the mapping area, the theoretical minimum control requirement is practically unrealistic.

Theoretical and practical studies (Ackermann, 1966, 1974 and Brown, 1979) showed that only planimetric points along the perimeter of the block, and relatively dense chains of vertical points across the block, are necessary to relate the image coordinate system to the object coordinate system. These measures also ensure the geometric stability of the block, and control the error propagation.

1. 1. 3. 1. Auxiliary Data as Control Information

Perimeter control for planimetry has reduced the number of control points and required terrestrial work for a photogrammetric block. However, the dense chains of vertical control demand additional surveys. A number of studies (Ackermann, 1984, Blais and Chapman, 1984, and Faig, 1979) have been carried out to reduce the number of control points, especially vertical points, using measured exterior orientation parameters at the time of photography. These studies showed that great savings in the number of vertical control points could be achieved.

1. 1. 3. 2. History of Auxiliary Data in Aerial Triangulation

The use of auxiliary data in aerial triangulation dates back to more than half a century ago. As mentioned by Zarzycki (1972), statoscope, horizon camera, and solar periscope were used to directly measure the exterior orientation parameters of the camera at the time of photography. A statoscope provides the ΔZ of the exposure stations using

differential altimetry. A horizon camera provides the rotation angles of the mapping camera with respect to the horizon. A solar periscope can also determine the rotation angles, but they are referred to the sun's location. Airborne ranging was also developed to determine the horizontal positions of the camera stations in order to support the airborne determination of large horizontal networks (Corten, 1960). Except for the statoscope, these instruments were not accepted for practical applications due to accuracy and economic reasons. The Airborne Profile Recorder (APR) was developed in 1960 and used extensively in Canada. This instrument provides the Z coordinate for a number of identifiable features that can be correlated to the profile. This can be achieved by using a statoscope to measure the movements of the aircraft with respect to an isobaric surface and a continuous record of the profile between terrain and aircraft, as shown in Figure 1.1.

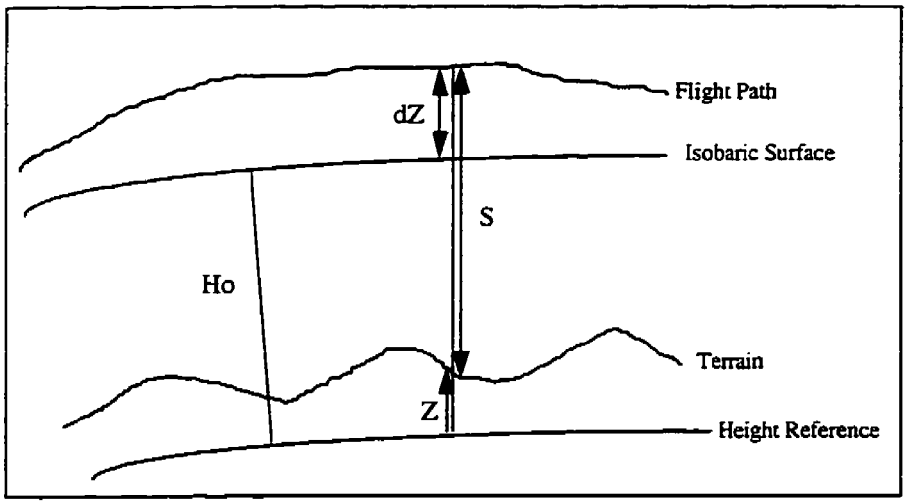

Figure 1. 1. Airborne Profile Recorder Concept

The height information can be derived as:

$$Z = Ho + dZ - S \qquad 1.1$$

Blais (1976) incorporated lake leveling information, which makes use of the condition that points along the shoreline of a lake have the same elevation. Gyroscopes were employed to determine the exterior orientation parameters, but gained little practical acceptance because of accuracy limitations (Corten and Heimes, 1976). With the advances in inertial and satellite positioning technology, the subject of direct measurements of exterior orientation parameters has gained increased attention in recent years. The Global Positioning System (GPS) can provide the 3D position of the exposure stations, while an inertial navigation system (INS) can determine the attitude of the exposure stations. Ackermann (1984) found that positioning data (X, Y, Z) are more effective than attitude data (ω, Φ, κ), as the latter imply a summation of errors that affect the final object coordinates. The integration of GPS and airborne photogrammetry will be discussed in Chapter 3. The integrated GPS-INS approach to fully recover the exterior orientation parameters is the newest technique (Schwarz, et al., 1993), but one of the problems is the high cost of INS.

1. 1. 4. GPS Assisted Aerial Triangulation

The Navstar Global Positioning System (GPS) has become generally available and has been considered fully operational on a world wide basis since 1993. It can be used for direct positioning practically anywhere on earth and at any time. GPS has already had a revolutionary impact in various disciplines which are involved with navigation and geodetic positioning. A real-time capability is required if GPS is used for navigation purposes. However, it was soon realized that GPS offers a very high accuracy for positioning in combination with post-processing methods.

Since the launch of GPS satellites in early 1980's, photogrammetrists realized the usefulness of GPS for their particular interests (e.g., aerotriangulation). There are four main areas in photogrammetry where GPS can be used (Ackermann, 1994):

1- Establishment of ground control points using terrestrial GPS,

2- GPS controlled survey flight navigation,

3- High precision camera positioning for aerial triangulation,

4- Positioning of other airborne sensors (e.g., laser scanners).

Aerial Triangulation (AT) determines the ground coordinates of a large number of object points and the exterior orientation parameters of aerial photographs using as few control points as possible. Direct determination of the exterior orientation parameters with sufficient accuracy is the main goal in mapping projects so that AT can be neglected. According to Lachapelle et al. (1993), the accuracy for attitude parameters derived from multiple-antenna GPS observations is approximately 10 arc minutes, which is still far from the accuracy of attitude determination using the conventional photogrammetric approach (i.e., photogrammetric block adjustment).

GPS assisted aerial triangulation allows for a significant reduction of ground control points to support photogrammetric mapping projects. Coordinates of camera exposure stations are derived for each instant of exposure using GPS positioning techniques. These GPS derived coordinates are introduced into the combined GPS-photogrammetric block adjustment as weighted observations, resulting in a reduction of the number of control points to a minimum.

1. 2. Objectives of the Research

Design and implementation of all engineering projects (e.g. road construction) requires complete three-dimensional information of the project site. This information can be obtained by producing topographic maps for the project area. Photogrammetric techniques, in which the photo is the basic input, represent some of the most economical methods to produce topographic maps (Combs et al., 1980). The measurements made on these photos are corrected for the different kinds of distortions introduced at the time of photography.

Conventional block adjustments (bundles or independent models) have been widely used to determine both photogrammetric point coordinates and the exterior orientation parameters of photography for mapping purposes.

The major impact of cost and time consumption for ground control establishment on any mapping project is the primary reason that photogrammetrists have been looking for a replacement of ground control by auxiliary data (e.g. GPS).

With airborne GPS technology, the position of the aircraft at the individual exposure stations can be precisely determined. These positions can then be introduced into the combined GPS-photogrammetric block adjustment as statistically weighted observations for the exposure stations, thereby reducing the number of ground control points to a minimum, if not completely.

The inherent geometry of a block and the common tie points in consecutive strips makes it possible to recover all three rotation angles in the combined block adjustment. Unfortunately, this method can not be used for a single strip, since the GPS coordinates of the exposure stations do not permit a reliable recovery of the roll angle of the aircraft. As a consequence, control introduced by airborne-GPS leaves an ill-conditioned, if not singular, system of normal equations. Ground control points can be used along the flight line to overcome this problem. A number of studies have been carried out in this area (Habib and Novak, 1994, Abdullah, 1997). However, there is still a need for some ground control points in these approaches.

A new technique for GPS controlled strip triangulation is proposed in this study. It is based on geometric constraints of man-made structures (e.g. high voltage towers, high rise buildings) located along the flight line. This new technique for single strip adjustment eliminates the need for multiple strips of photography and ground control points which significantly reduces both the time and the cost of the corridor mapping projects.

The main goals of this research are:

- to develop a comprehensive software package which can integrate GPS, geodetic, and photogrammetric observations,
- to optimize combined GPS-photogrammetric bundle block adjustments, especially for a large scale mapping,
- to investigate the reliability of the combined GPS-photogrammetric block,

- to investigate practical considerations for an airborne GPS-photogrammetric system, and
- to develop a new technique for GPS controlled strip triangulation using geometric constraints of man-made structures.

CHAPTER 2

GPS ASSISTED AERIAL TRIANGULATION: MATHEMATICAL MODELS AND PRACTICAL CONSIDERATIONS

In this chapter, techniques of conventional aerial triangulation are reviewed. This review encompasses various mathematical models, self-calibration techniques, additional parameters, and the associated mathematical models. The second part of this chapter deals with GPS assisted aerial triangulation, the mathematical model, and practical considerations. For the sake of completeness, a brief review of the Global Positioning System, and its mathematical models, is provided in Appendix A.

2. 1. Bundle Blocks

A bundle of rays that originates from an object point and passes through the projective centre to the image points (Figure 2.1) forms the basic computational unit of aerial triangulation. Bundle block adjustment means the simultaneous least squares adjustment of all bundles from all exposure stations, which implicitly includes the simultaneous recovery of the exterior orientation elements of all photographs and the 3D positions of the object points (Faig, 1985).

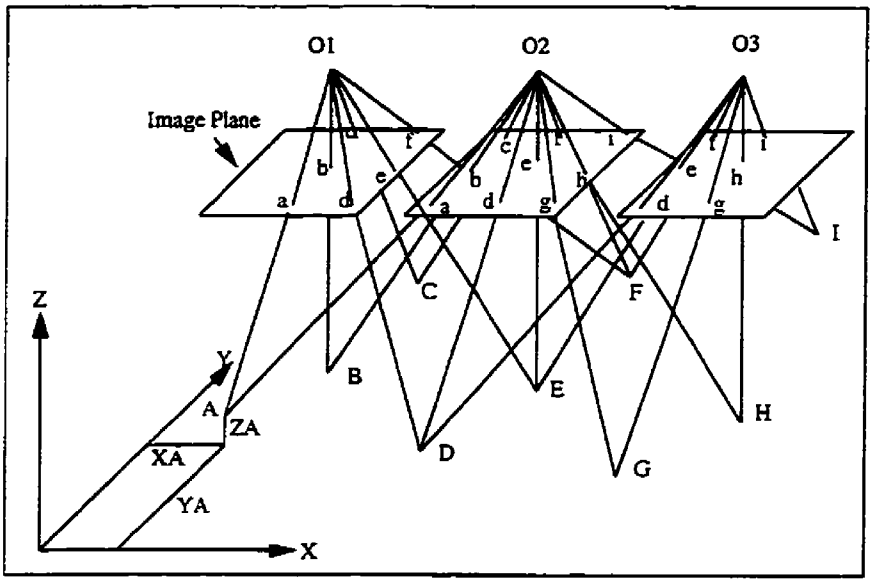

Figure 2.1 Bundle Blocks

The fundamental equation of aerial triangulation is the collinearity equation, which states that an object point, its homologous image point, and the perspective centre are collinear (Figure 2.2).

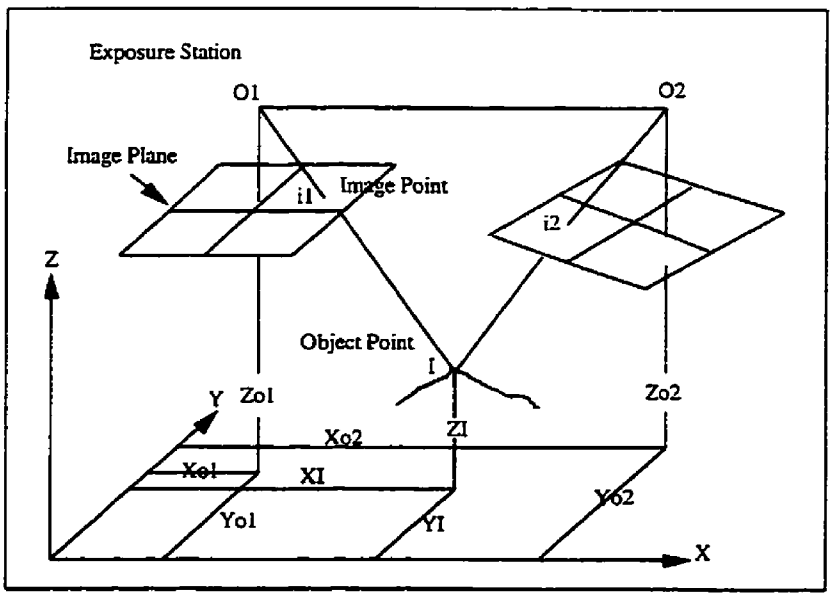

Figure 2.2 Concept of Collinearity Equation

The collinearity equations are given as:

$$F_x = x_i - x_o + c\frac{m_{11}(X_i - X_O) + m_{12}(Y_i - Y_O) + m_{13}(Z_i - Z_O)}{m_{31}(X_i - X_O) + m_{32}(Y_i - Y_O) + m_{33}(Z_i - Z_O)} = 0 \qquad 2.1$$

$$F_y = y_i - y_o + c\,k_y\frac{m_{21}(X_i - X_O) + m_{22}(Y_i - Y_O) + m_{23}(Z_i - Z_O)}{m_{31}(X_i - X_O) + m_{32}(Y_i - Y_O) + m_{33}(Z_i - Z_O)} = 0 \qquad 2.2$$

where

$$M = M_\kappa M_\Phi M_\omega = \begin{bmatrix} m_{11} & m_{12} & m_{13} \\ m_{21} & m_{22} & m_{23} \\ m_{31} & m_{32} & m_{33} \end{bmatrix} = \qquad 2.3$$

$$\begin{bmatrix} \cos(\Phi)\cos(\kappa) & \cos(\omega)\cos(\kappa)+\sin(\omega)\sin(\Phi)\cos(\kappa) & \sin(\omega)\sin(\kappa)-\cos(\omega)\sin(\Phi)\cos(\kappa \\ -\cos(\Phi)\sin(\kappa) & \cos(\omega)\cos(\kappa)-\sin(\omega)\sin(\Phi)\sin(\kappa) & \sin(\omega)\cos(\kappa)+\cos(\omega)\sin(\Phi)\sin(\kappa \\ \sin(\Phi) & -\sin(\omega)\cos(\Phi) & \cos(\omega)\cos(\Phi) \end{bmatrix}$$

and

(x_i, y_i) are the image coordinates,

(x_o, y_o) are the principal point coordinates,

c is the camera constant,

m_{ij} is an element of the 3D rotation matrix,

(X_i, Y_i, Z_i) are the object point coordinates,

(X_O, Y_O, Z_O) are the exposure station coordinates,

M is the rotation matrix,

(ω, Φ, κ) are the rotation angles, and

k_y is the scale factor for y axis in digital camera (this factor is 1 for a film-based camera).

In the standard case, there are 6 unknowns in the collinearity equations, namely, the exterior orientation parameters $(X_O, Y_O, Z_O, \omega, \Phi, \kappa)$. The three rotation angles (ω, Φ, κ) are implicit in the rotation matrix M (Equation 2.3). The principal point coordinates (x_o, y_o) and camera constant (c) are considered to be known for the basic bundle approach. However, this might not be true, as will be discussed later in this chapter. Strong imaging geometry plus a minimum of three ground control points are needed to solve for the six unknowns per bundle, which are then used to determine the unknown object coordinates of other measured image points.

2. 1. 1. Image Coordinate Measurement

A mono or stereo comparator is used to measure the image coordinates (x_i, y_i), which form the basic input into the bundle adjustment. Precision stereo comparators (e.g., Wild STK1) and mono comparators (e.g., Kern MK2) provide an accuracy at the level of 1-3 μm. Analytical plotters, such as AC1 in comparator mode, can also be used to measure the image coordinates providing 3-5 μm accuracy. It is recommended to observe each point at least twice, and to observe the fiducial/reseau marks. It is also necessary to

transfer points from one image to another when using a stereo comparator. However, if the points are targeted on the ground, point transfer is not required.

2. 2. Mathematical Formulations for Bundle Block Adjustment

F_x and F_y in Equations 2.1 and 2.2 may deviate from zero (i.e., perfect case) since the measured image coordinates include random and residual systematic errors. The collinearity equations are non-linear, therefore, they have to be linearized using Taylor's expansion. According to Chapman (1994), 6 different cases can be considered depending on the treatment of unknowns and observations. Case number 6, the most comprehensive case, is considered in this chapter, while the other cases are given in Appendix B.

2. 2. 1. Comprehensive Bundle Adjustment - Case # 6

* Observed photo coordinates,
* Observed object space coordinates,
* Unknown object space coordinates,
* Observed exterior orientation elements,
* Unknown exterior orientation elements,
* Observed geodetic measurements (e.g., distances),
* Unknown interior orientation and additional parameters,
* Observed interior orientation and additional parameters.

The observation equations are written as:

$$\begin{pmatrix} A_{EO} & A_S & A_{IO} \\ 0 & -I & 0 \\ -I & 0 & 0 \\ 0 & A_G & 0 \\ 0 & 0 & -I \end{pmatrix} \begin{pmatrix} \delta_{EO} \\ \delta_S \\ \delta_{IO} \end{pmatrix} = \begin{pmatrix} W_P \\ W_S \\ W_{EO} \\ W_G \\ W_{IO} \end{pmatrix} \qquad 2.4$$

where,

δ_{EO} is the correction vector of exterior orientation parameters,

δ_S is the correction vector of object space coordinates,

δ_{IO} is the correction vector of interior orientation parameters and additional parameters,

A_{EO} is the design matrix (exterior orientation parameters),

A_S is the design matrix (object space coordinates),

A_G is the design matrix of geodetic observations,

A_{IO} is the design matrix (derivatives of collinearity equations with respect to interior orientation and additional parameters),

W_P is the misclosure vector of image coordinates,

W_S is the misclosure vector of object point coordinates,

W_{EO} is the misclosure vector of exterior orientation parameters,

W_G is the misclosure vector of geodetic observation.

W_{IO} is the misclosure vector of the observed interior orientation and additional parameters, and

I is the identity matrix.

Interior orientation parameters include the camera constant, principal point coordinates, and Y scale factor for a digital camera scale bias. The equations for observed interior orientation and additional parameters are similar to those of observed exterior orientation parameters (Equations B.20 to B.25). The correction vector, $\bar{\delta}$, is computed using the least squares method as:

$$N = \begin{pmatrix} A_{EO}^T P_P A_{EO} + P_{EO} & A_{EO}^T P_P A_S & A_{EO}^T P_P A_{IO} \\ A_S^T P_P A_{EO} & A_S^T P_P A_S + P_S + A_G^T P_G A_G & A_S^T P_P A_{IO} \\ A_{IO}^T P_P A_{EO} & A_{IO}^T P_P A_S & A_{IO}^T P_P A_{IO} + P_{IO} \end{pmatrix} \quad 2.5$$

$$U = \begin{pmatrix} A_{EO}^T P_P W_P - P_{EO} W_{EO} \\ A_S^T P_P W_P - P_S W_S + A_G^T P_G W_G \\ A_{IO}^T P_P W_P - P_{IO} W_{IO} \end{pmatrix} \quad 2.6$$

where

P_P is the weight matrix of image coordinates,

P_S is the weight matrix of object point coordinates,

P_{EO} is the weight matrix of exterior orientation parameters,

P_{IO} is the weight matrix of interior orientation and additional parameters.

$$\bar{\delta} = \begin{pmatrix} \delta_{EO} \\ \delta_S \\ \delta_{IO} \end{pmatrix} \quad 2.7$$

$$\bar{\delta} = N^{-1} U \quad 2.8$$

In order to compensate for systematic errors, such as lens distortion, atmospheric refraction and the digital camera scale bias, and improve the collinearity equation model, distortion or additional parameters ,$(\Delta x_p, \Delta y_p)$, are introduced into the basic collinearity equations as:

$$x_i - x_o + \Delta x_p = -c\frac{m_{11}(X_i - X_O) + m_{12}(Y_i - Y_O) + m_{13}(Z_i - Z_O)}{m_{31}(X_i - X_O) + m_{32}(Y_i - Y_O) + m_{33}(Z_i - Z_O)} \qquad 2.9$$

$$y_i - y_o + \Delta y_p = -c\,k_y\frac{m_{21}(X_i - X_O) + m_{22}(Y_i - Y_O) + m_{23}(Z_i - Z_O)}{m_{31}(X_i - X_O) + m_{32}(Y_i - Y_O) + m_{33}(Z_i - Z_O)} \qquad 2.10$$

where $(\Delta x_p, \Delta y_p)$ are functions of several unknown parameters and are estimated simultaneously with the other unknowns in the equations. A complete recovery of all parameters (exterior orientation, object space coordinates, interior orientation, and additional parameters) is possible under certain conditions without the need for additional ground control points. This approach is called a "self calibrating bundle block adjustment".

Two general principles should be considered when incorporating additional parameters (Faig, 1985):

* the number of parameters should be as small as possible to avoid over-parametrization, and to keep the additional computational effort small,

* the parameters should be selected such that their correlations with other unknowns are negligible, otherwise the normal equation matrix becomes ill-conditioned or singular.

Since usually the same stable, metric aerial camera is used to photograph the entire project area in one flight mission for most topographic mapping projects, the interior orientation parameters and additional parameters can be assumed to be the same for all photos. Brown (1976) calls this approach "block invariant" which is most favorable for computational efficiency. If different cameras are used for the area being mapped, then the " block variant" approach is applied. In this approach, the parameters are only valid for a group of photographs (Ebner, 1976). If a non-metric camera is used for close range applications, a "photo variant" approach can be applied, in which new additional parameters are considered for each photograph.

2. 2. 2. Mathematical Models for Additional Parameters

There are two main approaches for modeling additional or distortion parameters; the first approach models the physical causes of image deformation (physical model), while the second approach empirically models the effects of image deformation (algebraic model).

2. 2. 2. 1. Physical Model

Four types of distortion are considered in this approach, namely, radial lens distortion, decentering distortion, and film shrinkage, and non-perpendicularity of the comparator axes in the case of film-based imagery. Thus; the model may be written as:

$$\Delta x_p = dr_x + dp_x + dg_x \qquad 2.11$$

$$\Delta y_p = dr_y + dp_y + dg_y \qquad 2.12$$

where,

$(\Delta x_p, \Delta y_p)$ are total distortions in x and y axes,

(dr_x, dr_y) are the contributions of radial lens distortion,

(dp_x, dp_y) are the contributions of the decentering lens distortions, and

(dg_x, dg_y) are the contributions of the film shrinkage and non-perpendicularity of the comparator axes.

The radial lens distortion may be expressed as:

$$dr = k_1 r^3 + k_2 r^5 + k_3 r^7 \qquad 2.13$$

or in x and y components:

$$dr_x = \frac{(x - x_o)}{r} dr = (k_1 r^2 + k_2 r^4 + k_3 r^6)(x - x_o) \qquad 2.14$$

$$dr_y = \frac{(y - y_o)}{r} dr = (k_1 r^2 + k_2 r^4 + k_3 r^6)(y - y_o) \qquad 2.15$$

where,

k_1, k_2, k_3 are the coefficients of the polynomial,

r is the radial distance of the measured point from the principal point,

(x_o, y_o) are the principal point coordinates, and

(x, y) are the measured image coordinates.

The decentering lens distortion model is given as (Brown, 1966):

$$dp_x = p_1\left(r^2 + 2(x - x_o)^2\right) + 2\,p_2 (x - x_o)(y - y_o) \qquad 2.16$$

$$dp_y = p_2\left(r^2 + 2(y - y_o)^2\right) + 2\,p_1 (x - x_o)(y - y_o) \qquad 2.17$$

where

(dp_x, dp_y) are the decentering distortions in the x and y directions, and

p_1, p_2 are the coefficients of the decentering distortion model.

The affinity model is used to model film shrinkage and non-perpendicularity of the comparator axes (Moniwa, 1977):

$$dg_x = A(y - y_o) \tag{2.18}$$

$$dg_y = B(y - y_o) \tag{2.19}$$

where,

(dg_x, dg_y) are the distortions contributed by film shrinkage and non-perpendicularity of the comparator axes, and

A, B are the coefficients of the affinity model.

The total number of unknowns per image is 16 (6 exterior orientation, 3 interior orientation, and 7 additional or distortion parameters, $k_1, k_2, k_3, p_1, p_2, A, B$). One more unknown is added to the list of interior orientation parameters, y scale factor k_y, if a digital camera, for example, is used.

The disadvantage of using this method is that there could be high correlations between the additional parameters themselves, and/or with the interior and exterior orientation parameters, which can create singularity in the normal matrix of observation equations. In addition to this, the model may not efficiently detect or compensate for irregular image deformations.

2. 2. 2. 2. Mathematical or Algebraic Modeling

In this approach, the combined effects of all systematic errors are modeled using functions that do not necessarily describe the physical nature of the distortions. Orthogonal polynomials have been popular choices of algebraic models. El Hakim (1979) used spherical harmonics to model the systematic errors. His formulations are expressed as:

$$\Delta x_p = (x - x_o)T \tag{2.20}$$

$$\Delta y_p = (y - y_o)T \tag{2.21}$$

where, T is the harmonic function,

$$T = a_{00} + a_{11}\cos\lambda + b_{11}\sin\lambda + a_{20}r + a_{22}r\cos^2\lambda + b_{22}r\sin 2\lambda + a_{31}r^2\cos\lambda + b_{31}r^2\sin\lambda + a_{33}\cos 3\lambda + b_{33}\sin 3\lambda + \ldots\ldots \tag{2.22}$$

and

$$\lambda = \tan^{-1}\left(\frac{y - y_o}{x - x_o}\right) \tag{2.23}$$

where, a_{ij}, b_{ij} are the coefficients of harmonic function T.

Brown (1976) also introduced the following orthogonal functions:

$$\Delta x_P = a_1 x + a_2 y + a_3 xy + a_4 y^2 + a_5 x^2 y + a_6 x y^2 + a_7 x^2 y^2 + \qquad 2.24$$

$$\frac{x}{c}[a_{13}(x^2 - y^2) + a_{14} x^2 y^2 + a_{15}(x^4 - y^4)] +$$

$$x[a_{16}(x^2+y^2)^2 + a_{17}(x^2+y^2)^4 + a_{18}(x^2+y^2)^6]$$

$$\Delta y_P = a_8 xy + a_9 x^2 + a_{10} x^2 y + a_{11} x y^2 + a_{12} x^2 y^2 + \qquad 2.25$$

$$\frac{y}{c}[a_{13}(x^2 - y^2) + a_{14} x^2 y^2 + a_{15}(x^4 - y^4)] +$$

$$y[a_{16}(x^2+y^2)^2 + a_{17}(x^2+y^2)^4 + a_{18}(x^2+y^2)^6]$$

where

a_1 to a_{18} are the coefficients of an orthogonal function,

c is the camera constant,

(x, y) are the measured image coordinates.

The advantage of using this method is that the parameters of these functions are not correlated. Therefore, singularity of normal matrix can be overcome. Distortion or additional parameters can be solved, along with other unknown parameters, in a bundle block adjustment by implementing both the physical and algebraic models. These techniques improve the accuracy of the bundle block adjustment when compared with the basic bundle block adjustment.

2. 2. 2. 3. Results from Conventional Self Calibration Blocks

El Hakim (1979) summarized the results of studies carried out by Grün (1978) and Salmenpera et al. (1974) as :

2.1. Self Calibration Block Adjustment Results

	Block Parameters		Without Self-Calibration			With Self-Calibration		
	Scale	Size	σ_0	μ_{XY}	μ_Z	σ_0	μ_{XY}	μ_Z
Grün	28000	104	5.3	8.8	15.8	3.3	5.2	12.2
Salmenpera	4000	94	5.4	4.5	8.5	5.1	3.4	7.8

All units are given in photo scale in μm and the overlap was 60%. As seen from Table 2.1, an improvement factor in the range of 1.3 to 1. 7 in planimetry, and 1.05 to 1.3 for height, can be achieved for the fully controlled blocks. It can be concluded that bundle block adjustment yields an absolute accuracy which is comparable to conventional terrestrial surveying (Faig, 1985).

2.2.3. Geodetic Observations in the Photogrammetric Block Adjustment

Conventionally, the adjustment of geodetic and photogrammetric measurements has been carried out in two separate steps. The terrestrial survey is adjusted to provide a

unique set of coordinates, and a variance-covariance matrix, for the ground control points, that are subsequently used as control for the photogrammetric solutions.

Combined photogrammetric-geodetic adjustment implies rigorous and simultaneous adjustment of all geodetic and photogrammetric observations, replacing the two steps solution with one step. This approach makes the error analysis and weighting of the observations more realistic. The program system GAP (General Adjustment Program) developed for this study, is an integrated software which accommodates GPS, photogrammetric, and geodetic observations. This program will be described in Chapter 3.

2. 2. 3.1. Mathematical Model

There are 9 types of geodetic measurements that can be handled by GAP, namely; slope distances, horizontal distances, zenith angles, horizontal directions, horizontal angles, 2D coordinate differences, 3D coordinate differences, height differences, and azimuth observations. The observation equation for photogrammetric measurements is given as:

$$F_P\left(\hat{X}_{EO}, \hat{X}_S, L_P\right) = 0 \qquad 2.26$$

where,

$\hat{X}_S$ is the object coordinates vector,

$\hat{X}_{EO}$ is the exterior orientation parameters vector, and

L_P is the photogrammetric measurements vector.

The observation equation for geodetic measurements can be written as:

$$F_G\left(\hat{X}_S, \hat{X}_{DIR}, L_G\right) = 0 \qquad 2.27$$

where

$\hat{X}_{DIR}$ is the vector of zero directions for horizontal direction observations, and

L_G is the geodetic measurements vector.

These equations are non-linear, and are linearized prior to the least squares adjustment. The linearized forms of these equations are:

$$W_P + A^P_{EO}\hat{X}_{EO} + A^P_S\hat{X}_S + \hat{B}_P\hat{V}_P = 0 \qquad 2.28$$

$$W_G + A^S_G\hat{X}_S + A^G_{DIR}\hat{X}_{DIR} + \hat{B}_G\hat{V}_G = 0 \qquad 2.29$$

where

W_P is the photogrammetric misclosure vector,

W_G is the geodetic misclosure vector,

A^P_{EO} is the derivative of the collinearity equation with respect to the exterior orientation parameters,

A^P_S is the derivative of the collinearity equation with respect to object point coordinates,

A^G_S is the derivative of the geodetic observations with respect to object point coordinates,

A^{G}_{DIR} is the derivative of the direction observations with respect to orientation parameter of the theodolite, and

$\hat{V}_P, \hat{V}_G$ are the residual vectors for image coordinates and geodetic observations.

These observations are combined and adjusted simultaneously using least squares techniques. The solution vector (unknown parameters) is computed using the following formula:

$$\hat{X} = (\overline{A}^T \overline{PA})^{-1} (\overline{A}^T \overline{PW}) \qquad 2.30$$

where

$\overline{A}$ is the design matrix composed of various design matrices,

$\overline{P}$ is the weight matrix and function of covariance matrix of various observations, and

$\overline{W}$ is the misclosure vector.

The normal equation matrix becomes more general by including geodetic observations into the block adjustment. Some measures (e.g., reordering of unknowns) have to be taken to keep the computational effort within reasonable limits. One of the advantages of integrating different observation types for coordinating points is that often a solution can be achieved, even in cases where any one of the approaches alone may be under-determined.

2. 3. Control Requirements

Any block comprised of two or more overlapping photographs requires to be absolutely positioned and oriented relative to the ground coordinate system. The 3D spatial similarity transformation with 7 parameters (3 rotations, 3 translations, 1 scale) is most frequently utilized for absolute orientation. Two horizontal and three vertical control points are used for the minimum optimal geometry. Due to some influences caused by point transfer errors and extrapolations beyond the mapping area, use of only the theoretical minimum control is unrealistic.

Theoretical and practical studies (Ackermann, 1966, 1974 and Brown, 1979) show that planimetric points along the perimeter of the block and relatively dense chains of vertical points across the block are necessary to relate the image coordinate system to the object coordinate system, to ensure the geometric stability of the block, and to control the error propagation.

The control requirements are different for mapping purposes and photogrammetric point determination projects. A spacing of 8-10 base lengths in planimetry along the perimeter of the block, dense cross chains (every 2nd strip) at both ends, and 6-8 base lengths in between for vertical control, are recommended for regular mapping. Ebner (1972) concluded that dense perimeter control (e.g., every two base lengths) and a dense net of vertical points within the block (e.g., every 2 base lengths perpendicular to the strip

direction) and every 4 base lengths along the strip direction, are required for photogrammetric point determination.

The number of control points can be reduced by changing flight parameters, increasing sidelap, and using multiple coverage. Molenaar (1984) found that if the terrestrial surveys were laid out solely to establish perimeter control (e.g., by a traverse), it may lead to a weak geometric configuration, therefore, some cross connections would strengthen the geometry and absolute accuracy.

2. 3. 1. Auxiliary Data As Control Entities

Perimeter control for planimetry has reduced the number of control points in required terrestrial work for a photogrammetric block. However, the dense chains of vertical control demand additional surveys. A number of studies (Ackermann, 1984, Blais and Chapman, 1984, Faig, 1979) have been carried out to reduce the number of control points, especially vertical points, using measured exterior orientation parameters at the time of photography. These studies showed that great savings in vertical control points could be achieved.

2. 3. 2. Mathematical Models for Auxiliary Data

Auxiliary control can be integrated into a photogrammetric block adjustment as additional observation equations, properly weighted, and adjusted together with the other data. Ackermann (1984) used the following observation equations for the statoscope, APR, and attitude data in his independent model block adjustment program (PAT-M):

$$V_j^{Stat} = Z_j^{PC} - Z_j^{Stat} - (a_0 + a_1 X_j + ...) \quad 2.31$$

$$V_j^{APR} = Z_j - Z_j^{APR} - (b_0 + b_1 X_j + ...) \quad 2.32$$

$$V_j^{\omega} = \omega_j - \omega_j^{Nav} - (e_0 + e_1 X_j + ...) \quad 2.33$$

$$V_j^{\Phi} = \Phi_j - \Phi_j^{Nav} - (d_0 + d_1 X_j + ...) \quad 2.34$$

$$V_j^{\kappa} = \kappa_j - \kappa_j^{Nav} - (e_0 + e_1 X_j + ...) \quad 2.35$$

where,

V_j is the residual,

Z_j^{PC} is the Z coordinate of exposure station,

Z_j^{Stat} is the elevation provided by statoscope,

Z_i^{APR} is the Z coordinate of an identifiable feature in the aerial photo,

ω_j is the roll angle,

κ_j is the yaw angle,

Φ_j is the pitch angle,

X_j is the X coordinate along strip, and

$a_j,.....,e_j$ are the coefficients of the polynomials used to model the systematic errors introduced from auxiliary data.

2. 4. Results Obtained from Previous Studies

Ackermann (1974) used statoscope data for a block of 60 km length without the need for interior vertical control. Studies carried out by Faig (1976 and 1979) and El Hakim (1979) showed that the use of statoscope with some lake information can completely meet vertical control requirements within a block for small and medium scale mapping. Ackermann (1984) has also used flight navigation data as auxiliary control in block triangulation, and demonstrated that the requirements for horizontal control can be reduced for small scale mapping.

2. 5. Reliability Analysis

Aerial triangulation has become a powerful tool for point determination during the last two decades. The main reason is the rigorous application of adjustment theory, which enabled simultaneous recovery of exterior orientation parameters and object point coordinates. The refinement of the collinearity model to compensate for systematic errors led to a further increase in accuracy by a factor of two or three. Today, an accuracy of the

adjusted coordinate residuals of 2 to 3 μm, expressed at the photo scale, can be achieved if the full potential is used (Förstner, 1985).

The effects of unmodelled errors, especially gross errors, had not been studied thoroughly until a few years ago. Each block adjustment has to handle a certain percentage of gross errors, which are generally detected and eliminated via residual analysis. However, there does not exist an accepted criterion for an appropriate stopping point in the process of elimination of possibly erroneous observations. Therefore, undetected gross errors may remain. These, hopefully, do not adversely affect the results. This leads to the theory of the reliability of adjusted coordinates.

2. 5. 1. The Concept of Reliability

The theory of reliability was developed by Baarda (1968) to evaluate the quality of least squares adjustment results of geodetic networks. According to Baarda, the quality of an adjustment includes both precision and reliability (Figure 2. 3)

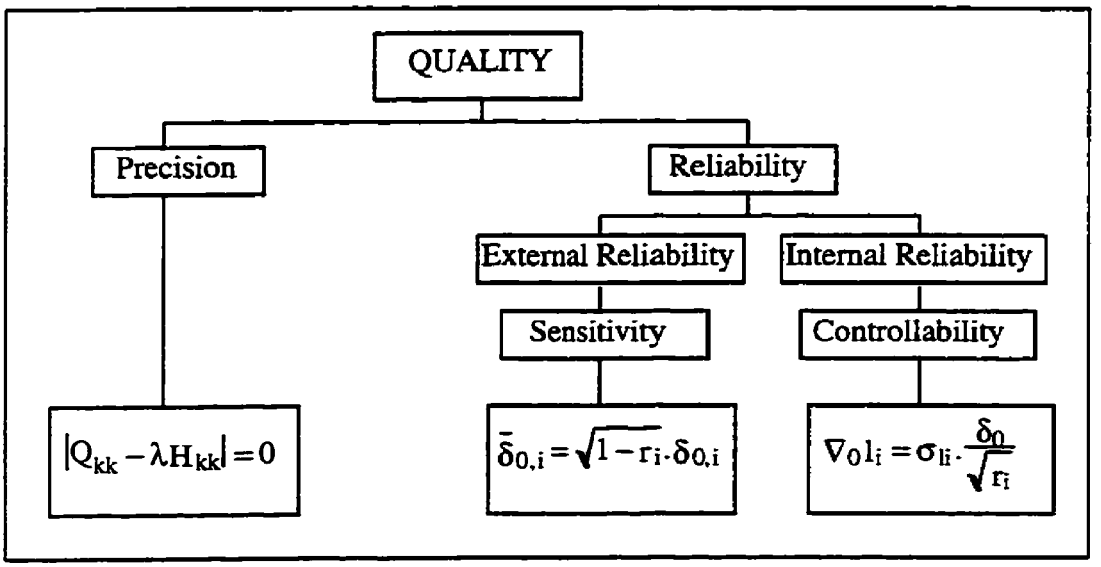

Figure 2. 3. Quality Evaluation of Adjustment (from Förstner, 1985)

Precision evaluation consists of comparing the covariance matrix, Q_{kk}, of the adjusted coordinates with a given matrix, H_{kk} (criterion matrix). The error ellipsoid derived from Q_{kk} should lie inside the error ellipsoid described by H_{kk}, and should be as similar to H_{kk} as possible. This provides a check on whether or not a required accuracy has been achieved.

As for reliability, Baarda distinguishes between internal and external reliabilities. Internal reliability refers to the controllability of the observations, and is described by the lower bounds of gross errors which can be detected within a given probability level. The effect of non-detectable gross errors on the adjustment results is described by external reliability factors, which indicate the amount by which the coordinates may be deteriorated in the worst case.

2. 5. 2 Reliability Measures

The linearized observation equation for a block adjustment can be written as:

$$\bar{l} + \bar{v} = A\hat{X} + a_0 \qquad ; \qquad P_{ll} \tag{2.36}$$

with the vector $\bar{l}$ containing the observations, l_i, and the residual vector, $\bar{v}$, containing the residuals v_i, the design matrix, A, the estimated vector, $\hat{X}$, of the unknown parameters (e.g., object point coordinates, transformation parameters, additional parameters), a constant vector, a_0, resulting from the linearization process, and the weight matrix, P_{ll}, which is the inverse of the variance-covariance matrix of the observations. The solution vector is derived using least squares method as:

$$\hat{X} = \left(A^T P_{ll} A\right)^{-1} A^T P_{ll} \left(\bar{l} - a_0\right) \tag{2.37}$$

The variance-covariance matrix of the residuals can be obtained from (Förstner , 1985):

$$Q_{vv} = Q_{ll} - A\left(A^T P_{ll} A\right)^{-1} A^T \tag{2.38}$$

and the direct relationship between the residuals and observations is:

$$\bar{v} = -Q_{vv} P_{ll} \left(\bar{l} - a_0 \right) \qquad 2.39$$

Because $Q_{vv} P_{ll}$ is idempotent, its rank equals its trace, which is equal to the total redundancy, r = n-u, where n is the number of observations, and u is the total number of unknowns.

$$\text{rank}\left(Q_{vv} P_{ll}\right) = \text{trace}\left(Q_{vv} P_{ll}\right) = \sum_{i=1}^{n} \left(Q_{vv} P_{ll}\right)_{ii} = r \qquad 2.40$$

The diagonal elements of, $\left(Q_{vv} P_{ll}\right)_{ii}$, reflect the distribution of the redundancy in the observations.

2. 5. 2. 1. Redundancy Numbers

The redundancy number, defined as:

$$r_i = \left(Q_{vv} P_{ll}\right)_{ii} \qquad 2.41$$

is the contribution of observation l_i to the total redundancy number, r (Förstner, 1985). These numbers range from 0 to 1. Observations which have $r_i = 1$ are fully controllable, and observations with $r_i = 0$ can not be checked. Lower redundancy numbers indicate that observations linked to these numbers can not be controlled, and errors on these

observations would be difficult to detect using the statistical outlier test. Average redundancy numbers for photogrammetric blocks range between 0.2 and 0.5. An average value of 0.5 is an indication of a relatively stable block.

The practical application of Baarda's reliability theory is to determine the magnitude of blunders that can not be detected on a given probability level, α_0, when accepting a level of risk, β_0, of committing Type II error (i.e., accepting the hypothesis that no blunders are present , when in fact, blunders are present) (Vaníček et al., 1991). Assuming that all observations are burdened with blunders, the objective is to find the minimum size of blunder in each observation that can still be detected.

2. 5. 2. 2 Internal Reliability

Internal reliability represents the maximum blunder in an observation undetectable with selected α_0 (the significance level) and $(1-\beta_0)$, (the power of the test). It is defined as (Li and Jie, 1989):

$$\nabla_0 l_i = \sigma_{li} \cdot \frac{\delta_0}{\sqrt{r_i}} = \sigma_{li} \cdot \delta_{0,i} \qquad 2.42$$

where,

σ_{li} is the standard deviation of the ith observation l_i,

δ_o is the non-centrality parameter,

$\delta_{0,i} = \delta_0 / \sqrt{r_i}$ is the internal reliability factor for observation l_i, and

$\nabla_0 l_i$ is the minimum blunder that can be detected statistically.

With a significance level of 1% and power of 93%, the non-centrality parameter is equal to 4. The example of ground control observation is considered here. If the redundancy number for the X coordinate of a ground control point is 0.65, and the standard deviation of this observation is 3 cm, then the minimum blunder that can be detected using a statistical outlier test is 15 cm.

The average local redundancy is considered as a measure of the overall reliability of one group of observations. It is defined as (Li and Jie, 1989):

$$r_k = \sum_{j=1}^{n_k} r_j / n_k \qquad 2.43$$

where, n_k is the number of members in the kth group of observations, and r_j is the local redundancy of the jth observation in the kth group.

2. 5. 2. 3. External Reliability

External reliability measures the effect of undetected blunder ($\nabla_0 l_i$) in the observation on the unknown parameters, obtained through the least squares adjustment. In

the case of photogrammetric block adjustment, it shows the reaction of the unknown parameters of the block (e.g., object point coordinates) to the undetected blunders in the observations (e.g., GPS coordinates of camera exposure stations). The external reliability factor is defined as (Li and Jie, 1989):

$$\bar{\delta}_{0,i} = \sqrt{1 - r_i} \cdot \delta_{0,i} \qquad 2.44$$

where, $\bar{\delta}_{0,i}$ is the external reliability factor for observation l_i. Table 2.2 gives an indication of ranges of acceptable reliability measures. For the same example given in previous section, the external reliability factor for the X coordinate of the ground control observation is 2.93, which is categorized as good according to Table 2.2.

Table 2. 2. On the Evaluation of the Reliability Measures (From Förstner, 1985)

	Good	Acceptable	Bad	Not Acceptable
r_i	$r_i > 0.5$	$0.1 < r_i \leq 0.5$	$0.04 < r_i \leq 0.1$	$r_i \leq 0.04$
$\delta_{0,i}$	$\delta_{0,i} < 6$	$6 \leq \delta_{o,i} < 12$	$12 \leq \delta_{o,i} < 20$	$\delta_{o,i} \geq 20$
$\bar{\delta}_{0,i}$	$\bar{\delta}_{o,i} < 4$	$4 \leq \bar{\delta}_{0,i} < 10$	$10 \leq \bar{\delta}_{0,i} < 20$	$\bar{\delta}_{o,i} \geq 20$

2. 6. GPS Supported Aerial Triangulation

The main purpose of aerial triangulation (AT) is the determination of ground coordinates for a large number of terrain points, and the exterior orientation parameters of aerial photographs using as few control points as possible. A favourable scenario in mapping projects is to have available the exterior orientation parameters with sufficient accuracy that the AT can be neglected. The affordable accuracy for attitude parameters using multi-antenna GPS technique is approximately 10 arc minutes (Lachapelle et al., 1993), and still far from what can be obtained from a conventional block adjustment (5 arc seconds). Therefore, aerial triangulation is still one of the important steps in mapping and can not be avoided.

The integration of GPS measurements into photogrammetric blocks allows the accurate determination of coordinates of the exposure stations, thus reducing the ground control requirements to a minimum. Therefore, the goal is to improve the efficiency of AT by avoiding ground control points almost completely (Lapine, 1991). The combined adjustment of photogrammetric data and GPS observations can be carried out by introducing GPS observation equations into the conventional block adjustment. An empirical investigation by Frieβ (1991) showed that, in addition to the high internal accuracy of GPS aircraft positions (σ=2 cm), drift errors may occur due to the ionospheric and tropospheric errors, satellite orbital errors, and uncertainty of the initial carrier phase ambiguities. These drift errors become larger as the distance between the

monitor and remote stations increase. Of the mentioned errors, incorrect carrier phase ambiguities are the major contributor to the drift errors in the derived positions.

The following sections concentrate on the application of GPS in aerial triangulation, and deal with combined GPS photogrammetric block adjustment, its mathematical models, and practical considerations.

2. 6.1. GPS Observable used in Precise Photogrammetric Applications

There are three types of positioning information that can be extracted from GPS satellite signals: pseudorange (code), carrier phase, and phase rate (Doppler Frequency). The high accuracy required for aerotriangulation, demand the use of GPS phase measurements. In order to eliminate the effects of systematic errors inherent in these observations, double difference GPS phase measurement techniques are used. The reason is that most GPS errors affecting positioning accuracy are highly correlated over a certain area, and can be eliminated or reduced. The observation equation for DGPS phase measurement is given in Appendix A, Equation A. 15.

The terms $\nabla\Delta d_\rho$, $\nabla\Delta d_{ion}$, and $\nabla\Delta d_{trop}$ in Equation A.15 are generally small or negligible for short monitor-remote distances (e.g. <10-20 km). However, the term $\nabla\Delta d_\rho$ becomes more significant due to Selective Availability (SA), and may introduce some negative effects on integer carrier ambiguity recovery. The satellite and receiver clock

errors are eliminated using the DGPS method, but the receiver noise is amplified by a factor of 2. The phase observable is used extensively in kinematic mode, where the initial ambiguity resolution can be achieved using static initialization or "On The Fly" methods. Accuracy at the centimeter level can be obtained if cycle slips can be detected and recovered (Cannon, 1990). The accuracy of kinematic DGPS is a function of the following factors (Lachapelle, 1992):

- separation between the monitor and the remote station,
- the effect of Selective Availability,
- the receiver characteristics and ionospheric conditions.

2. 6. 2. Combined GPS-Photogrammetric Block Adjustment

The observation equations for the camera projection centres are incorporated into the conventional block adjustment. The observation equation should take into account the eccentricity vector between the antenna phase centre and the projection centre of the camera. This vector is usually determined using geodetic observations, and expressed relative to the camera frame coordinate system (Figure 2. 4). The observation equations are given as (Ebadi and Chapman, 1995):

$$\begin{pmatrix} V_{Xi} \\ V_{Yi} \\ V_{Zi} \end{pmatrix}^{GPS} = \begin{pmatrix} X_i \\ Y_i \\ Z_i \end{pmatrix}^{GPS} - \left(\begin{pmatrix} X_i \\ Y_i \\ Z_i \end{pmatrix}^{PC} + M_{\kappa\Phi\omega}^{T} \times a \right) \qquad 2.45$$

where,

$(X_i, Y_i, Z_i)^{PC}$ are the coordinates of the exposure stations,

$(X_i, Y_i, Z_i)^{GPS}$ are the coordinates of the antenna phase centre,

$(V_{Xi}, V_{Yi}, V_{Zi})^{GPS}$ are the GPS residuals,

a is the offset vector, and

M is the rotation matrix.

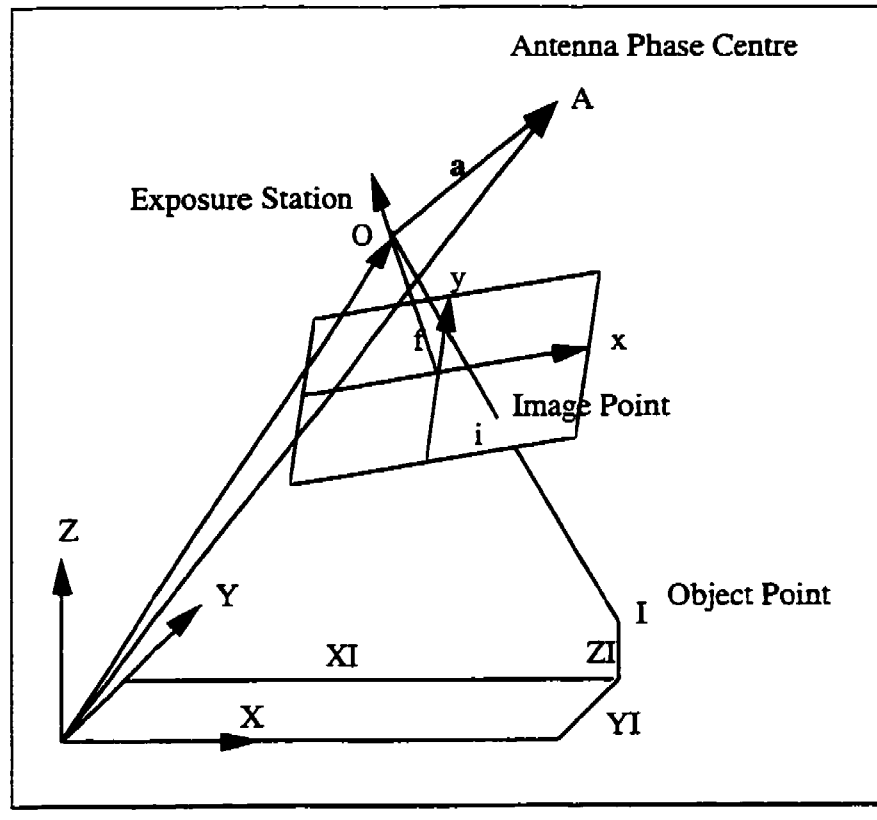

Figure 2. 4. Geometric Model For GPS Observation Equation

Ackermann and Schade(1993) introduced a special approach to take care of GPS errors caused by inaccurate ambiguities. In their approach, ambiguities are resolved using pseudorange observations at the beginning of each strip; therefore, the GPS positions of the exposure stations tend to drift over time. Six linear unknown parameters per strip (3 offsets and 3 drifts) are added to the observation equations of the exposure stations to account for these effects. These equations are given as:

$$\begin{pmatrix} X_i \\ Y_i \\ Z_i \end{pmatrix}^{GPS} + \begin{pmatrix} V_{Xi} \\ V_{Yi} \\ V_{Zi} \end{pmatrix}^{GPS} = \begin{pmatrix} X_i \\ Y_i \\ Z_i \end{pmatrix}^{PC} - \left(\begin{pmatrix} a_x \\ a_y \\ a_z \end{pmatrix} + \begin{pmatrix} b_x \\ b_y \\ b_z \end{pmatrix} (t_i - t_o) \right) \qquad 2.46$$

where,

$(X_i, Y_i, Z_i)^{PC}$ are the unknown coordinates of the exposure stations,

$(X_i, Y_i, Z_i)^{GPS}$ are the GPS coordinates of the camera exposure stations,

$(V_{Xi}, V_{Yi}, V_{Zi})^{GPS}$ are the GPS residuals,

(a_j, b_j) are the unknown drift corrections which are common for all observation equations of each strip,

t_i is the GPS time observed for each exposure and is treated as constant in the bundle block adjustment, and

t_o is the reference time for each strip and is treated as a constant value.

The drift parameters approximate and correct the GPS drift errors of the exposure stations in the combined block adjustment. Certain datum transformations can also be accommodated by these parameters. Depending on the data collection and processing techniques, drift parameters may be chosen stripwise or blockwise. In the case of stripwise processing, one set of parameters has to be introduced for each strip while in the blockwise case, one set of drift parameters suffices for the entire block. The determinability of these parameters should be guaranteed according to the ground control configuration and flight pattern (Frieβ, 1992). The geometry of the combined GPS-photogrammetric block is determined as in the conventional case (standard overlap and standard tie-pass point distribution).

2. 6. 3. Ground Control Configuration for GPS-Photogrammetric Blocks

Theoretically, as long as the datum transformation is known, no control points are needed to carry out the GPS-photogrammetric block adjustment, since each exposure station serves as a control point. If a coordinate system other than WGS84 is required for the final object coordinates, then ground control points are required to define the datum. For this purpose, four control points are usually used at the corners of the block.

The situation is different when drift parameters are included. The inclusion of drift parameters weakens the geometry of the block. To overcome this problem, various ground control configurations can be utilized to strengthen the geometry, and enable

recovery of all unknowns in the block adjustment. The GPS-photogrammetric blocks can be made geometrically and numerically stable and solvable for all unknowns in 3 ways (Ackermann and Schade, 1993):

(a) - If the block has 60% side lap (Figure 2. 5, case a),

(b) - If 2 chains of vertical control points across the front ends of the block are used (Figure 2. 5, case b),

(c) - If 2 cross strips of photography at the front ends of the block are taken (Figure 2. 5, case c).

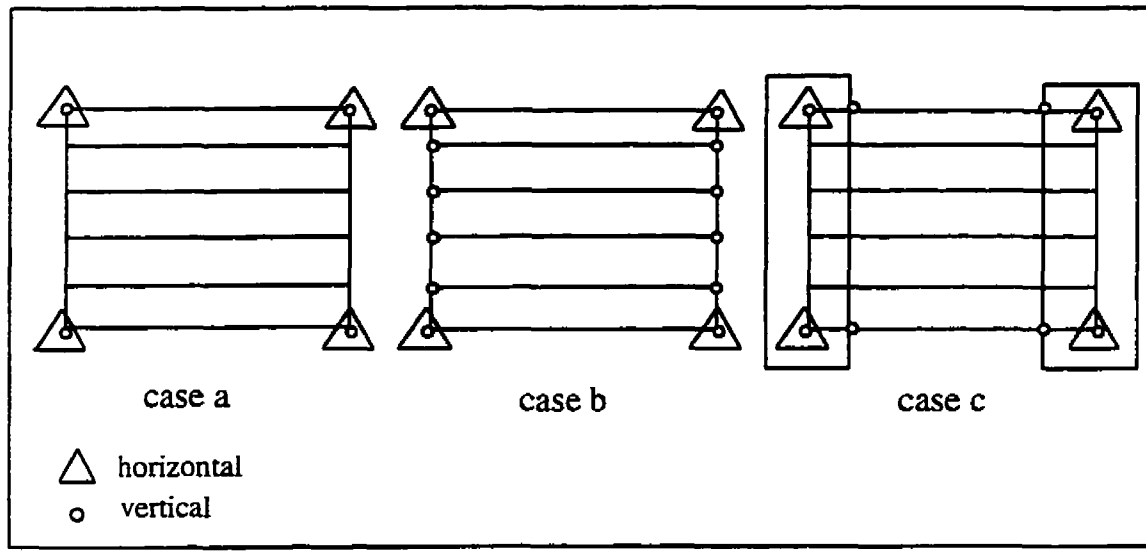

Figure 2. 5. Ground Control Configurations for GPS Assisted Blocks

Case (c) (2 cross strips) is usually recommended for GPS aerial triangulation due to its economic efficiency. The use of pairs or triplets of ground control points at the perspective locations in the cross strips is suggested for stronger geometry and higher reliability. Cross strips must be strongly connected to all overlapping strips, by measuring and transferring all mutual points, in all combinations. The same procedure applies to ground control points. They should be measured in all images in which they appear. It

may be required to have more than 2 cross strips and 4 ground control points if the blocks have irregular shape.

2. 6. 4. Problems Encountered and Suggested Remedies

2. 6. 4. 1. Antenna-Aerial Camera Offset

GPS provides the coordinates of the antenna phase centre and not, as desired, the projection centre of the camera (Frieβ, 1987). This happens because the phase centre of the antenna and the rear nodal point of the aerial camera lens can not occupy the same physical point in space (Lucas, 1987). If the camera is operated in a locked-down mode, the relative motion of the camera's projective centre with respect to the antenna can be avoided. In this case, the offset between the camera projection centre and the antenna phase centre is constant with respect to the camera fixed coordinate system (Figure 2. 4).

The offset vector can be surveyed using geodetic methods and measured with respect to the image coordinate system, or alternatively treated as an unknown quantity and solved together with other unknowns in a block adjustment. However, the latter case requires more extensive control.

The GPS positions of the antenna phase centre have to be reduced to the camera exposure stations. Since an external coordinate system is considered for the coordinate

reduction, the attitude of the camera must be known. The attitude parameters can be obtained by an initial block adjustment run.

2. 6. 4. 2. Synchronization Between Exposure And GPS Time

To interpolate exposure station positions from GPS positions, the instants of exposure must be recorded using the receiver time scale with precise synchronization to GPS time (Frieβ, 1987). The measuring rate for GPS observations must be 1 Hz or greater, as the speed of survey aircraft is on the order of 50 to 100 m per second (Ackermann and Schade, 1993). The photogrammetric camera should be equipped with a shutter synchronized electronic signal, providing an accuracy better than 1 ms.

2. 6. 4. 3. Geodetic Datum

GPS provides coordinates in the WGS84 system, which is a geocentric Cartesian coordinate system centred at the mass centre of the earth. However, the reference systems usually used in aerial triangulation are the local coordinate systems referred to local ellipsoids. Planimetric coordinates may be obtained by transforming from WGS84 to the local coordinate system (e.g., UTM), implying that there is still a need for minimum ground control points to carry out the transformation. The transformation between these two coordinate systems can also be based on published formulas (Colomina, 1993). The transformation of height requires knowledge of the geoid and its undulation (Faig and

Shih, 1989). It is also possible to carry out the GPS aerial triangulation in a localized vertical coordinate system, and apply the transformation thereafter (Ackermann and Schade, 1993).

2. 6. 4. 4. Ambiguity Resolution

This problem can be handled in a number of ways. It can be approximately determined from the pseudorange observed in the C/A or P codes. Calibrating N (by occupying a known point at the airport) is another solution. The unknown N can also be determined using "On The Fly" ambiguity resolution methods (Hatch, 1990, Abidin, 1993, Chen, 1994). Inaccurate approximation of ambiguity creates drift errors in the GPS positions of exposure stations. Ambiguity resolution is still one of the most challenging parts of kinematic GPS positioning. No matter what method is chosen for ambiguity resolution, GPS drift errors can not be avoided.

2. 6. 4. 5. Cycle Slip

Cycle slips are discontinuities in the time series of the carrier phase measurements as measured in the GPS receiver. These occur when:

- parts of the aircraft obstruct the inter-visibility between the antenna and satellite,
- multipath from reflection of some parts of the aircraft (Krabill et al., 1989),
- receiver power failure,

- low signal strength due to the high ionospheric activity or external source (e.g., radar).

Some approaches for cycle slip detection and correction are:

- using receiver with more than 4 channels to obtain redundant observations,
- integrating GPS with INS or other sensors (Schwarz et al., 1993),
- using dual frequency receivers,
- applying OTF ambiguity resolution techniques,
- locking on new course GPS positions derived from C/A code pseudorange after signal interruption (Ackermann and Schade, 1993).

2. 6. 5. Accuracy Performance of the GPS-Photogrammetric Blocks

GPS-photogrammetric blocks yield high accuracy due to the fact that these blocks are effectively controlled by the GPS air stations which act practically as control entities. The advantages are that there is little error propagation, and the accuracy distribution is quite uniform throughout the block. Accuracy does not depend on the block size. The accuracy of these blocks are determined by the intersection accuracy of the rays having measurement accuracy of σ_0 (Ackermann and Schade, 1993).

Ground control points are no longer required for controlling the block accuracy. They may provide the datum transformation, for which a few points only are sufficient.

The geometry of the block may be weakened by introducing GPS shift and drift parameters, but the required accuracy is still maintained. Such general accuracy features have been confirmed by theoretical accuracy studies (Ackermann and Schade, 1993), based on the inversion of the normal equation matrices. These studies showed that the standard deviations of the tie points for a simulated block controlled with 4 ground control points and only one set of free datum parameters is quite uniform, and the overall RMS accuracies are $1.4\sigma_0$ .S (horizontal) and $1.9\sigma_0$ .S (vertical), where S is the scale of photography.

Ackermann and Schade (1993) found that the block accuracy deteriorates if the GPS camera positioning accuracy decreases. GPS assisted blocks do not strongly depend on high GPS camera positioning accuracy, except for very large scale blocks. Similar accuracies could be achieved in conventional aerial triangulation only with a large number of ground control points. The theoretical studies (Ackermann, 1992, Burman and Tolegård, 1994) have established the very high accuracy performance of GPS blocks even in the case of additional parameters. The results are valid for the whole range of photo scales which are used in practice for mapping purposes, except for very large scale and photogrammetric point determination. According to Ackermann (1994), GPS assisted triangulation for large scale mapping (i.e., scale > 1:6,000) warrants further investigation. Part of this research deals with large scale mapping and its associated problems (i.e., timing error, incorrect ambiguity resolutions), and recommended solutions.

The theoretical and practical precisions obtained from simulated and real blocks carried out in this study will be given in Chapter 4.

2. 6. 6. Practical Considerations in GPS Airborne Photogrammetry

There are some practical problems to be considered before the process can be fully operational. These problems consist of selecting and mounting a GPS antenna on the aircraft, the receiver and camera interface, and the determination of the antenna-aerial camera offset. A solid consideration of the operational requirements, and their effect on flight plan, will lead to a successful photogrammetric mission.

2. 6. 6. 1. GPS Antenna

The GPS antenna should be mounted on the aircraft in such a way that it can receive the GPS signals with a minimum of obstruction and multipath. Potential places include the fuselage directly over the camera or the tip of the vertical stabilizer (Curry and Schuckman, 1993).

The advantage of fuselage location is that the antenna phase centre can be located along the optical axis of the camera, which simplifies the measurement of the offset vector. However, the fuselage location is more subject to multipath and shadowing of the antenna depending on wing placement. The vertical stabilizer location is usually less

sensitive to multipath and shadowing. Another advantage is that the actual mount of the antenna can be simplified, since some aircrafts have already a strobe light mount in the same location, which can be used for antenna mounting. However, the measurements of the antenna offset vector is more complicated. Once the antenna and camera have been mounted in the aircraft, it is not necessary to remeasure the offset vector for subsequent flight missions. As a rule of thumb, the best location for the GPS antenna is the one which can receive the GPS signals with minimum obstruction/interference. This location varies for different aircraft types. It should also be noted that making any kind of holes in the aircraft for antenna mounting must be done by a certified aircraft mechanic. Possible locations for antenna are shown in Figure 2. 6.

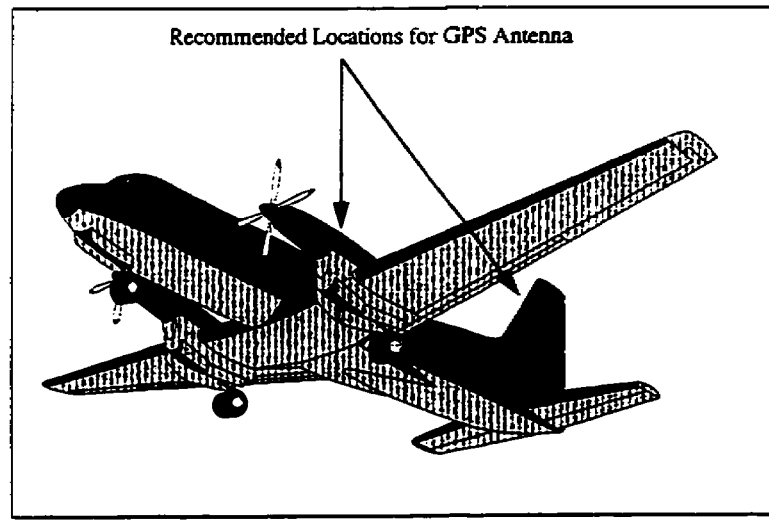

Figure 2. 6. GPS antenna locations on the aircraft

2. 6. 6. 2. Receiver and Camera Interface

The photogrammetric camera and the GPS receiver must be connected in such a way that exposure times can be recorded and correlated with the GPS time of antenna phase centres. Modern aerial cameras send a pulse corresponding to the so called "centre of exposure" to the receiver. These pulses are repeatable to some tens of nanoseconds. Older cameras can also be modified to send an exposure pulse to the receiver, but the repeatability is not as good as modern cameras. There may be some pulse lag which will need calibration.

A GPS receiver records signals at regular epochs set by the user, such as every one second. However, the camera exposure can occur at any time, and therefore the camera position at the instant of exposure should be interpolated from the GPS position of the antenna phase centre. Theoretically, the aerial camera can record exposure times with high accuracy and the interpolation can be based on these times. However, GPS receivers have an extremely accurate time base, therefore; it is preferred to record exposure times in the receiver. Most receivers have a simple cable connection from the camera. The camera pulse is sent to the receiver whenever an exposure occurs. The event time and an identifier are recorded in the receiver data file. GPS receivers can also send an accurate Pulse-Per-Second (PPS) signal that is used to trigger the camera at the even second pulse nearest to the designed exposure time. In order to use the exposure pulse to mark the occurrence of an event, the instant of a camera exposure should be exactly defined. The pulse is usually triggered when the fiducials are exposed onto the film in forward motion

compensation cameras. An image is created as soon as enough photons hit the silver halide crystals to cause the ground control targets to begin to be exposed (Curry and Schuckman, 1993). The errors caused by these timing issues are small, but can be modeled by introducing correction parameters to the bundle block adjustment program.

After the flight mission and film processing, the individual frames and the GPS event markers should be correlated. Some cameras can accept data from the receiver by imprinting the time and approximate coordinates onto the film. Lacking such a system, the camera clock can be set to GPS time so that GPS time is recorded for every frame simplifying the matching to event markers.

2. 6. 6. 3. Antenna-Aerial Camera Offset

The GPS receivers record position data for the GPS antenna phase centre at the instant of the exposure, but the coordinates of the exposure stations are required for the block adjustment. The offset vector between these two points should, therefore, be determined. If the location of the antenna is directly along the camera optical axis, the offset vector comprises a single vertical component. If not, a more sophisticated measurement method is required. The antenna offset can be surveyed using geodetic techniques (e.g., angular and distance measurements to the fiducial marks of the camera and to estimated location of the antenna phase centre). The antenna manufacturer is usually able to provide the location of the antenna phase centre to centimetre level

accuracy. The measurements of the offset vector are carried out in the aircraft or camera coordinate system. The coordinates of the antenna phase centre are given in a geocentric coordinate system (e.g., WGS84). The bundle block adjustment is performed in a ground-based coordinate system using the exposure station coordinates as weighted observations. Since the aircraft attitude changes with respect to the ground coordinate system, three orientation parameters, known as roll, pitch, and yaw, should be available to transfer the 3D antenna position to the camera's exposure stations. The bundle block adjustment program can be modified in such a way that it resolves the offset vector into the ground coordinate system at every iteration based on the calculated values of the attitude parameters. Coordinates for the exposure stations can then be updated. A formulation for this modification is given in Section 2. 6. 2. It is the antenna position that is actually constrained, with appropriate weight, while the camera exposure station moves about in ground space with respect to the antenna.

If the camera is not operated in a locked mode, the components of the antenna offset vector in the camera coordinate system will change. Therefore, the orientation angles in flight, for each frames should be recorded and used later in the block adjustment. A gyro-stabilized camera mount can be used for this purpose.

2. 6. 6. 4. Planning and Concerns for Flight Mission

The key to a successful GPS photogrammetry flight is careful mission planning. All GPS receiver manufactures provide planning software, which helps to determine satellite constellation for a particular day, time, and location. Flights should be planned for a period during which at least six or seven satellites are available, so that if phase lock between one or two satellites is lost during a turn, carrier phase processing can still continue. Even if only C/A code pseudorange data are collected and processed, additional satellites improve the geometry and increase the redundancy. The location of the master station has to be carefully planned to minimize multipath and obstruction effects.

Another parameter to be considered is the satellite cut-off elevation angle. It is recommended to record data from satellites which are 15 degrees or more above the horizon to reduce the errors introduced by atmosphere. The elevation mask can be programmed in the receiver or set in the planning software. However, it is advantageous to set a lower mask on the receivers during data acquisition which will help later to detect and correct for cycle slips during turns. Low elevation satellites can usually be ignored by post processing software.

All GPS receivers provide PDOP (Positional Dilution of Precision), which is an indicator of the strength of the satellite geometry. PDOP should be less than 5. A flight should not be planned and executed when this parameter is greater than 7 or 8 during any

portion of the mission. There could be brief spikes in PDOP when satellites rise and set. It may be possible to process through a PDOP spike, and still achieve good results on either side of spike.

The GPS data rate should be chosen according to the required accuracy of the photogrammetric project. Normally, a 1 Hz or 2 Hz rate is sufficient. Depending on memory configuration, GPS receivers can record data from five to six satellites at a 2 Hz rate for three to five hours in dual frequency mode. Data can be logged to an external device (e.g., PC) for longer flights.

The receivers at both the master and remote stations should begin logging at approximately the same time. Only data collected simultaneously at both receivers can be post-processed.

Static initialization for the aircraft receiver is required in carrier phase mode. This can be done by remaining stationary on the runway for 5-10 minutes, and performing a fast static survey to compute the base line between master and remote stations, or by physically lining up the aircraft antenna over a known point on the runway, measuring the height of the antenna and collecting a few seconds of data. It has to be remembered that continuous phase lock must be maintained on at least 4 satellites once the static initialization has been done. The ambiguity can also be resolved using so called "On The

Fly" techniques. If possible, data should be collected in such a way that both carrier and code post-processing methods can be applied.

It is advisable to check the camera before take-off by shooting a few test exposures with the camera connected to the receiver. Most receivers can indicate that an event has been recorded.

The banking angle of the aircraft should be restricted to 20-25 degrees during a turn, depending on the satellite geometry. If carrier phase data are being collected, smaller banking angles will extend the flight duration. The receiver itself has to be monitored for sufficient battery power and satellite tracking.

The maximum distance allowable between monitor and remote stations should be chosen in such a way that the errors contributed from atmosphere are negligible.

After completing the flight, it is useful to align the antenna over a known point and collect a few seconds of data, or to carry out a second fast static survey if continuous kinematic data are being collected. In this way, the data can be processed backward, if necessary. The data should also be immediately downloaded to a computer and checked for integrity. The photo coverage of the project area has to be evaluated upon completion of the flight.

CHAPTER 3

GAP (GENERAL ADJUSTMENT PROGRAM)

3. 1 Introduction/Overview

GAP is an integrated GPS, photogrammetric, and geodetic least squares adjustment program developed for this research. It can be used to perform least squares adjustment of geodetic networks (e.g., distances, directions, azimuths), photogrammetric blocks (e.g., image coordinates, exterior orientation parameters) or combined geodetic photogrammetric blocks. It can also incorporate GPS derived positions of the exposure stations into the block adjustment.

GAP was originally developed in Standard FORTRAN 77, and then ported to FORTRAN 90. One of the important features of FORTRAN 90 is the capability for dynamic memory allocation. The routines of this program are portable; no machine dependent features and no operating system calls are embedded in the code.

3. 2 Sparse Matrix Solution

The bundle block adjustment usually requires the solution of a large system of non-linear equations, with sparse structured and symmetric coefficient matrices. It can be

shown that, the normal equations for a least squares problem are symmetric. The first objective is to exploit the structure of normal equations by storing only the upper (or lower) triangular portion of normal matrix N (equation 2.5). The unknown parameters, X, can be ordered such that the non-zero elements of N fall in a diagonal band, whose width is small compared to the dimension of the system. Figure 3. 1. shows an example of this band storage structure.

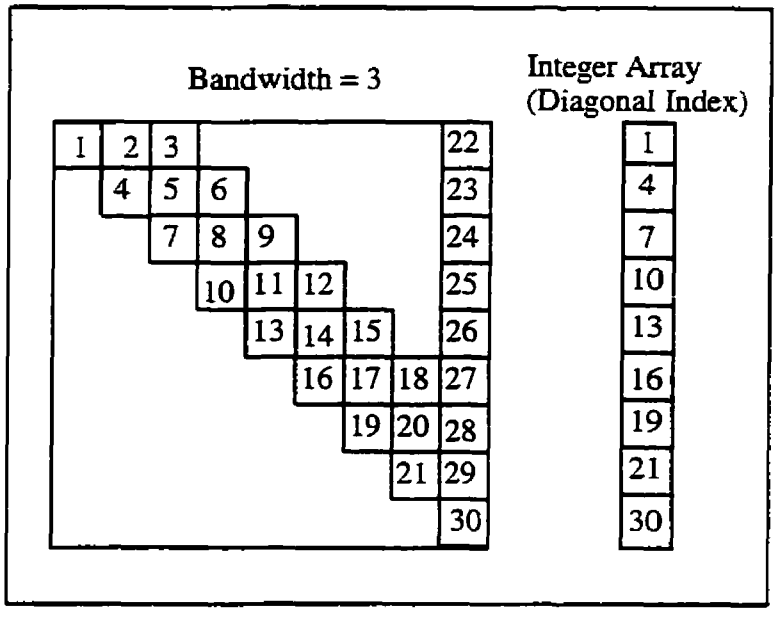

Figure 3. 1. Fixed Bandwidth Storage Structure (from Milbert, 1984)

In the example shown, all non-zero elements fit into a bandwidth of three. This structure can be described by storing the array indices of the diagonal elements in an integer array. If the bandwidth is one, the system is diagonal. Conversely, if the bandwidth is equal to the order of the normal matrix, then the system is full and sparse structure is not exploited. Greater savings in storage and execution times can be achieved

by using a variable bandwidth (profile) structure (Jennings, 1977). Figure 3. 2. shows this structure.

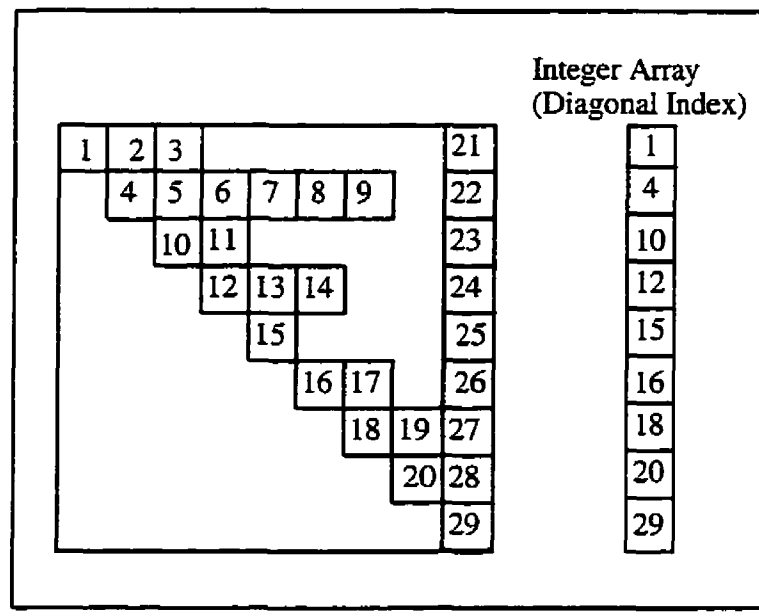

Figure 3. 2. Variable Bandwidth Storage Structure (from Milbert, 1984)

The structure is again described by an index array. GAP is able to process large least squares system by exploiting the sparse non-zero structure of a problem. Speed in execution is attained by using a static data structure (Milbert, 1984), meaning that the rows of the system are stored end-to-end in a single array. The price paid for this rapid processing is that the structure of each least squares problem should be known before the equations are accumulated and solved. GAP consists of two modules: the first module performs the analysis of the structure of a least squares problem stored in an integer array, while the second module solves the normal equations using the predetermined structure.

The elements of the normal equations are saved in a real array to further improve storage. The first module carries out the following tasks:

* initialization of an integer array to store the address of the diagonal elements,

* accumulation of the connectivity information based on graph theory (George and Liu, 1995), and

* analysis of the structure, and subsequent minimization of the bandwidth of the normal equations.

King's algorithm (King, 1970), originally applied to simultaneously solve the equations derived from network systems, is used to reorder the unknowns.

Once a structure has been determined, the least squares problem is ready to be solved. The contribution of each observation equation (e.g., image coordinates, exterior orientation parameters, GPS observations, ground control points) is accumulated one at a time into the normal equations (i.e., summation of the normal equations). After all the observations have been processed, the system is solved using a cholesky factorization approach. singularities can be detected by using a small positive, singularity tolerance.

In addition to the solution vector, $\hat{X}$, of the least squares solution, statistic information (e.g., variances of unknowns, which is the diagonal elements of $\sum \hat{x}$) can be obtained by inverting the normal matrix, N. Hanson (1978) showed that the inverse elements of the normal equations can be computed within the profile in place at no

greater cost than computing only the diagonal elements of the inverse. Variances of the adjusted observations and variances of the residuals can also be derived to perform a reliability analysis, if desired.

Data abstraction and modularity which are important factors for structured programming, have been considered in the development of GAP. Data abstraction separates the logical view of the data from the internal storage structure, while modules perform specific tasks and make a minimum number of assumptions about processes in other parts of the program (Milbert, 1984). The modules were designed as subprograms sharing common variables, in order to allow the user ease in discarding routines not needed for a particular application.

3. 3 Program Organization

The main flowchart of the program is shown in Figure 3. 3. All observations (e.g., photo coordinates, control points, exterior orientation parameters, geodetic observations) are treated as weighted observations with appropriate weights. Therefore, to treat orientation angles as unknown parameters to be solved, high standard deviations must be assigned to these angles to reflect the uncertainty in the parameters. On the other hand, to constrain the positions of exposure stations (e.g., GPS data), low standard deviations should be considered for these positions based upon the expected accuracy of these observations.

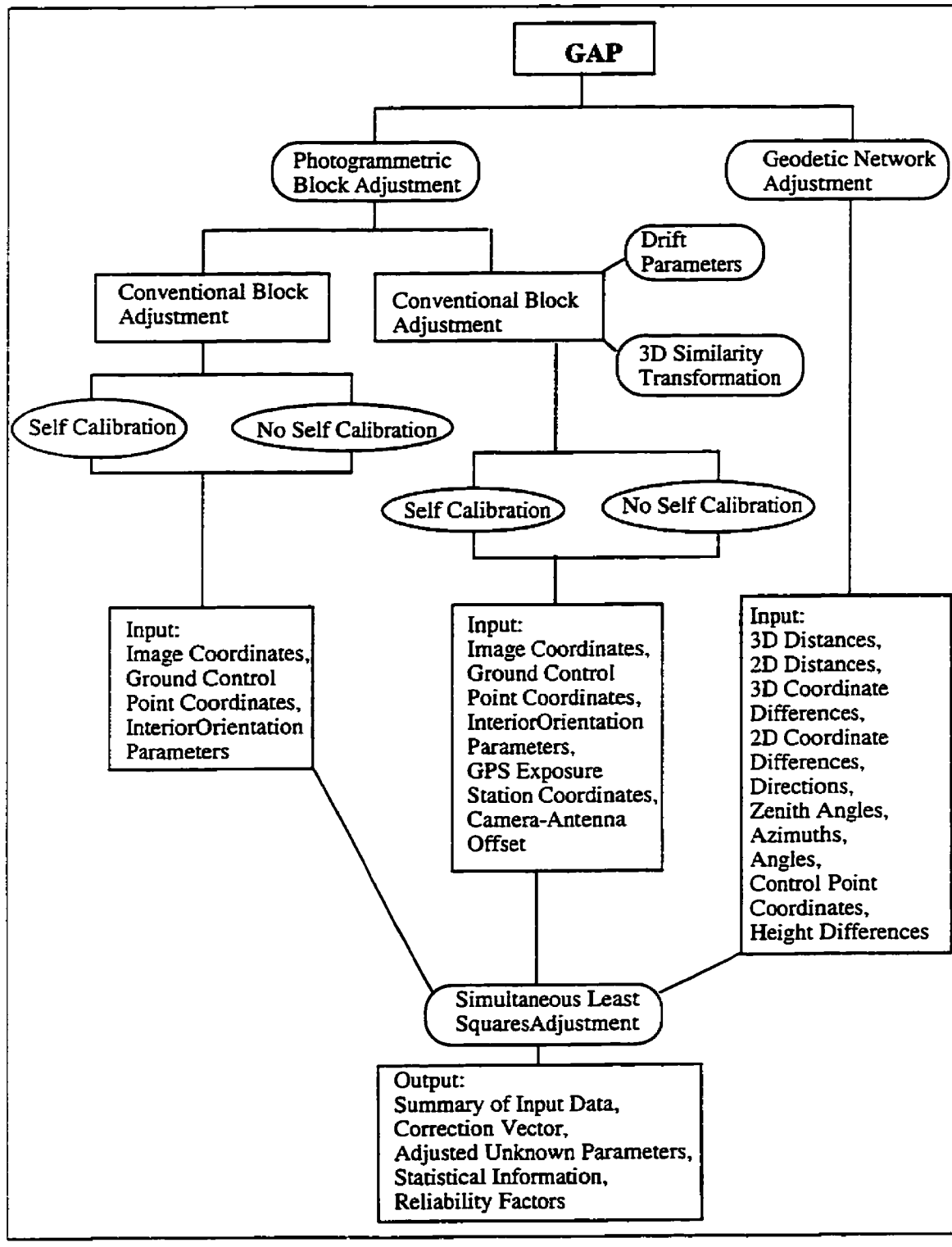

Figure 3.3. Flowchart of GAP

Due to the huge number of unknowns for a large block of photography, the "KING" reordering scheme (King, 1970) was adopted to minimize the bandwidth of the normal equations, and reduce the memory and CPU requirements. GAP can be run in both conventional block adjustment mode in which all 6 exterior orientation elements are solved as unknowns using ground control points, and GPS assisted block adjustment mode where coordinates of exposure stations are constrained using GPS data.

In GPS assisted aerial triangulation, the antenna should be located directly over the camera perspective centre for best results. In this case, there is a Z shift (Z coordinate in GPS_OFFSET); otherwise, the camera should be locked in place during the flight or the crab angle should be recorded whenever changed. The standard deviations of exposure stations should be selected in such a way that they reflect the accuracy of GPS camera stations.

3. 4 Advanced Program Features

GAP also supports self-calibrating bundle block adjustment. This means that, in addition to the interior orientation parameters, additional parameters can also be estimated to further improve the accuracy. There are typically 4 interior orientation parameters: the camera constant, the principal point coordinates, and the y-axis scale factor for the case of a CCD camera. GAP permits photowise, stripwise, or blockwise solution of these parameters. In order to solve for interior orientation parameters, it is

necessary to include standard deviations for these parameters when applying self calibration. Principal point coordinates are difficult to estimate in a self-calibration mode with aerial photography due to a high correlation with the camera leveling angles. Thus, these parameters should be constrained, and their standard deviations should be set to small values (i.e., large weights). The y-axis scale factor is used when there is a scale difference between the x and y photo axes. This is normally applicable to CCD cameras, but may be useful to improve the results of conventional block adjustment.

GAP can also solve for GPS drift parameters by including the GPS exposure time of each photo, and an index vector, in order to apply them on stripwise basis. It is important that the GPS be processed in a special way to take advantage of the drift and offset parameters being solved for each strip. It is also necessary to add cross strips to the block to make it possible to solve for these extra parameters (6 per strip) with a minimum ground control configuration (4 GCPs).

GAP can also perform a rigorous reliability analysis, in which the redundancy numbers, internal and external reliability factors of the observations are computed, based on the standardized residuals. The statistical information pertaining to the adjustment parameters can be obtained by setting the appropriate flag in the input file. This requires that the least squares normal matrix be inverted.

CHAPTER 4

RESULTS OF GPS ASSISTED AERIAL TRIANGULATION

This chapter deals with the results of GPS-photogrammetric block adjustments obtained using both simulated and real data. Results from a simulated block triangulation incorporating GPS-observed exposure stations are presented first, after which the results from a medium scale mapping are discussed.

4. 1 Simulated Large Scale Mapping Project

As mentioned in Chapter 1, to the author's knowledge, a thorough investigation has not yet been carried out for GPS assisted aerial triangulation, specifically as applied to large scale mapping and cadastral point determination. In these cases, the required accuracy of the camera exposure stations is less than 0.5 m. Therefore, reduction and elimination of GPS errors (e.g., timing errors, atmospheric errors, and especially errors introduced from incorrect ambiguities) are important issues to be considered for large scale GPS-photogrammetric blocks.

There are mainly two reasons that GPS has not been used for large scale mapping in the past; the satellite configuration was not complete until 1993, and also, intelligent and advanced ambiguity resolution techniques were not developed until recent years.

Both the precision and reliability of bundle block adjustment with GPS data were theoretically investigated using simulated data. The variance-covariance matrix of unknown parameters (Q_{XX}), and the variance-covariance matrix of residuals (Q_{VV}), and the weight matrix of observations (P_{ll}), as well as independent check points, were used to aid both precision and reliability analyses.

This study demonstrates the potential of GPS, even for large scale mapping projects. The simulated block was made up 10 strips. The block parameters are shown in Table 4. 1.

Table 4. 1. Information of Simulated Block

Number of Photos	230
Number of Strip	8 + 2 Cross Strips
Terrain Elevation Difference	150 m
Photo Scale	1: 5,000
Focal Length	152 mm
Average Flying Height	900 m
Forward Overlap	60%
Side Overlap	30% & 60%
Photograph Format	23 cm x 23 cm
Precision of Image Coordinates	0.005 mm
Precision of GPS Data	0.02 - 1.0 m
Precision of Ground Control Points	0.02 m & 0.1 m

4. 1. 1. Methodology

Image coordinates for all pass points and tie points were derived using the collinearity equations (equations 2.1 and 2.2) based on simulated values for camera exposure station coordinates, and attitude and ground coordinates of tie or pass points. The image coordinates were contaminated with pseudo-random noise in order to better simulate the real situation. The test design of GPS camera exposure stations is composed of different accuracies ranging from 2 cm to 1 m. Configurations of ground control points (GCPs) are shown in Figure 4. 1.

A - No ground control points,

B - 4 Ground control points at the corners of the block,

C - Full ground control Points,

D - Four pairs of ground control points and cross strips.

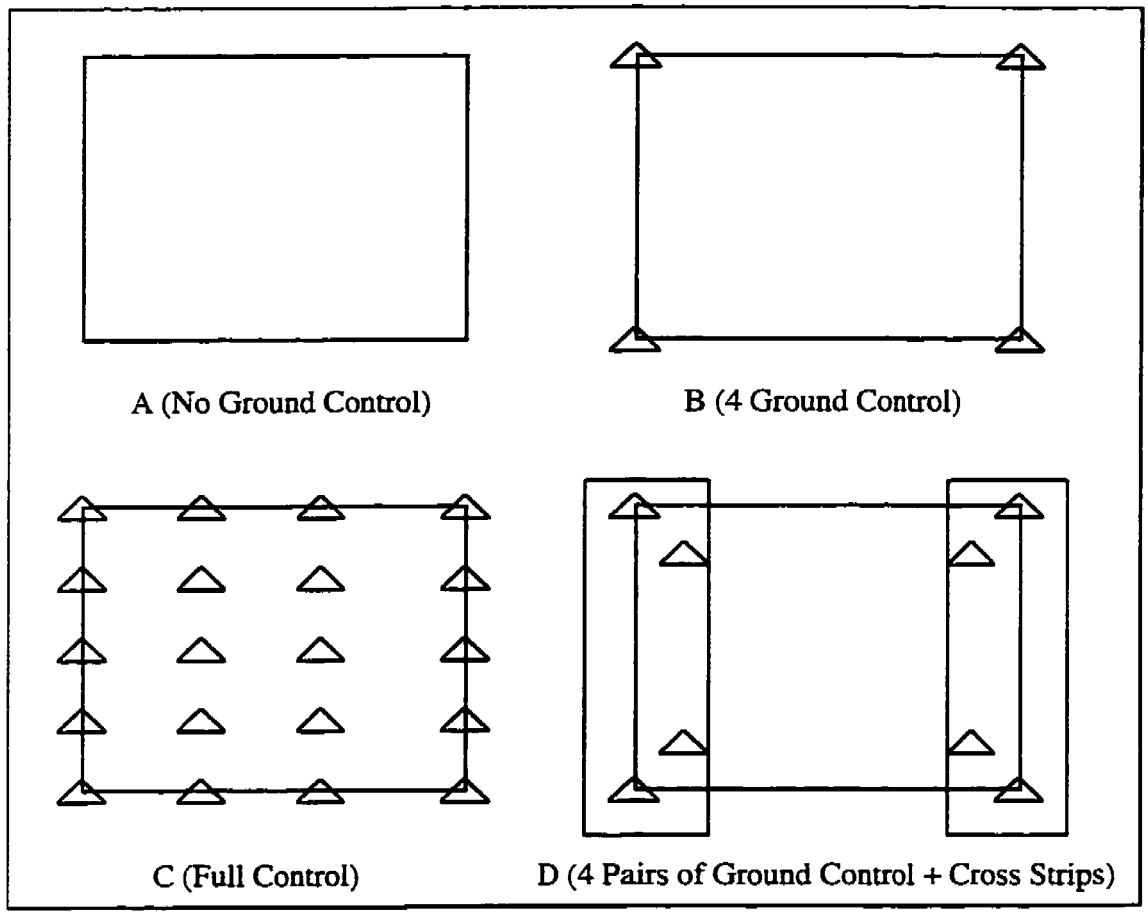

Figure 4. 1. Ground Control Configurations

There are two more configurations, E and F, which are almost the same as B and D, but with 60% sidelap. Among these configurations, version C is a conventional block adjustment and was considered for comparison.

The main objective is to test and analyze various scenarios for GPS-photogrammetric mapping projects. These tests include various ground control configurations, different sidelap, various accuracies for GPS coordinates of camera exposure stations, different ground control point accuracies, and cross strips.

These 6 configurations of ground control points for the simulated block form 6 main experiments carried out in this part of the research. However, it should be mentioned that within each of these experiments, several block adjustments were executed, varying the accuracy of ground control points (i.e., 0.02 m and 0.1 m) and GPS derived positions of camera exposure stations (i.e., 0.02 - 1.0 m).

The block adjustments were performed using the previously described program, GAP. For both precision and reliability analyses, the matrices Q_{XX} and $Q_{VV}P$ are computed by the program. A local coordinate system was adopted for the datum of the object points.

The results are based on the adjustments of the simulated block for the 6 experiments described above. They will be presented in two parts. In the first part, the theoretical and practical precisions will be derived for various scenarios, and reported in graph format to facilitate interpretation. The reliability measures obtained from these experiments will be presented and discussed in the second part. These results will also be shown in graph format.

It is expected to obtain relatively good results for experiment E (i.e., better than 3 cm accuracy for GPS accuracy of 0.5 m or better). Lower accuracy is expected from Experiment A, which has 30% sidelap and no ground control point (i.e., accuracy at the

level of 6 cm or better for GPS accuracy of 1 m or better). The expectation for other experiments is that their practical precision or accuracy will fall between 3 cm and 6 cm.

4. 1. 2. Precision Analysis of Simulated GPS-Photogrammetric Block

The covariance matrix of three-dimensional object points is generally considered as a measure of theoretical precision:

$$D(X) = \sigma_0^2 Q_{XX} \tag{4.1}$$

where, Q_{XX} is the cofactor matrix of the object points and σ_0^2 is the *a priori* variance factor. The theoretical precision in one coordinate direction of the ith object point is given by:

$$m_i = \sigma_0 \sqrt{(Q_{XX})_{ii}} \tag{4.2}$$

The average theoretical precision of n object points is computed as:

$$\overline{m} = \sigma_0 \sqrt{tr(Q_{XX})/3n} \tag{4.3}$$

The average practical precision (i.e., accuracy) in each of the X, Y, and Z coordinate directions are:

$$\overline{\mu}_X = \sqrt{\frac{\sum \Delta X^2}{n}} \tag{4.4}$$

$$\bar{\mu}_Y = \sqrt{\frac{\Sigma \Delta Y^2}{n}} \qquad 4.5$$

$$\bar{\mu}_Z = \sqrt{\frac{\Sigma \Delta Z^2}{n}} \qquad 4.6$$

where, $\Delta X, \Delta Y$, and ΔZ are differences between the adjusted and simulated coordinates of an object point. The simulated object points serve as check points in this simulated block.

The theoretical precision of the photogrammetric block is determined by inverting the normal matrix of the observation equations in a least squares bundle block adjustment. However, accuracy or practical precision is obtained by comparing the computed coordinates of object points and coordinates derived from an independent source. Theoretical and practical precisions converge to the same value if there are no systematic errors and biases in the observations, and observations are close to their true values.

Figures 4. 2 - 4. 4 show the practical precisions of all object points and Figures 4. 5 - 4. 7 depict the theoretical precisions obtained from the inversion of normal matrix, respectively. In all these figures, the ground control accuracy was assumed to be 0.02 m. The program GAP was executed for various configurations of ground control with different GPS accuracy of camera exposure stations.

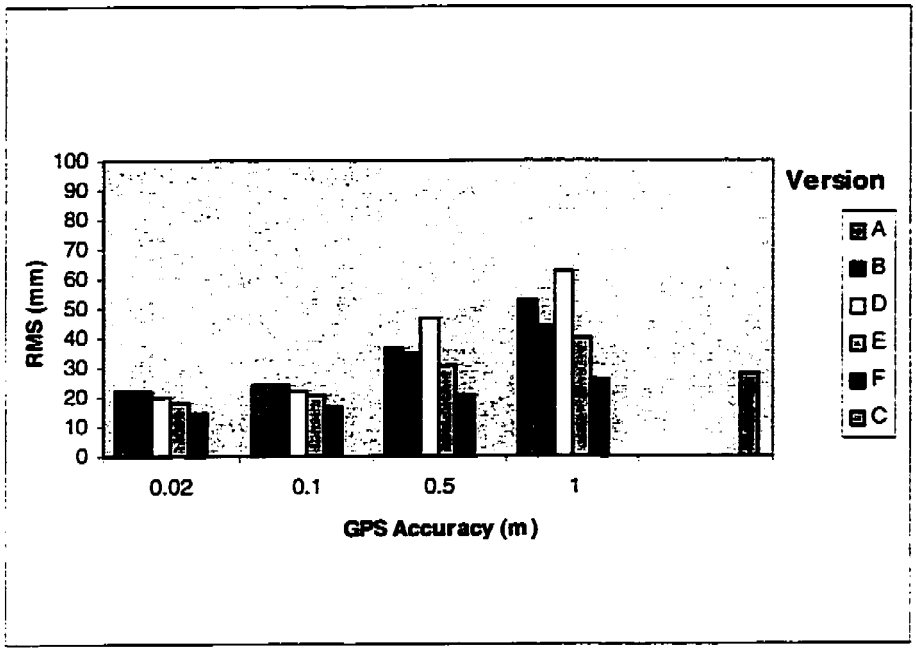

Figure 4.2. Accuracy of X Coordinate of Object Points

(Ground Control Accuracy = 0.020 m)

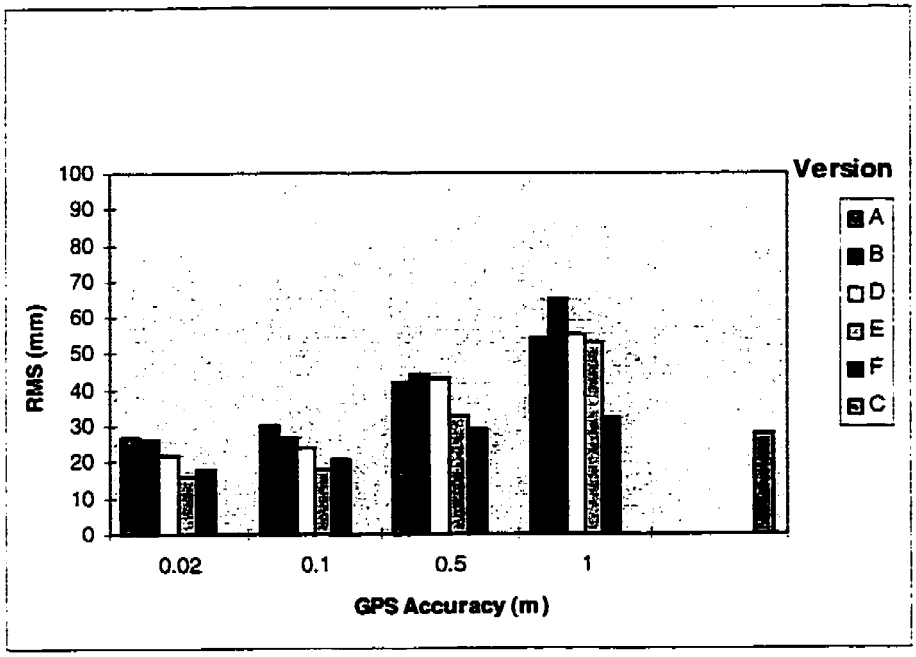

Figure 4.3. Accuracy of Y Coordinate of Object Points

(Ground Control Accuracy = 0.020 m)

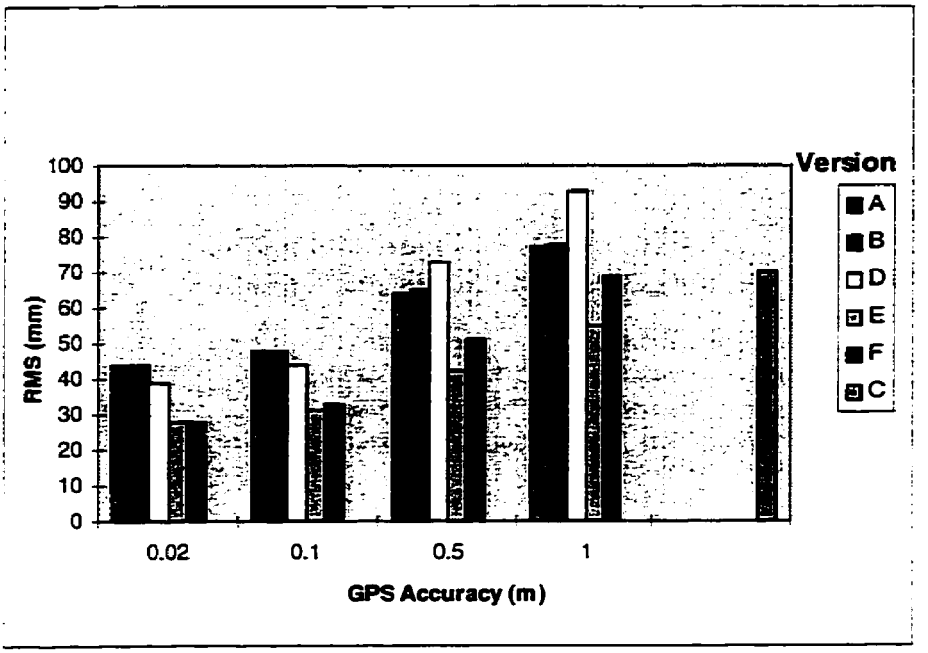

Figure 4.4. Accuracy of Z Coordinate of Object Points

(Ground Control Accuracy = 0.020 m)

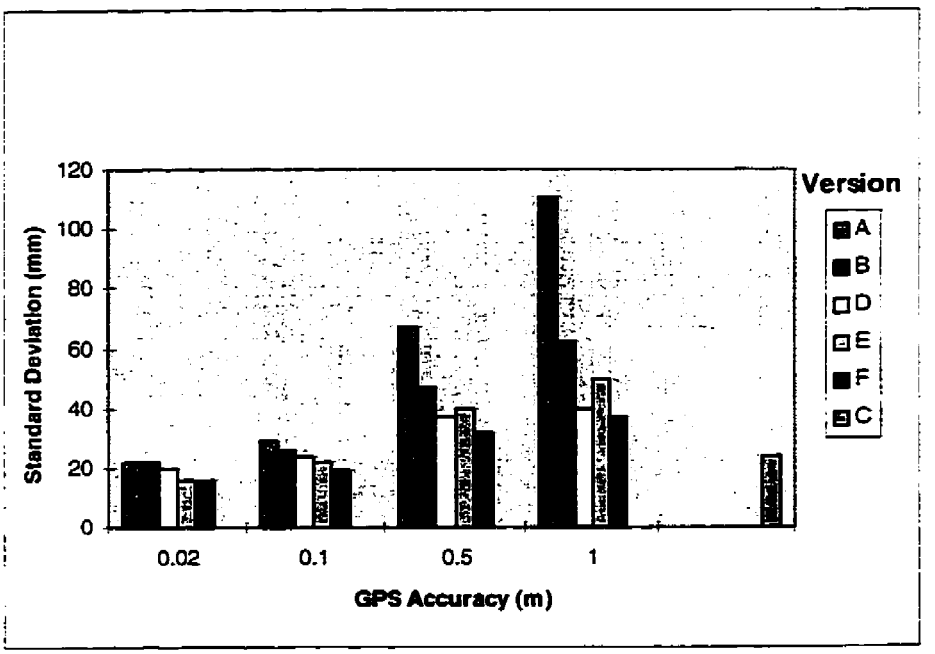

Figure 4. 5. Standard Deviations of X Coordinate of Object Points

(Ground Control Accuracy = 0.020 m)

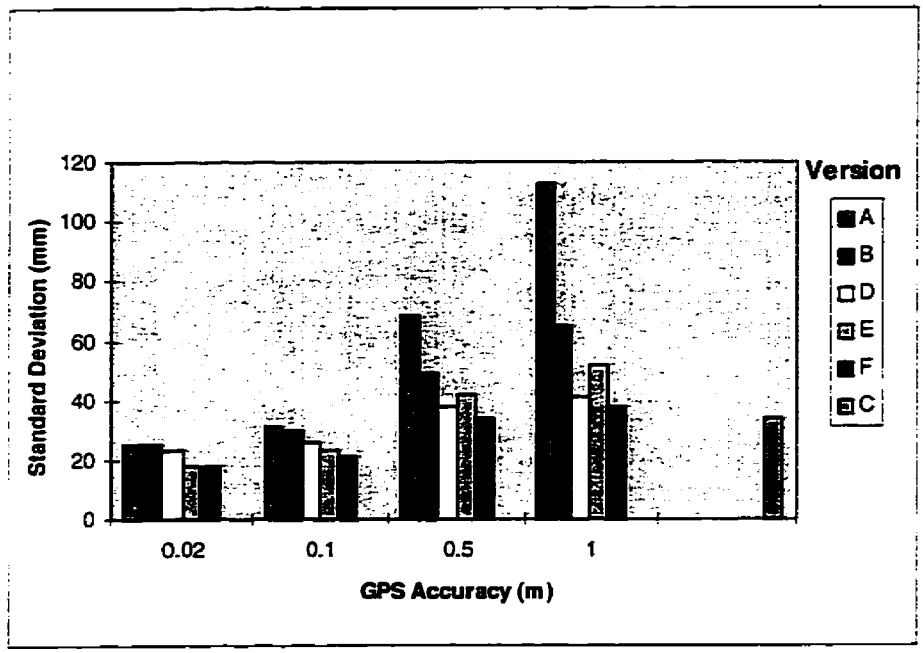

Figure 4. 6. Standard Deviations of Y Coordinate of Object Points

(Ground Control Accuracy = 0.020 m)

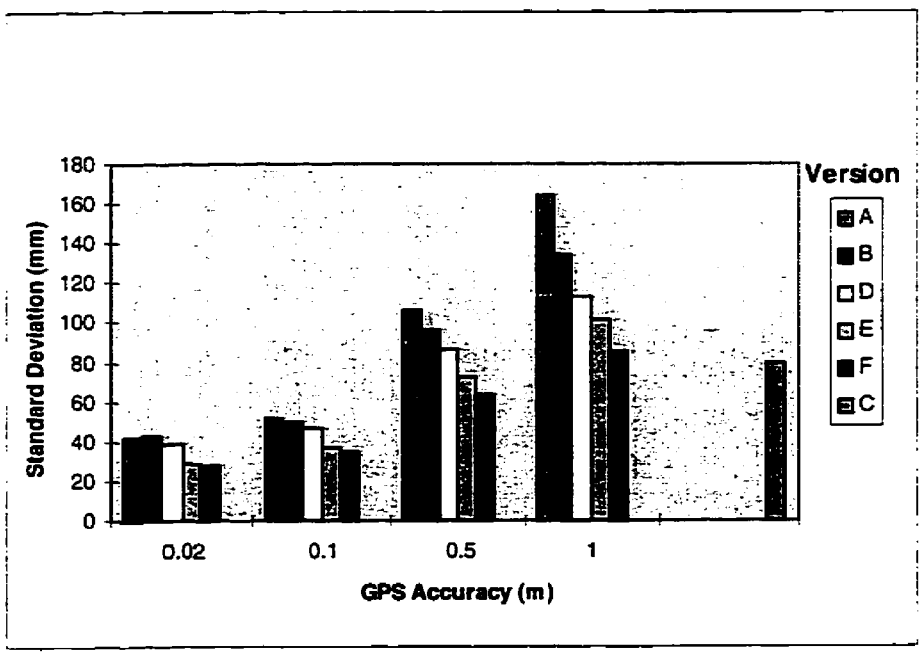

Figure 4. 7. Standard Deviations of Z Coordinate of Object Points

(Ground Control Accuracy = 0.020 m)

The following conclusions can be derived from examination of these figures:

* Based on Figures 4.2 - 4.4, if the accuracy of the camera exposure stations is better than 0.1 m, especially in height, then the adjusted coordinates are better than those obtained from conventional block adjustment (configuration C) regardless of whether the ground control points are used or not.

* The adjusted points are more precise than the GPS data with which the adjustment was performed (Figures 4.2 - 4.4). This implies that the precision of point determination can reach centimetre level, provided the camera station accuracy is at the decimetre level.

* Based on Figures 4.5 - 4.7, the standard deviations of the adjusted object points decrease as the accuracy of GPS-derived camera exposure stations deteriorates. The rate of deterioration is high for configurations A, B, and D, but increasing sidelap overcomes this problem (configurations E and F).

* The best results compared to those of conventional block adjustment were obtained from configuration F, which includes 4 pairs of control points at the corners of the block, 60% sidelap, and cross strips (Figures 4.2 - 4.4).

* The accuracy obtained from configuration A (no ground control) and configuration B (4 ground control) are practically the same when the GPS exposure stations have 0.02 m accuracy (Figures 4.2 - 4.4). It should be mentioned that there was no datum deficiency

for this simulated block. Therefore, it can be concluded that the GPS-photogrammetric block adjustments can be executed without ground control points, provided that the datum transformation is known. The planimetric transformation between WGS84 and the local coordinate system typically involves a straightforward procedure, but the height transformation requires knowledge of the geoid.

Figures 4.8 - 4.10 show the accuracy for the same block when ground control point accuracy is increased from 0.02 m to 0.1 m. As shown in these figures, there is a 9% average deterioration in accuracy, which implies, to some extent, the insensitivity of GPS controlled blocks to ground control points.

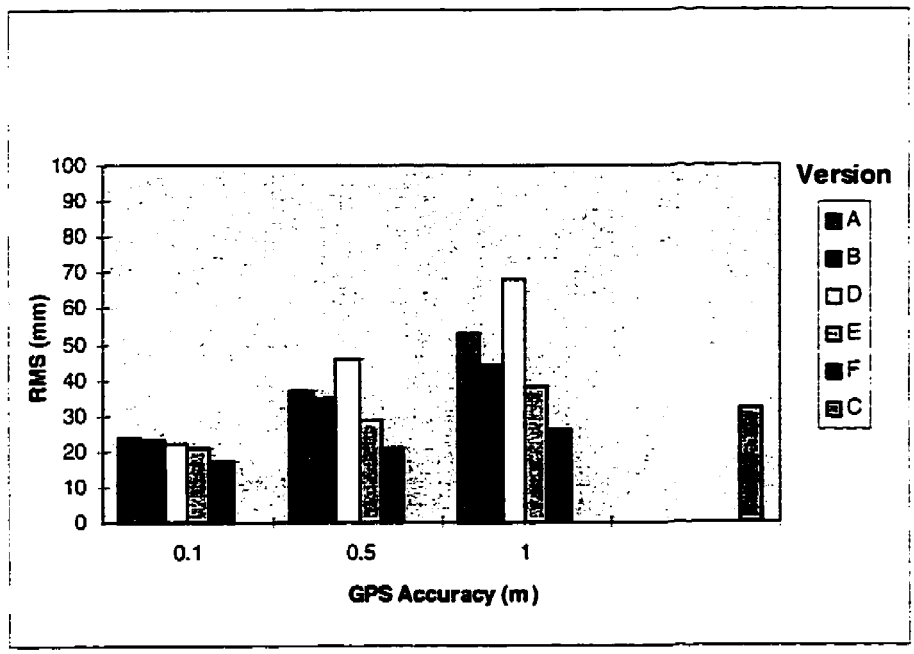

Figure 4.8. Accuracy of X Coordinate of Object Points

(Ground Control Accuracy = 0.1 m)

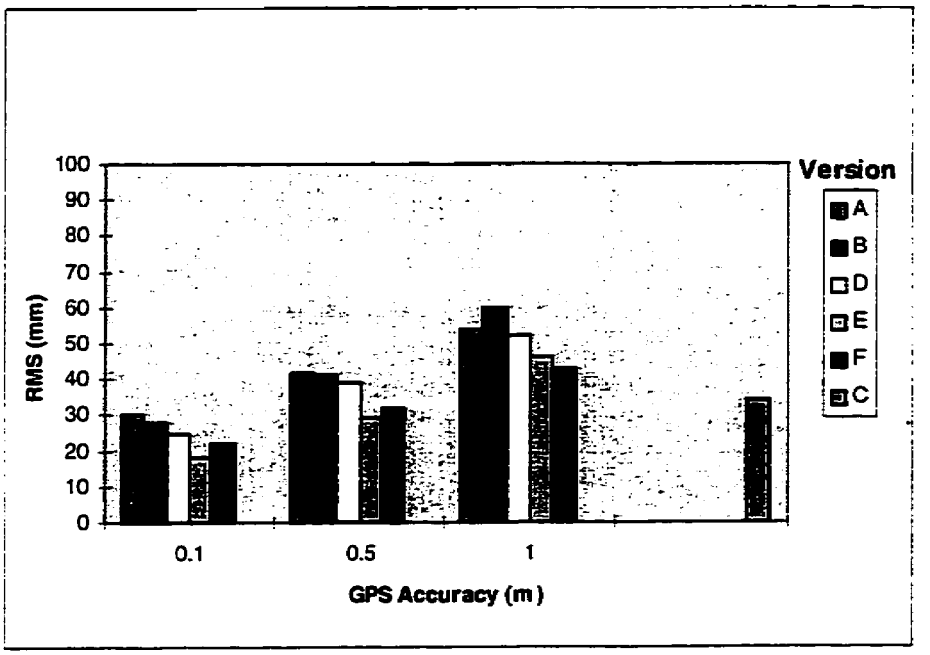

Figure 4.9. Accuracy of Y Coordinate of Object Points

(Ground Control Accuracy = 0.1 m)

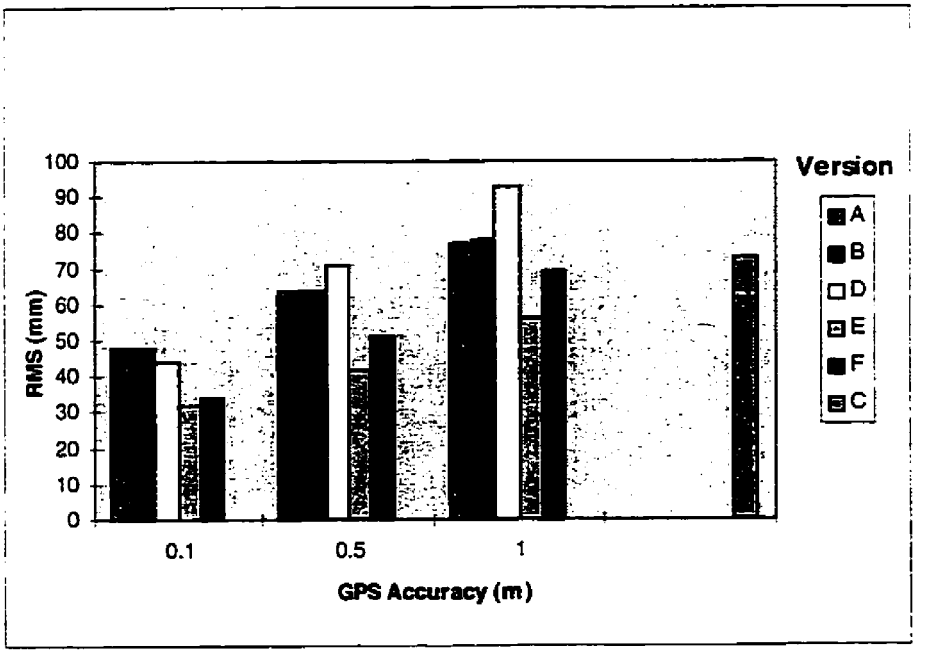

Figure 4.10. Accuracy of Z Coordinate of Object Points

(Ground Control Accuracy = 0.1 m)

The distribution of the theoretical precision of the object points obtained from inversion of the normal matrix for the upper right part (i.e., a subset of the total project area) of the block, and for various configurations, are shown in Figures 4.11 through 4.19. The following statements can be developed from these figures:

* For GPS-photogrammetric blocks, the theoretical precision is worse both at the corners and edges of the block (especially for blocks with no ground control, Figures 4.11 - 4.13). Therefore, the flight strategy of extra strips and photos is recommended.

* The theoretical precision of adjusted object points in the interior part of the GPS-photogrammetric block is quite homogenous both in planimetry (configuration A or F), and height (configuration F), but this is not true for conventional blocks (configuration C). Thus, there is no need for vertical control points within the GPS-controlled blocks. The theoretical precision of the Z coordinates of object points, obtained from configuration A, is not completely homogeneous, due to the fact that sidelap was 30% for this configuration.

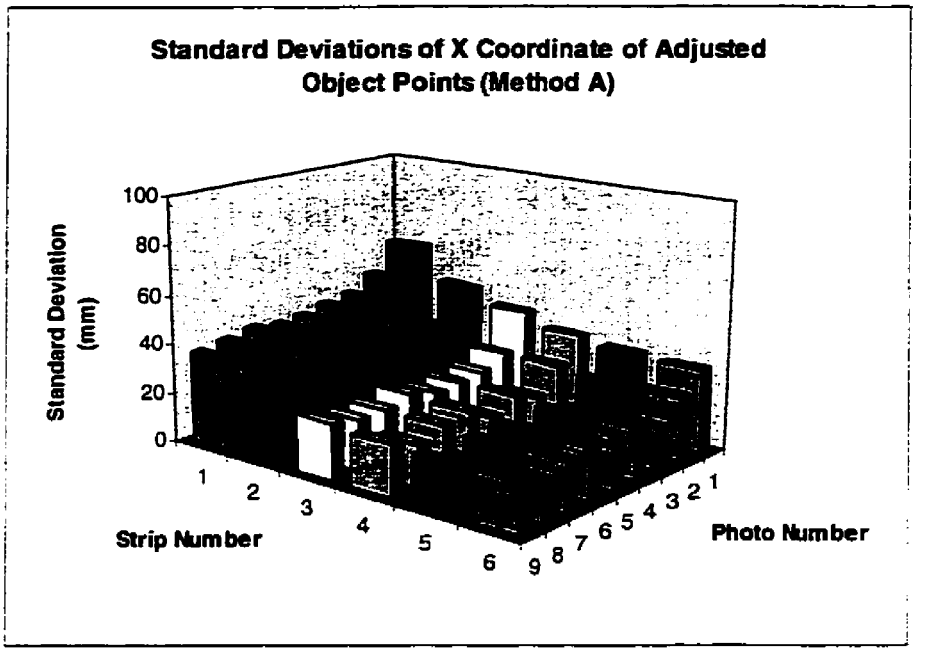

Figure 4. 11. Precision Distribution of X Coordinate of Object Points (Method A)

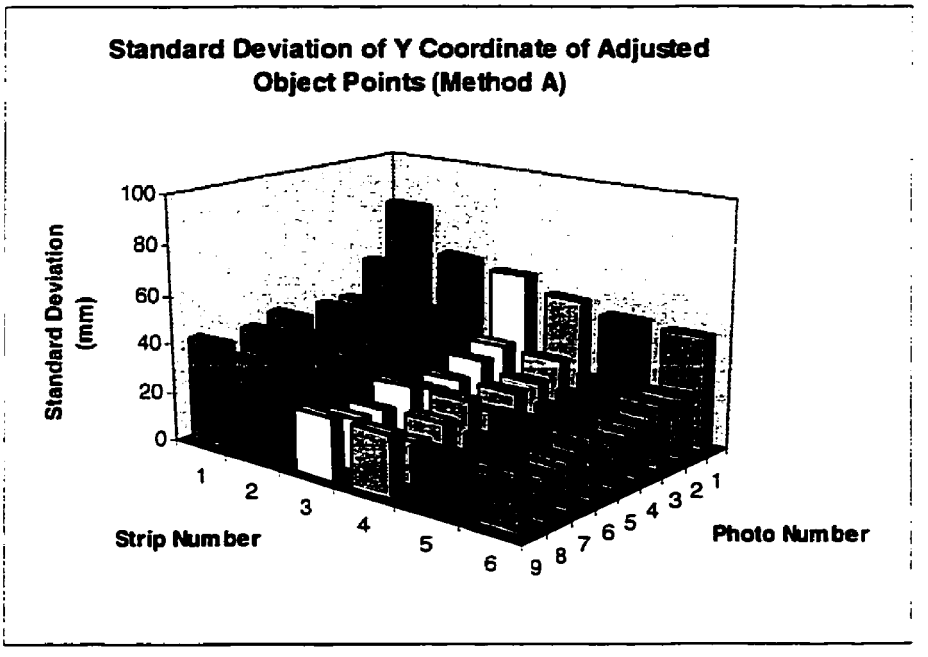

Figure 4. 12. Precision Distribution of Y Coordinate of Object Points (Method A)

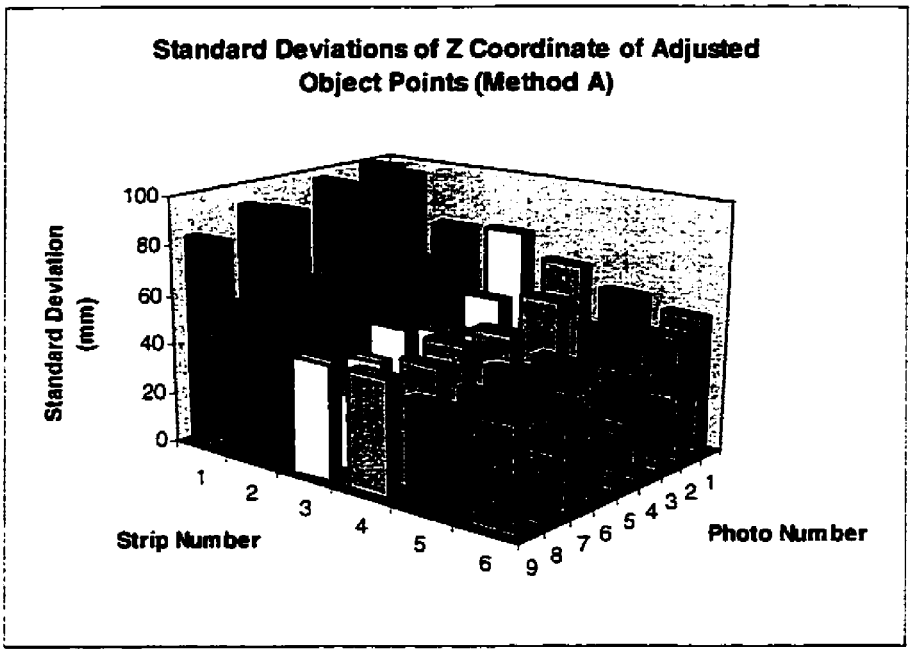

Figure 4. 13. Precision Distribution of Z Coordinate of Object Points (Method A)

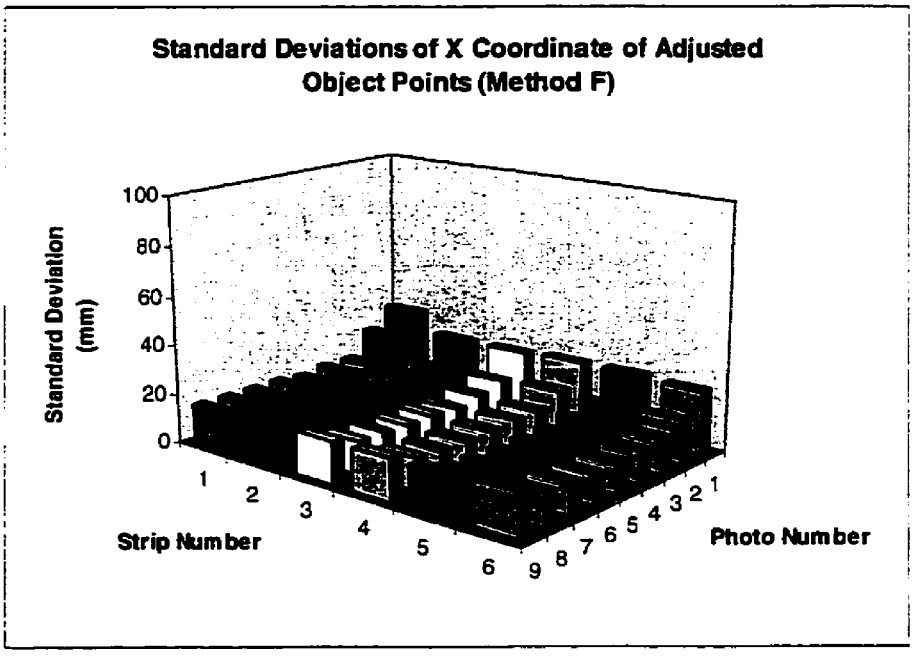

Figure 4. 14. Precision Distribution of X Coordinate of Object Points (Method F)

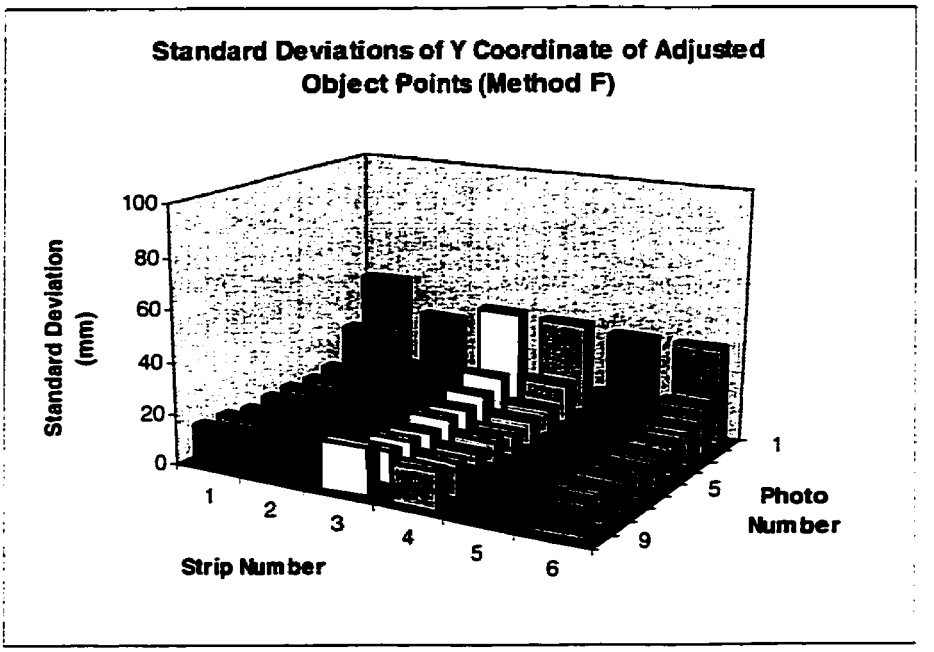

Figure 4. 15. Precision Distribution of Y Coordinate of Object Points (Method F)

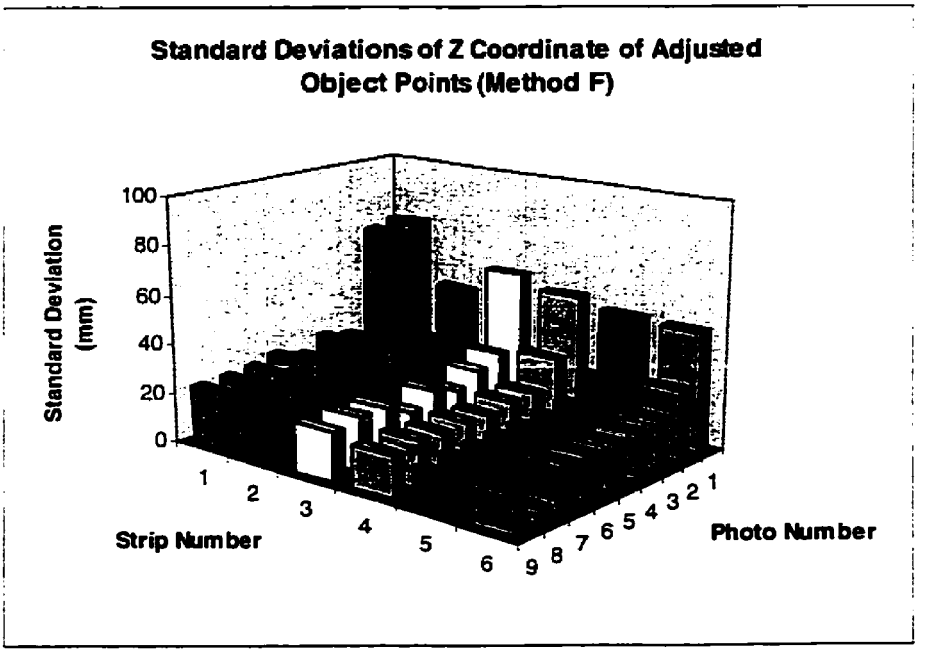

Figure 4. 16. Precision Distribution of Z Coordinate of Object Points (Method F)

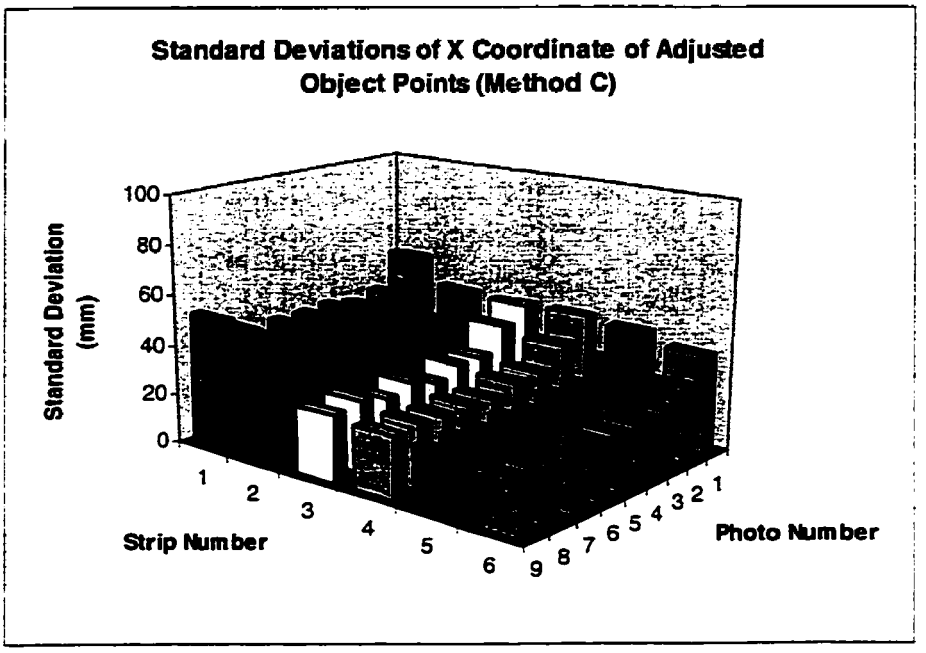

Figure 4. 17 Precision Distribution of X Coordinate of Object Points (Method C)

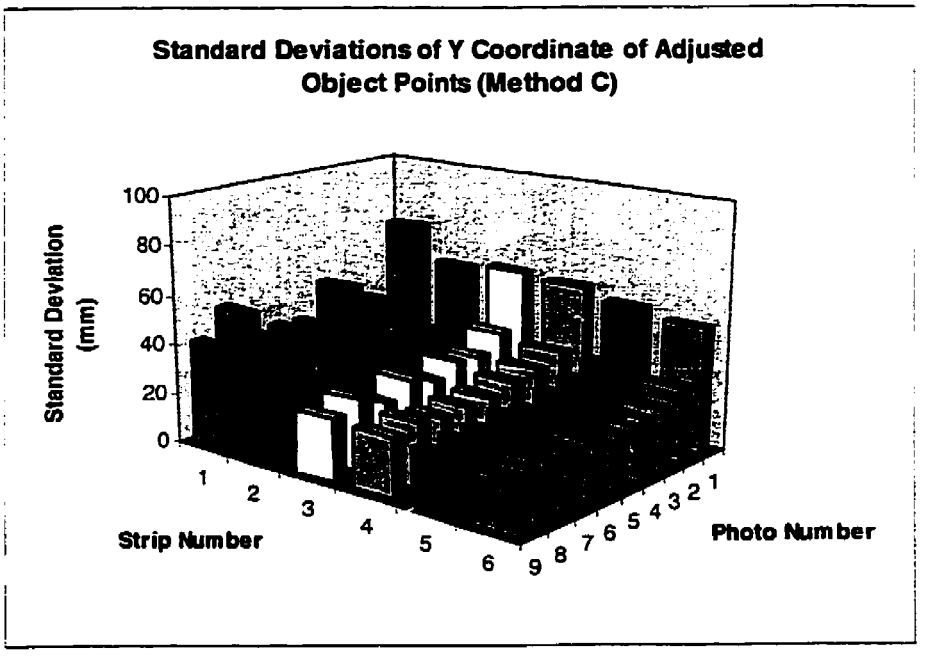

Figure 4. 18. Precision Distribution of Y Coordinate of Object Points (Method C)

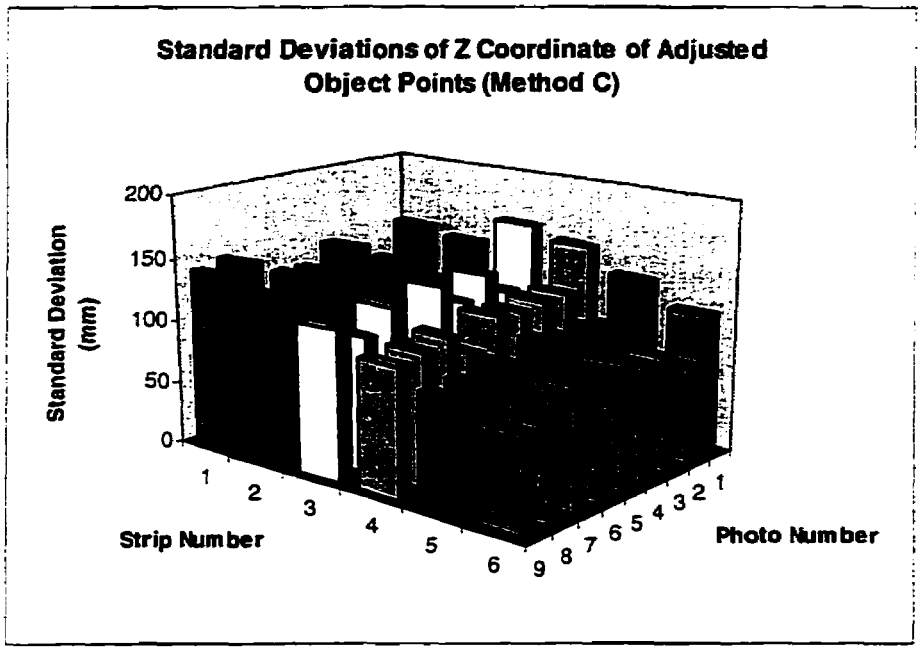

Figure 4. 19. Precision Distribution of Z Coordinate of Object Points (Method F)

4. 1. 3. The Reliability Analysis of Simulated GPS-Photogrammetric Block

Three measures of reliability; namely, redundancy numbers, internal reliability factors, and external reliability factors, were derived. Using a confidence level of 99%, and a power of 93%, the non-centrality parameter, δ_0, is equal to 4.0. Figures 4. 20 through 4. 27 show the global (i.e., average) redundancy numbers for image coordinates, GPS observations, and ground control points derived for various ground control configurations.

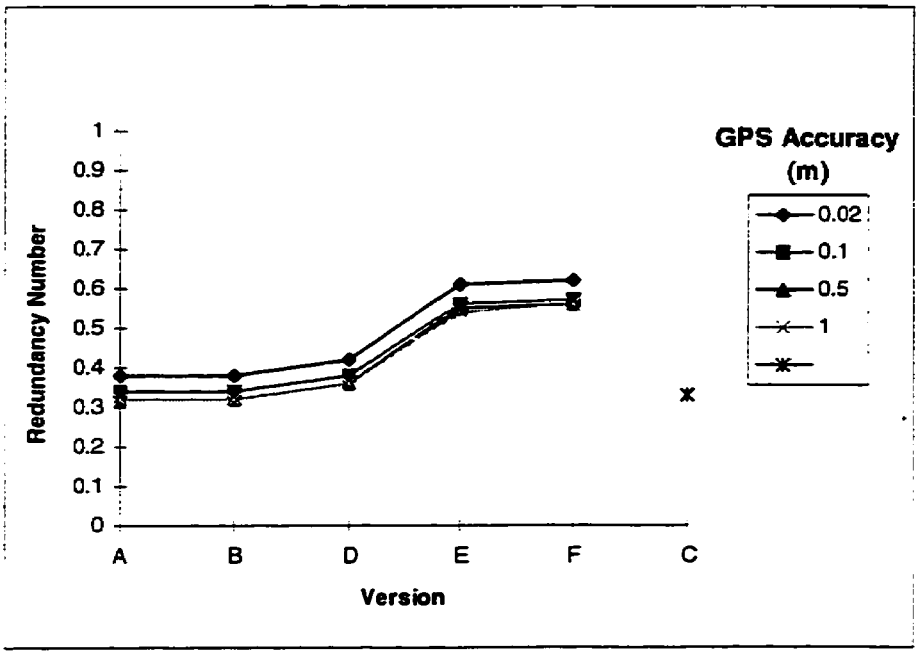

Figure 4. 20. Redundancy Numbers of x Coordinate of Image Points Obtained from Simulated Block

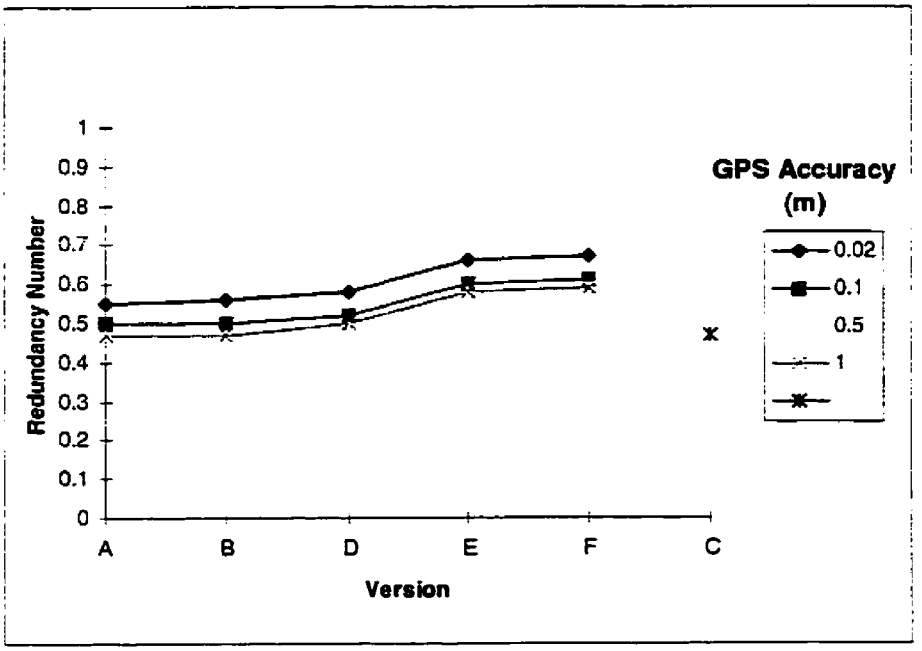

Figure 4. 21. Redundancy Numbers of y Coordinate of Image Points Obtained from Simulated Block

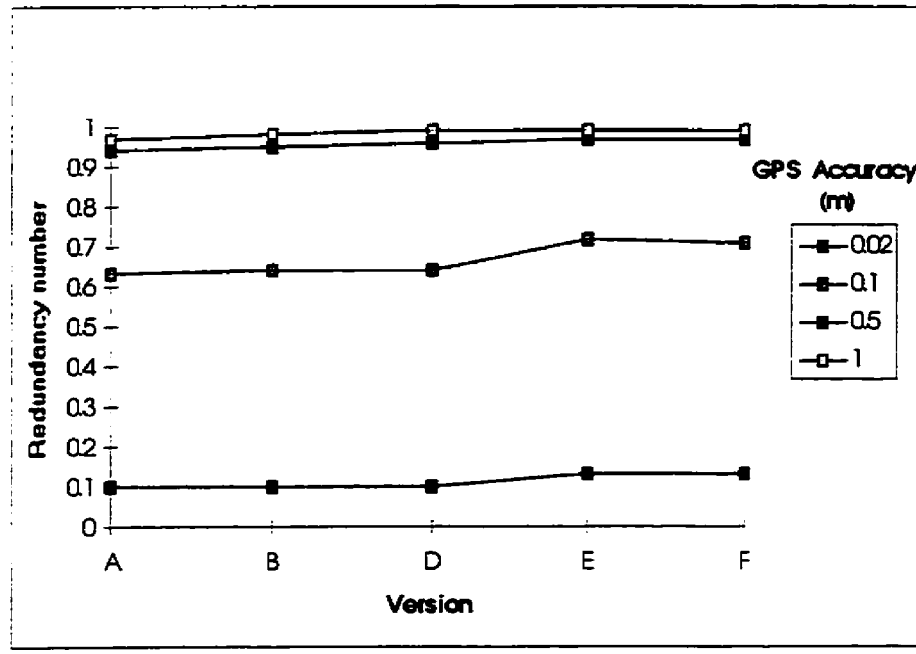

Figure 4. 22. Redundancy Numbers of X Coordinate of GPS Derived Exposure Stations Obtained from Simulated Block

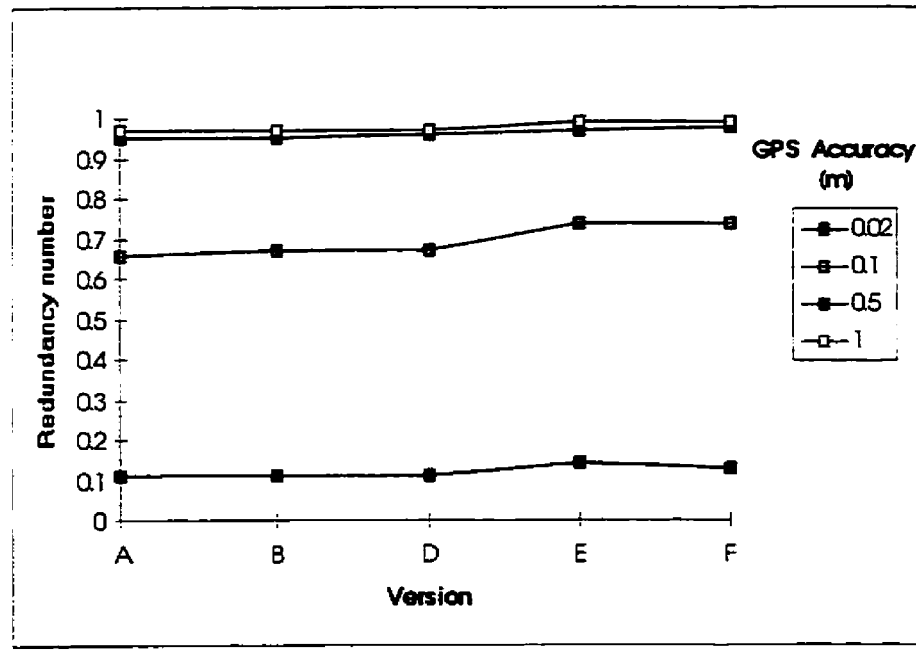

Figure 4. 23. Redundancy Numbers of Y Coordinate of GPS Derived Exposure Stations Obtained from Simulated Block

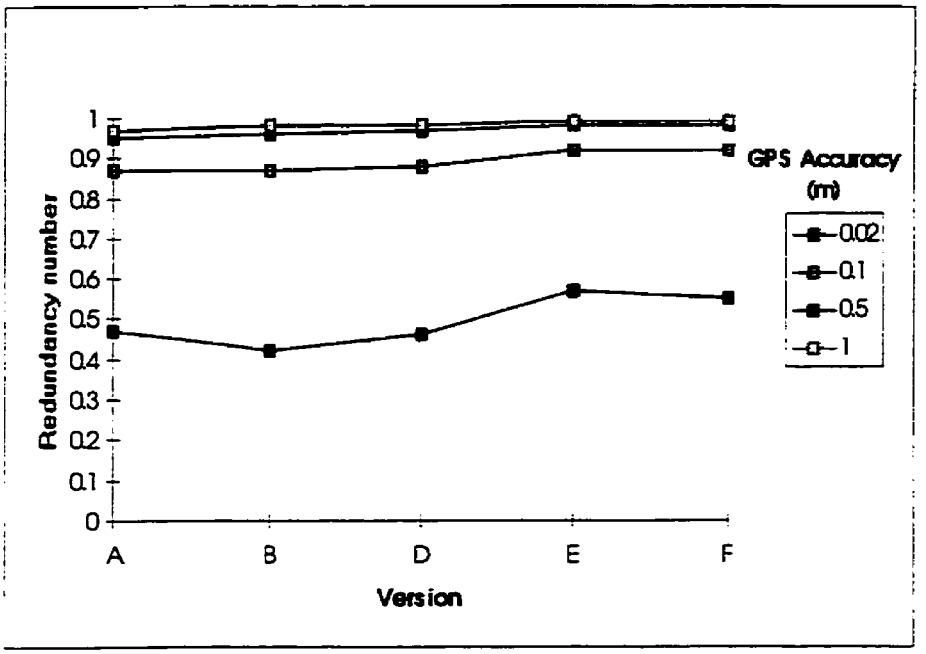

Figure 4. 24. Redundancy Numbers of Z Coordinate of GPS Derived Exposure Stations Obtained from Simulated Block

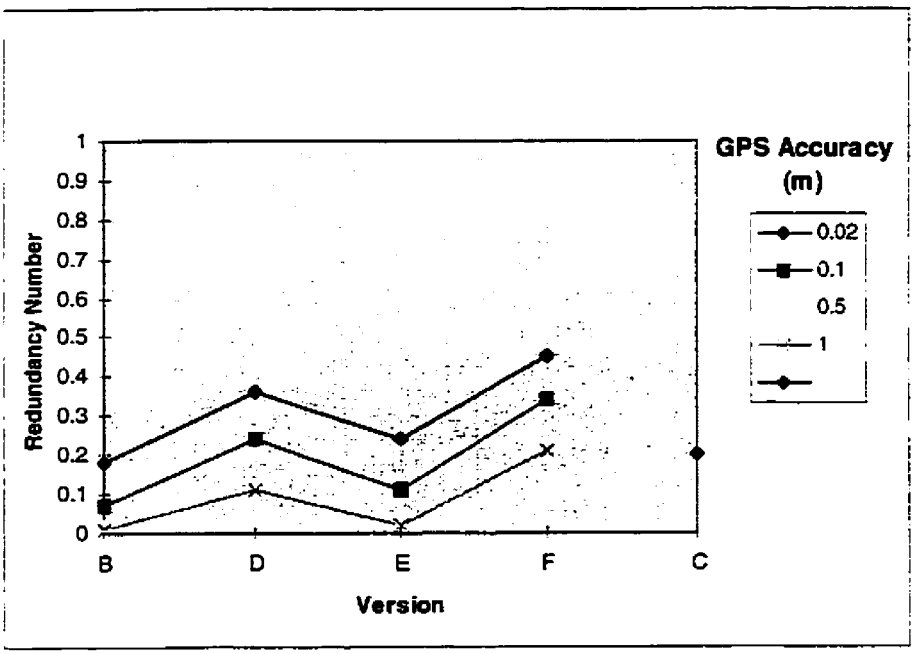

Figure 4. 25. Redundancy Numbers of X Coordinate of Ground Control Points Obtained from Simulated Block

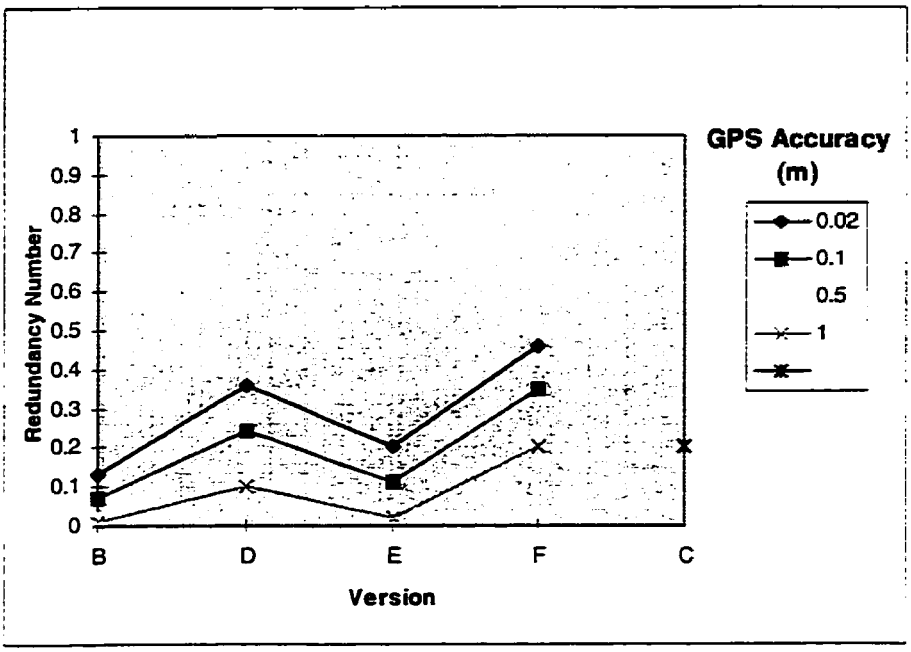

Figure 4. 26. Redundancy Numbers of Y Coordinate of Ground Control Points Obtained from Simulated Block

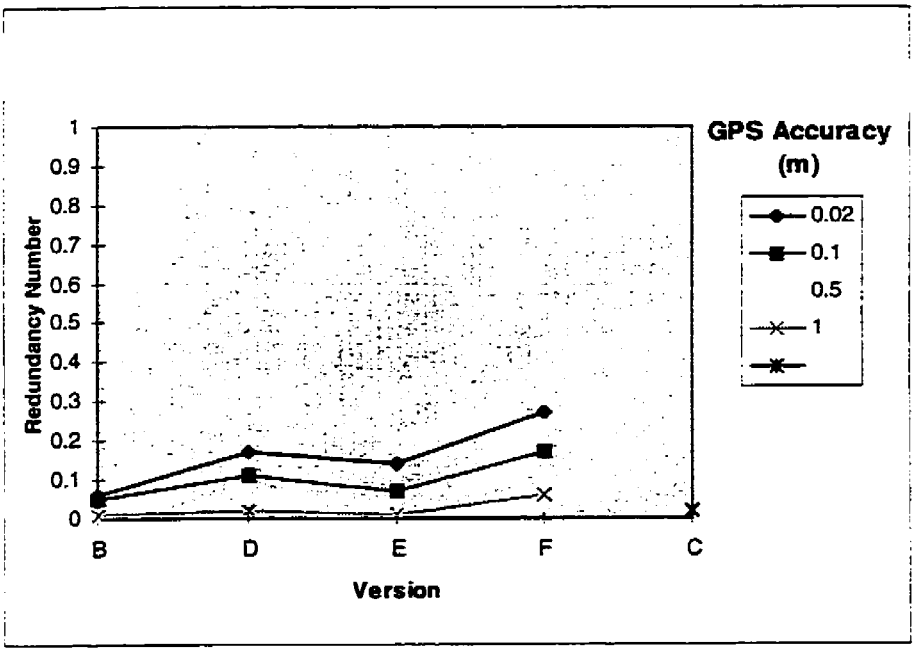

Figure 4. 27. Redundancy Numbers of Z Coordinate of Ground Control Points Obtained from Simulated Block

Based on these figures, the following statements can be made:

* In an aerial triangulation block incorporating GPS data, the reliability of image coordinates does not depend on ground control points at the corners of the block (Figures 4.20 and 4.21, results for configurations A and B). Therefore, from the reliability point of view, ground control points are not needed in a GPS assisted aerial triangulation.

* In a GPS assisted aerial triangulation, the average reliability of image points is not less than that in the conventional block adjustment (Figures 4.20 and 4.21). The reliability of image points increases by 13% with GPS data having 2 cm accuracy, compared to GPS data with 1 m accuracy.

* The more precise the GPS data, the smaller their local redundancy numbers become (Figures 4.22 - 4.24). For the two different GPS accuracies (0.1 m and 0.50 m), the redundancy numbers are 0.63 and 0.94, respectively. These values are "good" according to Table 2.2. But compared with the poor reliability of the control points (0.02-0.4) in the conventional block, the reliability of GPS data is at least 33% better, and more homogeneous over the entire block.

* It is well known that the reliability of ground control points in a conventional block adjustment is dependent on the location of the ground control points (Förstner, 1985). Therefore, the replacement of the ground control points with GPS data can alleviate the poor reliability of the control points as in a conventional block adjustment.

* Based on Figures 4.20 and 4.21, in a GPS-photogrammetric block 60% sidelap (configurations E and F) improves the redundancy numbers by 30%.

The effect of an undetected blunder in the observations on unknown parameters can be measured by external reliability. Figures 4. 28 through 4. 35 show the external reliability factors (ERF) for various groups of observations.

Blunders in GPS data, that can not be detected statistically, do not significantly affect the adjusted object points. The external reliability of GPS data is almost better than that of the ground control points located at the edges of the conventional block. The external reliability factors of image coordinates obtained from all ground control configurations are almost equal, or better than, those obtained from conventional block adjustment (Figures 4. 28 and 4. 29). The best results were achieved from configurations E and F, where 60% sidelap and cross strips have been included. If GPS provides accuracies ranging from 0.1 m to 0.5 m, then the external reliability factors of GPS data are between 1 and 3, producing reliable results (Figures 4. 30, 4. 31, and 4. 32).

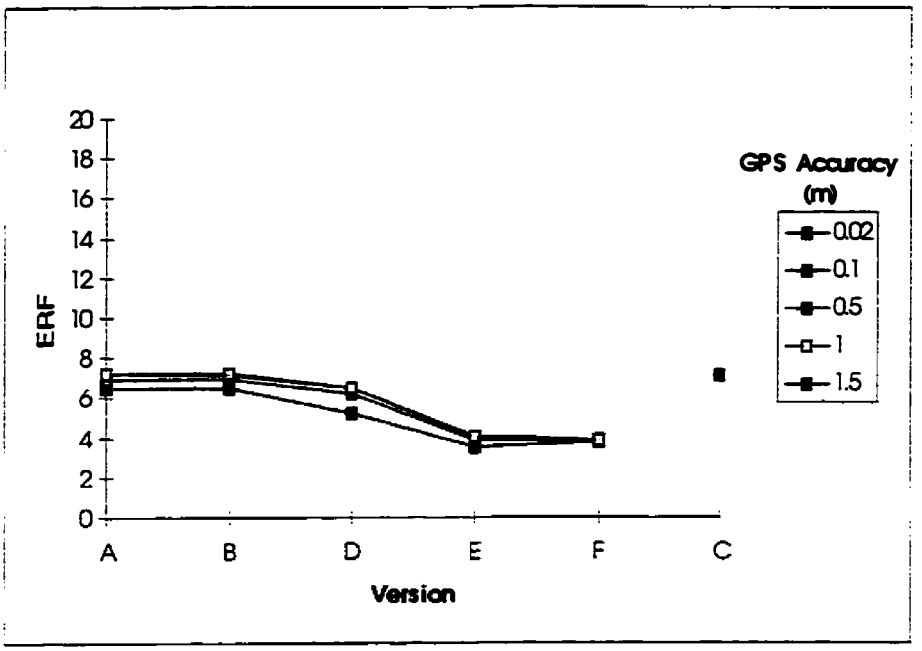

Figure 4. 28. External Reliability Analysis of x Coordinate of Image Points Obtained from simulated block

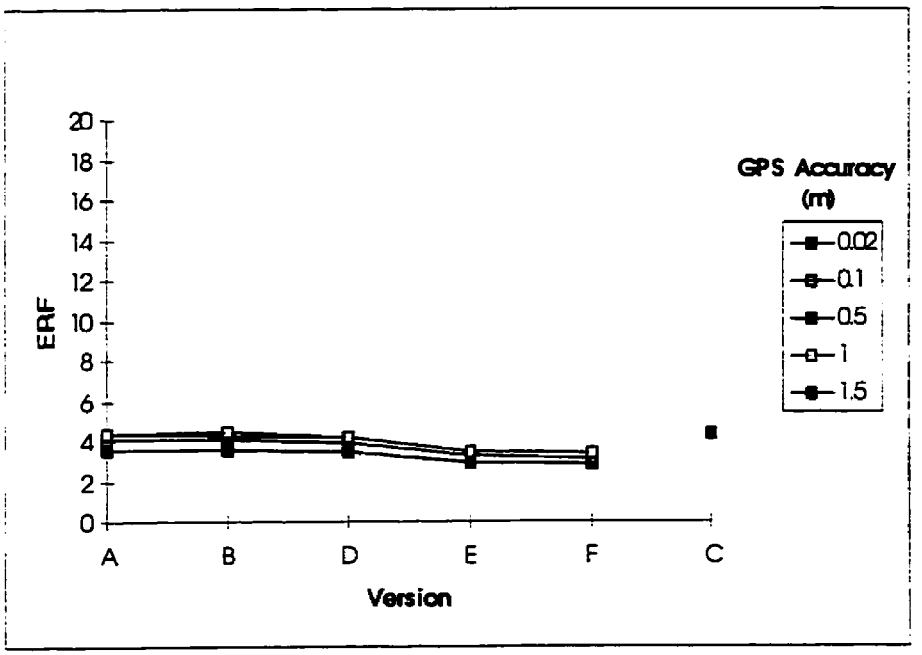

Figure 4. 29. External Reliability Analysis of y Coordinate of Image Points Obtained from Simulated Block

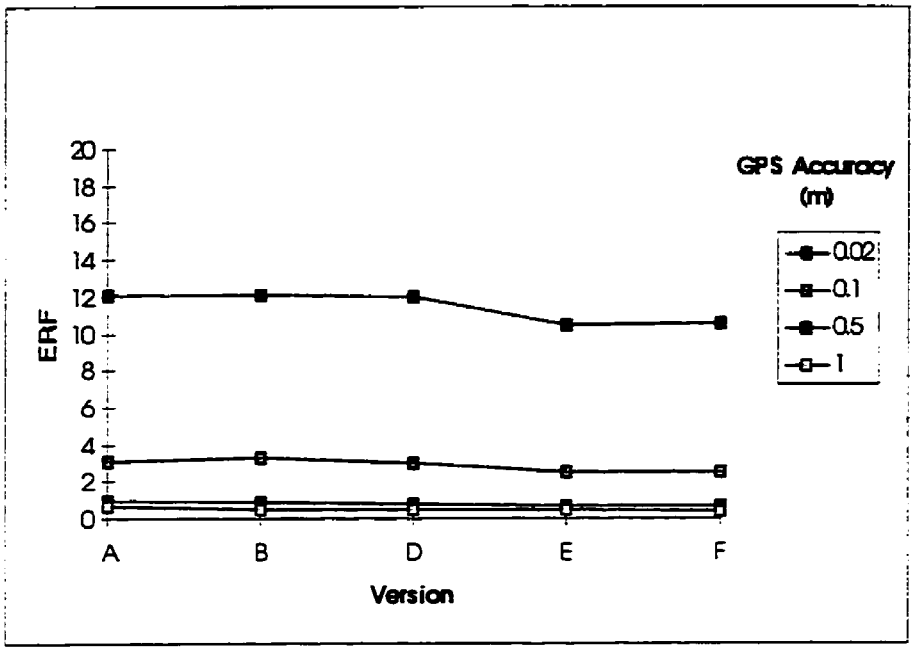

Figure 4. 30. External Reliability Analysis of X Coordinate of GPS Derived Exposure Stations Obtained from Simulated Block

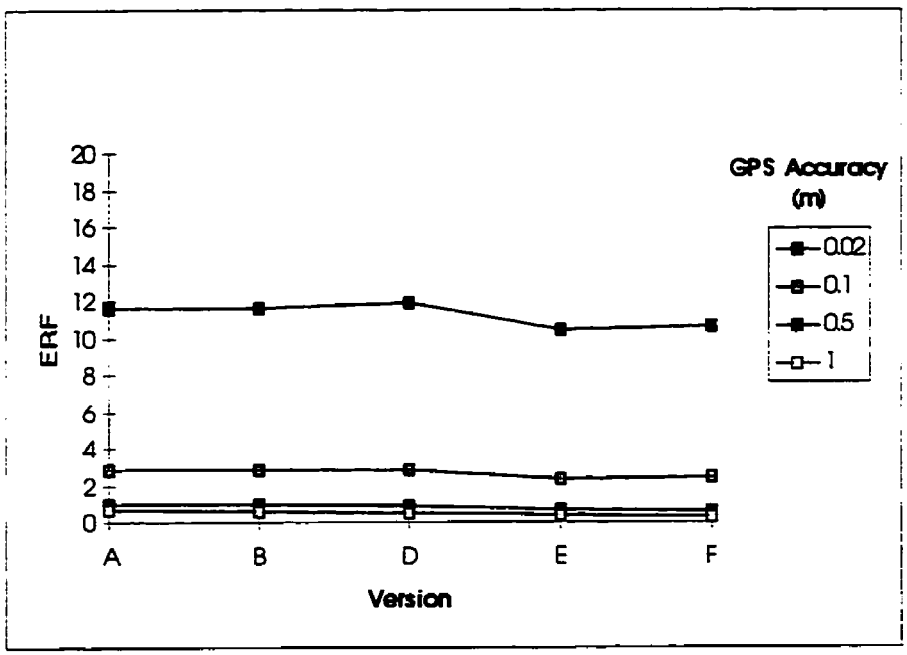

Figure 4. 31. External Reliability Analysis of Y Coordinate of GPS Derived Exposure Stations Obtained from Simulated Block

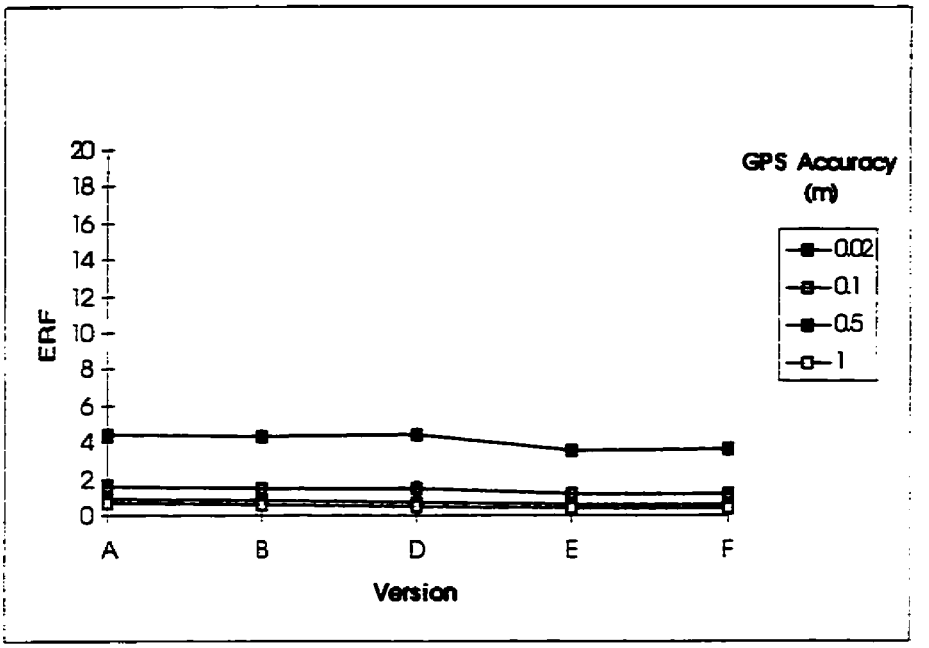

Figure 4. 32. External Reliability Analysis of Z Coordinate of GPS Derived Exposure Stations Obtained from Simulated Block

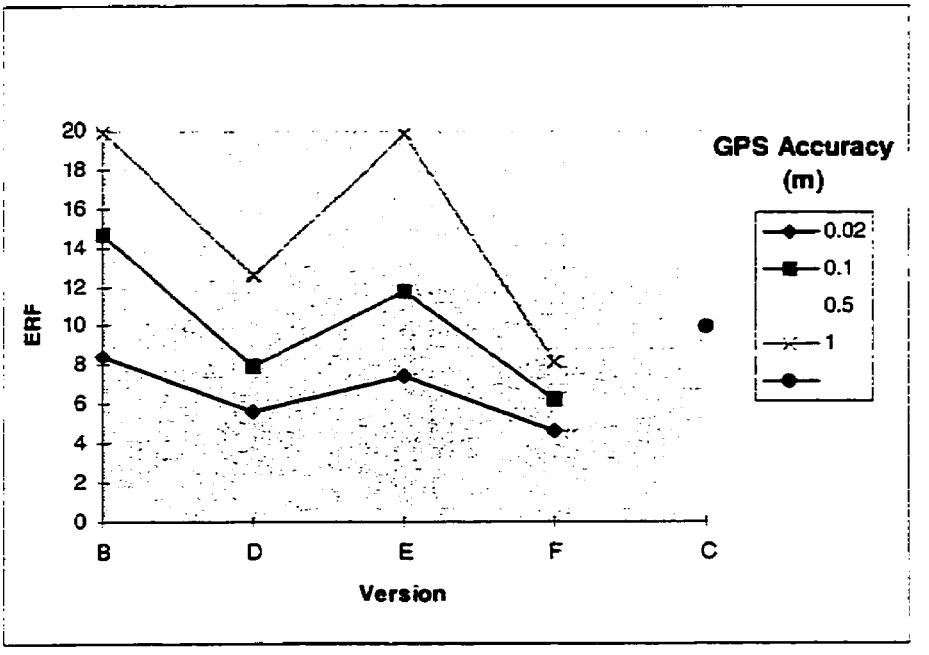

Figure 4. 33. External Reliability Analysis of X Coordinate of Ground Control Points Obtained from Simulated Block

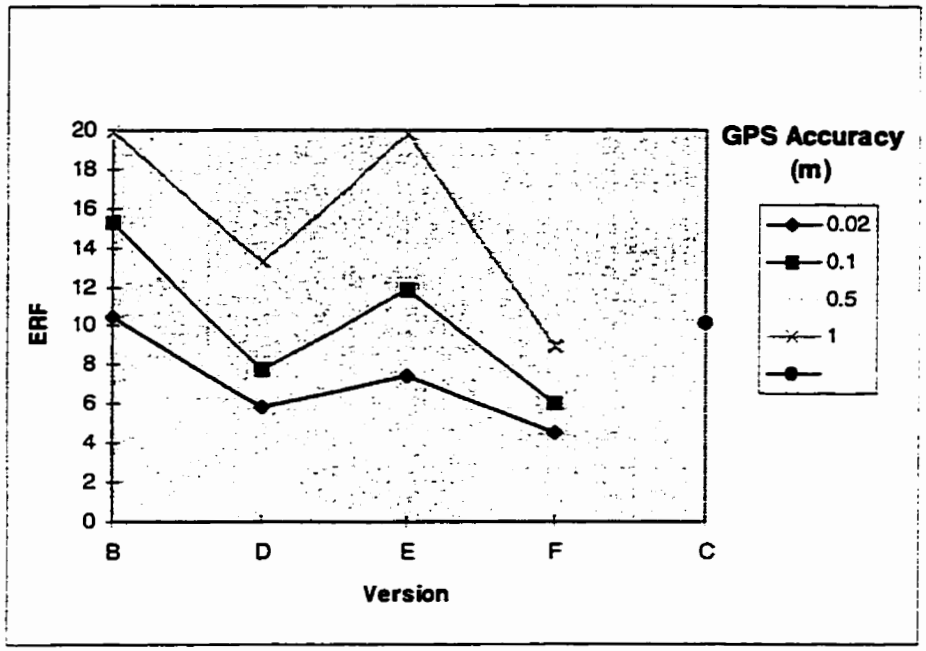

Figure 4. 34. External Reliability Analysis of Y Coordinate of Ground Control Points Obtained from Simulated Block

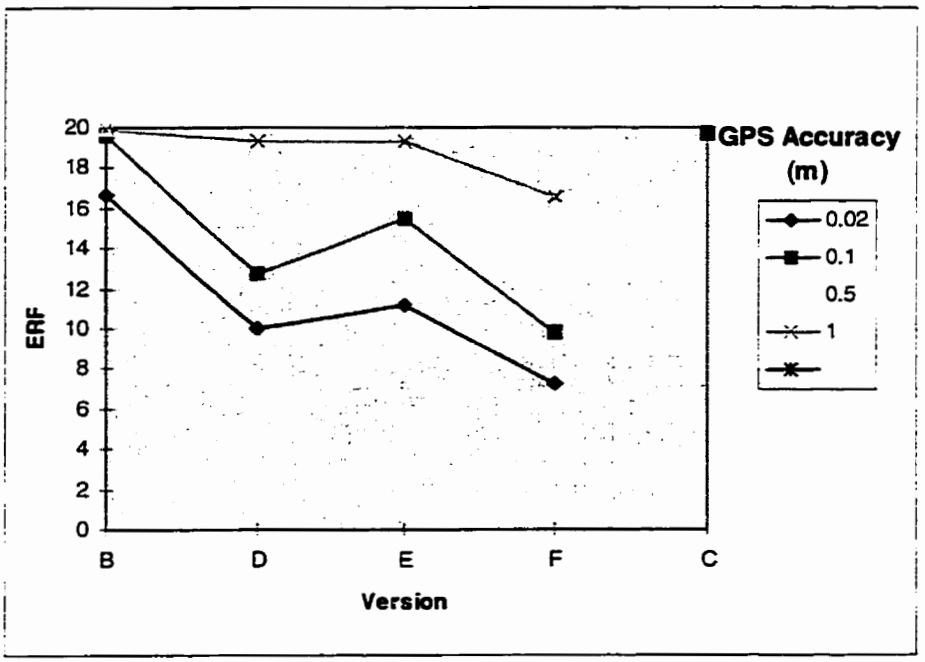

Figure 4. 35. External Reliability Analysis of Z Coordinate of Ground Control Points Obtained from Simulated Block

The external reliability factors of the image coordinates obtained from configurations A and B are the same, implying that the ground control points do not have a significant effect on this factor. In all previous figures for reliability analysis, global (average) values of various reliability measures were shown. Now, local redundancy and reliability factors of image points are considered. For this purpose, the local redundancy numbers and reliability factors of image coordinates for configurations A and C are shown in Figures 4. 36 and 4. 37.

Comparing Figures 4. 36 and 4. 37 shows that the local redundancy numbers and reliability factors obtained from GPS-photogrammetric block adjustment are 25% better than those achieved from the conventional block adjustment. This means that even if these measures of reliability are examined locally, the GPS assisted aerial triangulation provides more reliable results.

Configuration A

Corner of the block

	x	y	x	y
r_i	0.35	0.33	0.11	0.43
$\bar{\delta}_{0,i}$	5.45	5.72	11.22	4.62
r_i	0.37	0.43	0.14	0.56
$\bar{\delta}_{0,i}$	5.23	4.58	9.85	3.58
r_i	0.38	0.34	0.35	0.50
$\bar{\delta}_{0,i}$	5.11	5.57	5.52	3.98

Centre of the block

	x	y	x	y	x	y
r_i	0.67	0.57	0.68	0.58	0.67	0.57
$\bar{\delta}_{0,i}$	2.83	3.48	2.77	3.42	2.62	3.48
r_i	0.59	0.60	0.60	0.61	0.67	0.60
$\bar{\delta}_{0,i}$	3.30	3.23	3.28	3.20	3.31	3.20
r_i	0.67	0.57	0.68	0.58	0.67	0.57
$\bar{\delta}_{0,i}$	2.83	3.48	2.77	3.42	2.82	3.48

Figure 4. 36. Local Redundancy Numbers and Reliability Factors of Image Points

Configuration C

Corner of the block

	x	y	x	y
r_i	0.11	0.17	0.10	0.16
$\bar{\delta}_{0,i}$	11.78	8.96	12.05	9.23
r_i	0.12	0.37	0.14	0.51
$\bar{\delta}_{0,i}$	11.01	5.17	9.98	3.95
r_i	0.25	0.18	0.27	0.32
$\bar{\delta}_{0,i}$	6.91	8.47	6.61	3.95

Centre of the block

	x	y	x	y	x	y
r_i	0.56	0.44	0.58	0.44	0.57	0.44
$\bar{\delta}_{0,i}$	3.54	4.55	3.40	4.46	3.47	4.54
r_i	0.57	0.55	0.57	0.58	0.56	0.54
$\bar{\delta}_{0,i}$	3.50	3.60	3.44	3.39	3.54	4.69
r_i	0.56	0.44	0.58	0.44	0.57	0.44
$\bar{\delta}_{0,i}$	3.54	4.55	3.40	4.47	3.49	4.52

Figure 4. 37. Local Redundancy Numbers and Reliability Factors of Image Points

4. 2. Jackson Project (Medium Scale Mapping)

This project was designed to support planimetric mapping at the scale of "1:10,000". The project area is located in and around the city of Jackson, Tennessee, U.S.A., (Figure 4.38.), and was photographed using a film-based camera. Aerial triangulation was required to achieve ±0.75 m horizontal accuracy for the facility and land-based elements on the derived orthophotos and to support the generation of 5 m contours within the area covered by photography. The project parameters are given in Table 4. 2.

Table 4. 2. Project Parameters

Region: Jackson Utility Division, TN
Purpose: Planimetric Mapping at 1:10,000
Size of Project Area: 40 km by 20 km
Terrain Elevation Difference: 150 m
Photo Scale: 1:24,000
Number of Strips: (7 + 2 Cross Strips)
Number of Photos: 179
Number of Ground Control Points: 20 (Full)
Forward Overlap: 60%
Side Overlap: 30%

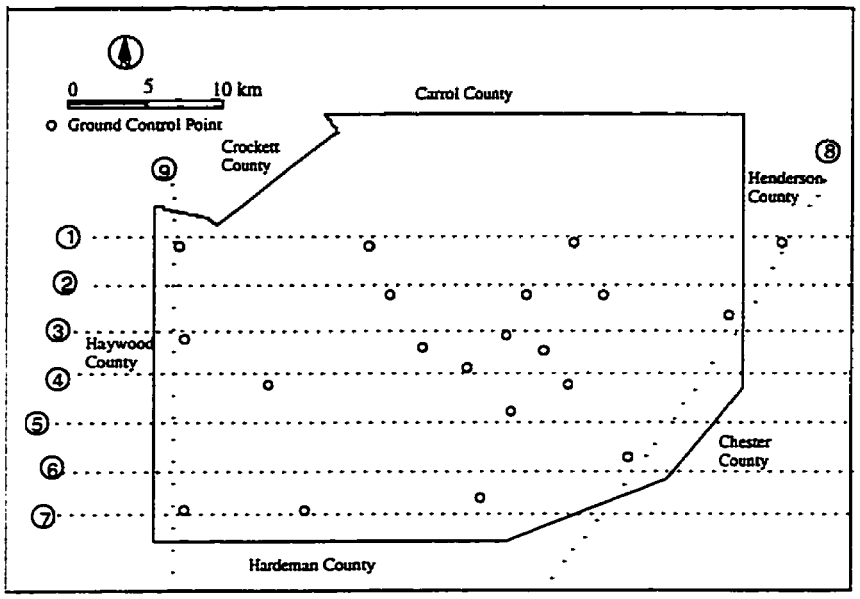

Figure 4. 38. The Study Area (from Greening et al., 1994)

4. 2. GPS Data Collection and Processing

GPS data were collected at a rate of 1 Hz using Trimble Navigation, Ltd. 4000 SSE dual frequency receivers. Two receivers were used; one as master station located approximately in the centre of the block, and the other one as remote station onboard the aircraft. Various methods were used to process these data due to the receiver capability of receiving both L1 and L2 carriers. Double difference GPS processing techniques were applied in all methods, in order to eliminate or reduce the effects of some of the GPS errors (e.g., timing errors and atmospheric errors). Static data were collected prior to take-off and after landing for ambiguity resolution, which also made possible the processing of data in reverse mode. The coordinates of the antenna phase centre at each epoch were determined using Kalman filtering techniques, and "On The Fly" ambiguity resolution

techniques, whenever needed. The initial cycle ambiguities were determined using the fixed baseline technique, and the data were then processed in a continuous kinematic mode. The GPS data set was continuous throughout the flight mission, except for one loss of lock at the beginning of the mission (while in static mode). The re-initialization was performed after flight mission to verify the correct determination of the ambiguities, and provide an independent check on the GPS data processing.

Twenty ground control points were established during an independent survey using conventional DGPS static and rapid static processing techniques. The accuracy of these points is within the range 10 mm + 10 ppm. Orthometric elevations were computed from the GPS-derived ellipsoidal heights by means of geoid undulations.

4. 3. Kinematic GPS Processing of Jackson Data Set

The Jackson data set was processed using GRAFNAV. Information about this program is given in Appendix C. The data were processed using various methods, due to the availability of both L1 and L2 carrier frequencies. These methods are described in the following sections. Indicator of the satellite geometry, PDOP (Positional Dilution of Precision) is shown in Figure 4. 39. As illustrated, for most of the time, the PDOP is less than 3, which is an acceptable value for airborne-GPS applications. Six to eight satellites were tracked for the entire mission. The master station was established in the centre of the photogrammetric block to minimize the distance between master and remote stations

which did not exceed 30 km. In all methods of processing, the GPS data rate was 1 Hz. The options used for each method are shown in Table 4. 3.

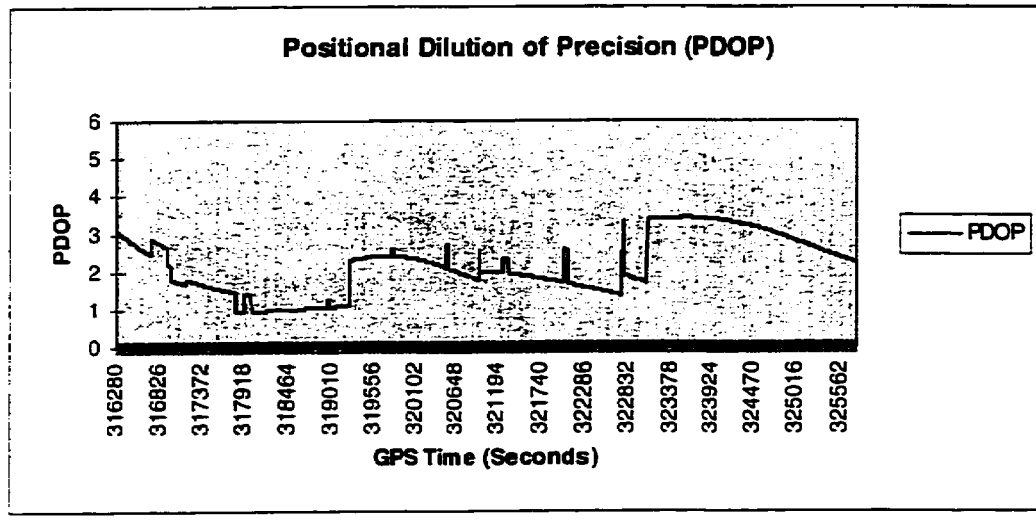

Figure 4. 39. PDOP for Jackson Data Set

Table 4. 3. Processing Methods of Jackson Data Set

	Dual Frequency	Single Frequency	OTF	Solution	Processing Mode
Method 1	Yes	No	Yes	Float	Forward
Method 2	No	Yes	Yes	Float	Forward
Method 3	Yes	No	Yes	Float	Reverse

According to the standards for medium scale mapping, the required accuracy for camera exposure stations is less than 1 m. The distance between the master and the

remote stations (baseline) was also less than 30 km. Therefore, in all GPS processing methods, the float solution was chosen. "On The Fly" ambiguity resolution option was activated to take care of loss of lock in the case of less than 4 satellites. Forward and backward processing procedures were used. Both dual and single frequencies were used to compare the results, and determine accuracy degradation due to the lack of L2 carrier phase. Relative ionospheric correction did not improve the results, thus, this option was turned off.

RMS values for L1 carrier phase data obtained from the three methods are shown in Figure 4. 40 - 4. 42. There are just 4 spikes of 6 cm in all cases, which are assumed to be caused mainly by multipath. RMS values are about 2 cm for all methods. There is a slight degradation in RMS when single frequency was used (Method 2). Comparison between Figures 4.40 and 4.42 show that the forward and reverse trajectories are compatible. One of the advantages of using dual frequency processing techniques is that it helps to resolve ambiguity values quicker, because of widelane carrier phase processing techniques. The mean of RMS values for these three methods are 16.4, 17.1, and 16.9 mm, and the standard deviations are 12.0, 13.5, and 12.5 mm, respectively. Method 1 provides better results by comparing these values. Although there is 1 mm degradation in the mean, and 2 mm in standard deviation, when single frequency is used, it is still an acceptable accuracy for medium scale mapping.

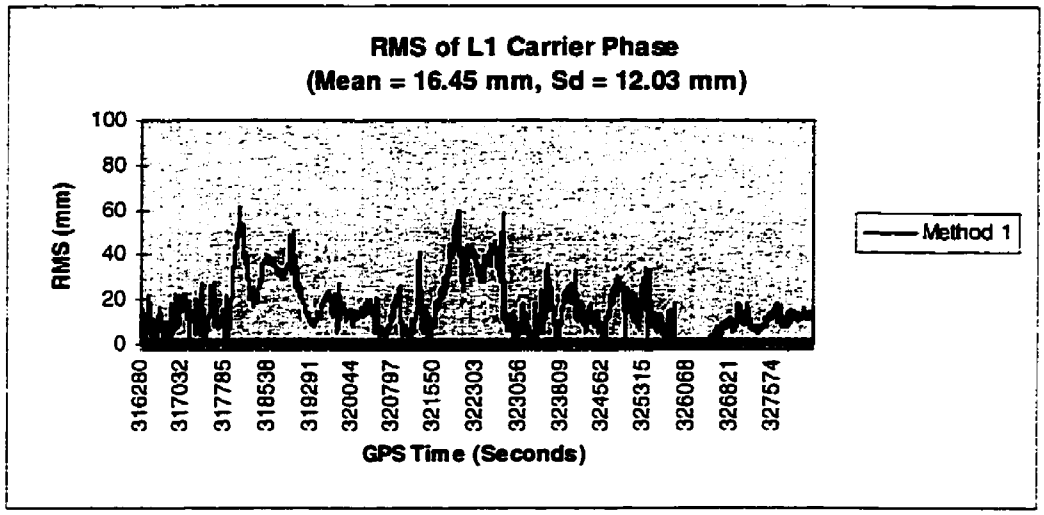

Figure 4. 40. RMS of L1 Carrier Phase Obtained from Method 1

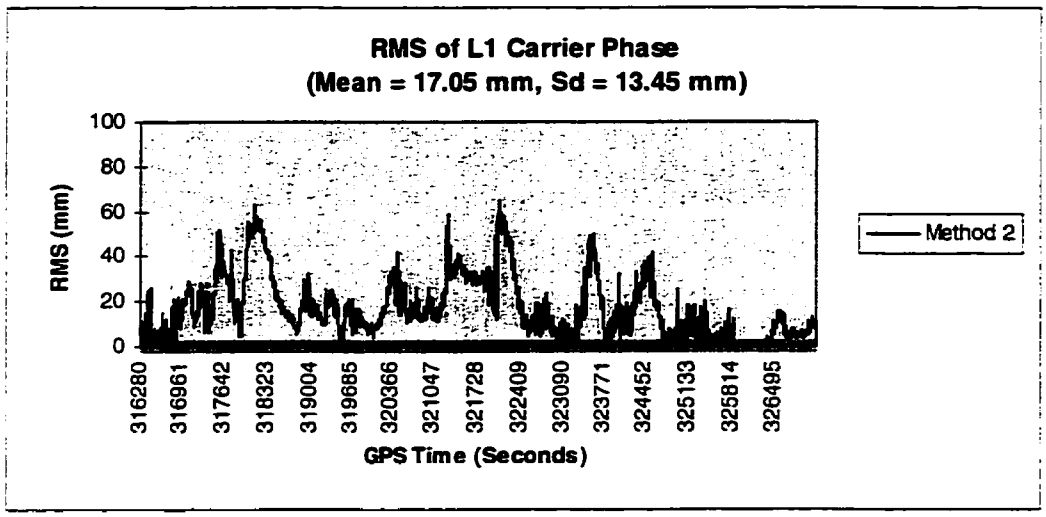

Figure 4. 41. RMS of L1 Carrier Phase Obtained from Method 2

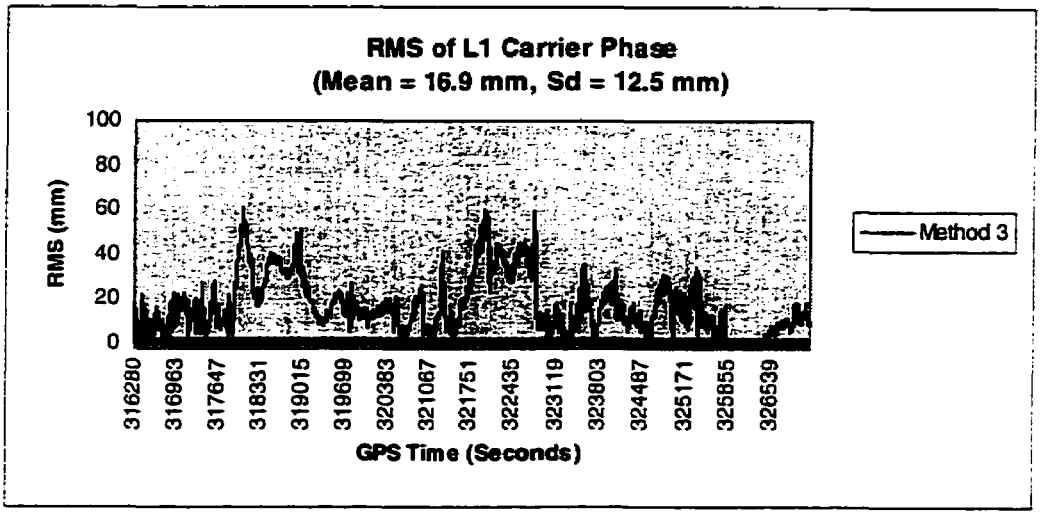

Figure 4. 42. RMS of L1 Carrier Phase Obtained from Method 3

GRAFNAV also generates a quality number, ranging from 1 to 6, which is a function of the geometry of the satellites, and RMS of the L1 carrier phase (1 is best and 6 is worst). The quality numbers for the three processing methods are shown in Figures 4. 43 - 4. 45. The quality number is 1 for almost the entire flight mission when using both L1 and L2 carrier frequencies. It was degraded a little when single frequency was chosen to process the data (Method 2). This number for Method 3 (reverse processing mode) is the same as that of Method 1.

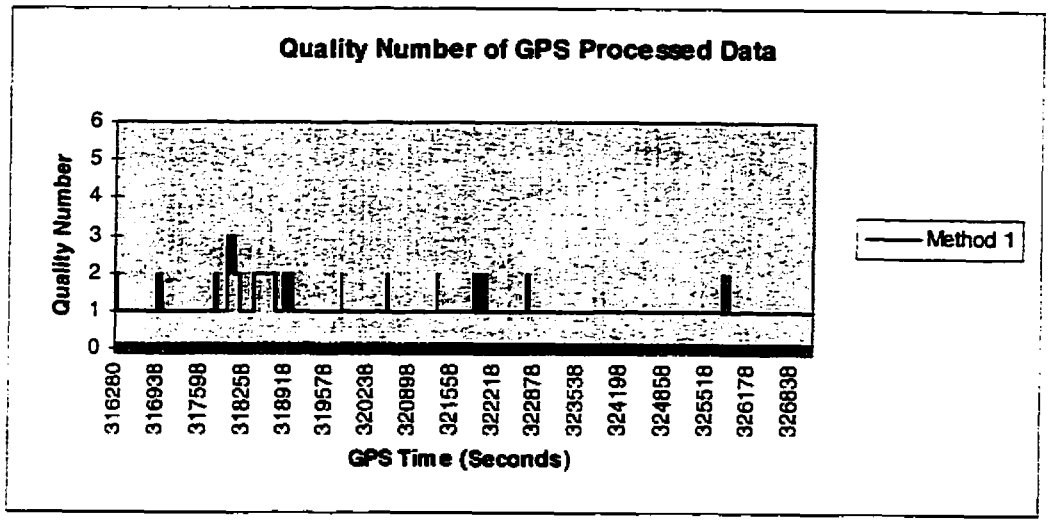

Figure 4. 43. Quality Number Obtained from Method 1

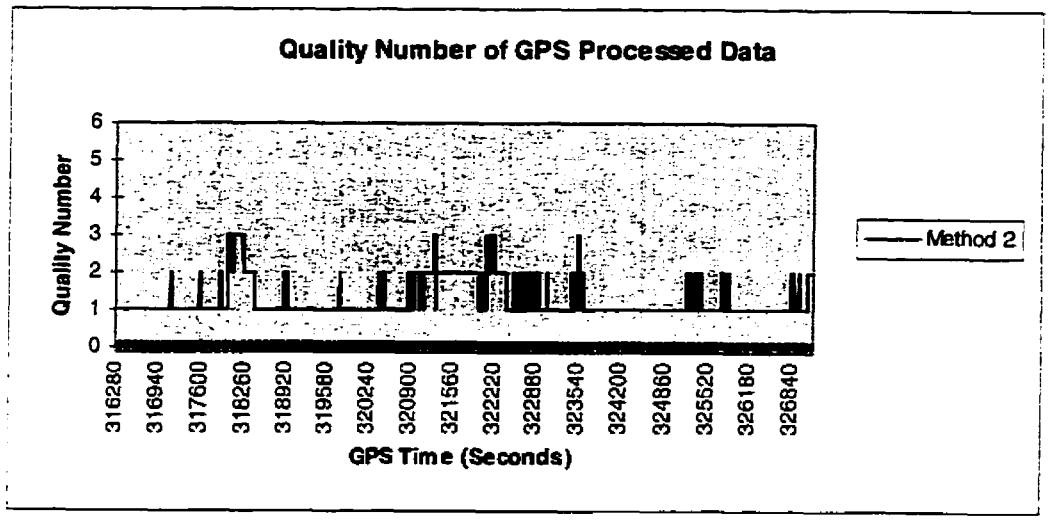

Figure 4. 44. Quality Number Obtained from Method 2

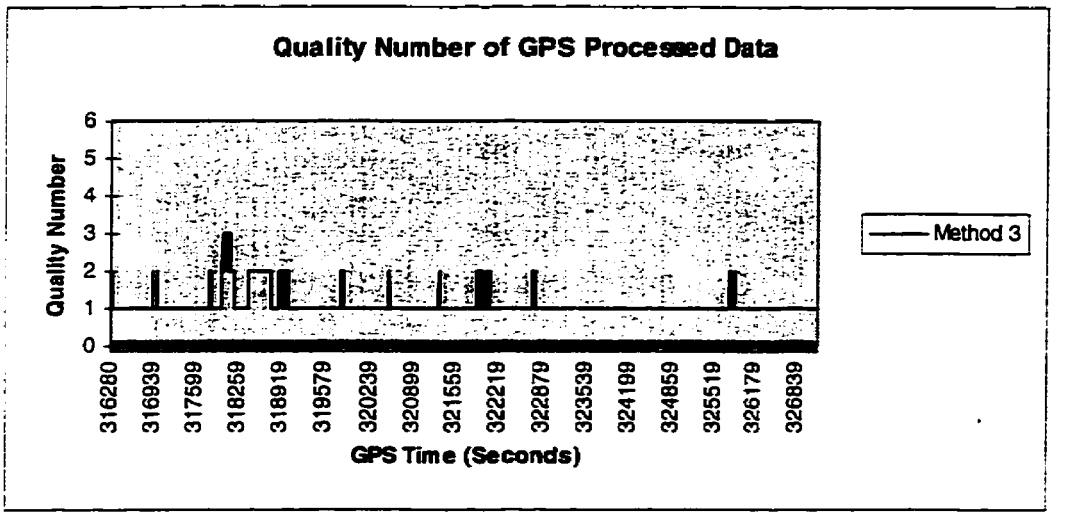

Figure 4. 45. Quality Number Obtained from Method 3

In order to see the behavior of ambiguities for the entire mission, ambiguity drifts as computed by GRAFNAV are shown in Figures 4. 46 - 4. 48. The mean values of ambiguity drifts for Methods 1, 2, and 3 are 0.0008, 0.0018, and 0.0009 cycles per second. The standard deviations of ambiguity drifts are 0.001, 0.0019, and 0.001, respectively. These values show that ambiguities were relatively constant for the entire flight mission. Although there are some spikes due to loss of lock on a particular satellite during banking in Figure 4. 47, these drifts are still acceptable.

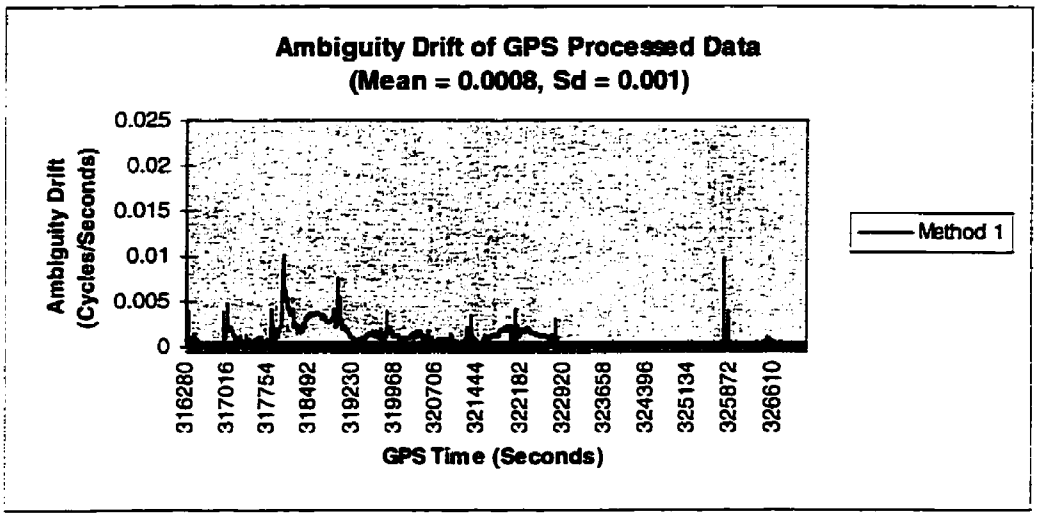

Figure 4. 46. Ambiguity Drift obtained from Method 1

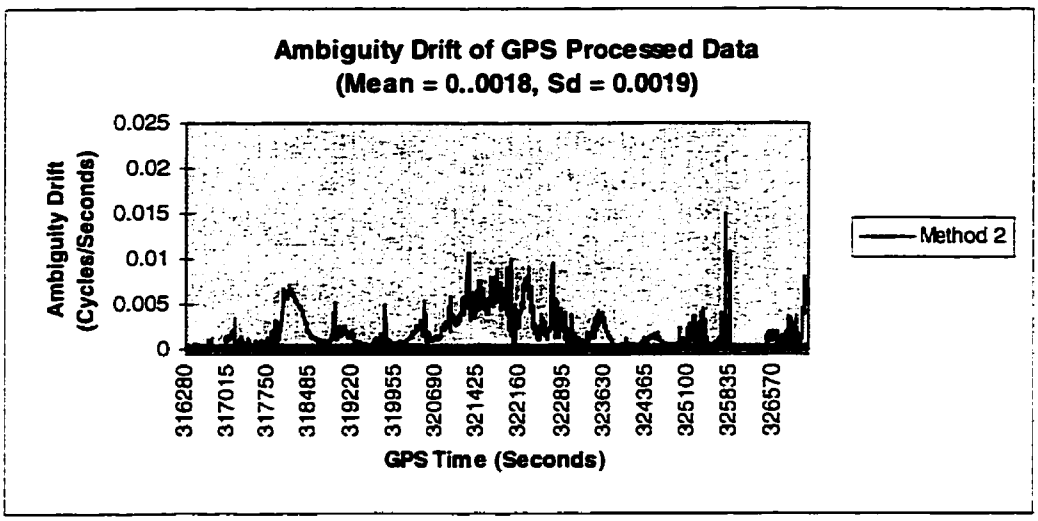

Figure 4. 47. Ambiguity Drift obtained from Method 2

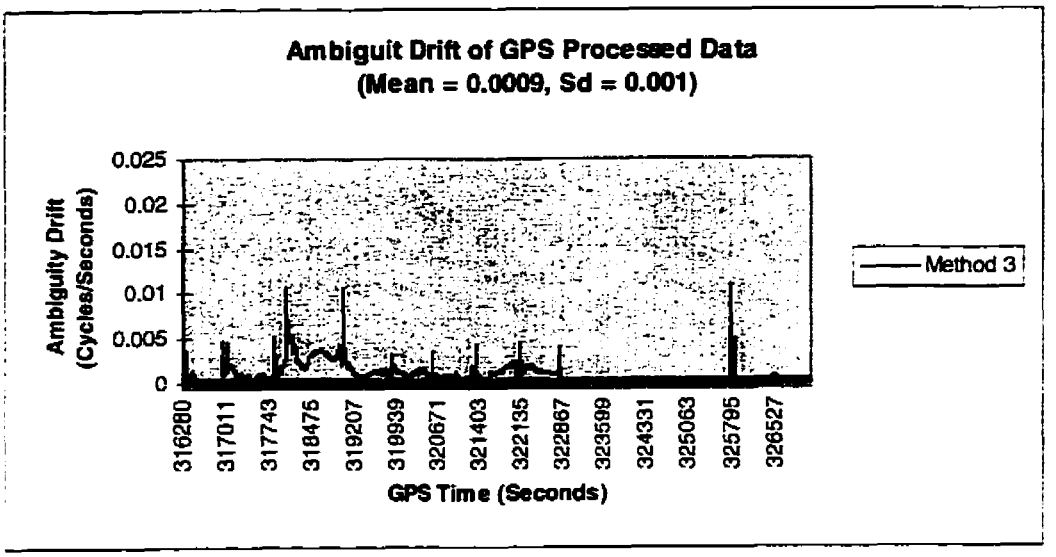

Figure 4. 48. Ambiguity Drift obtained from Method 3

The differences in X, Y, and Z from forward and reverse trajectories were computed. These differences are shown in Figure 4. 49. The X, Y, and Z differences are less than 10 cm for almost the entire mission, except one spike of 30 cm, which happened at the middle of mission due to an abrupt change in satellite geometry.

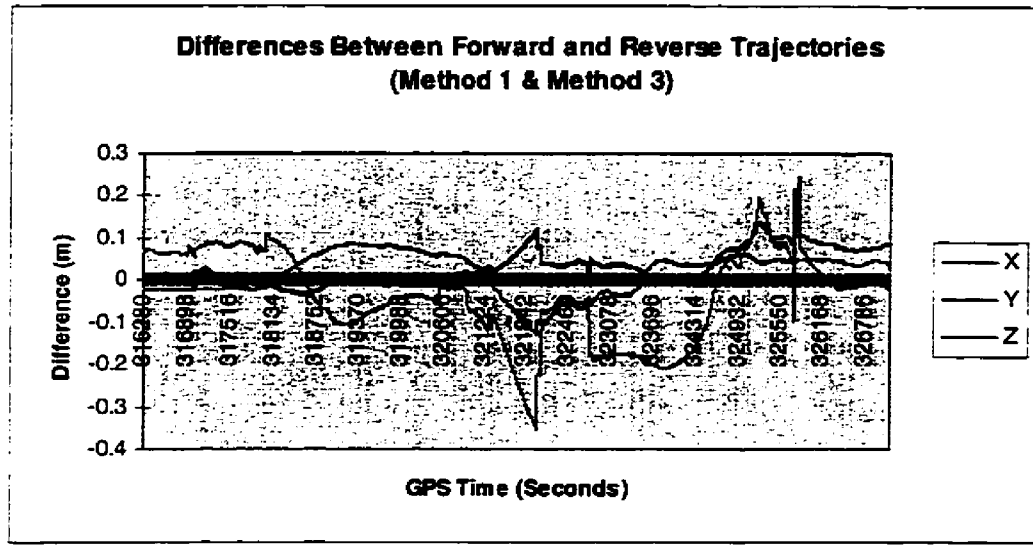

Figure 4. 49. Difference Between Forward and Reverse Trajectories

4. 4. Photogrammetric Processing of Jackson Data Set

The flowchart of the processing methodology for GPS-assisted aerial triangulation is shown in Figure 4. 50.

This rigorous and integrated approach to the GPS-assisted aerial triangulation has been successfully implemented on Jackson project. As known, the GPS-photogrammetric bundle block adjustment includes the simultaneous, rigorous, 3-dimensional least squares adjustment of reduced image coordinates, GPS camera exposure station coordinates, and ground control points, as well as other auxiliary information which may be available. These observation should be appropriately weighted.

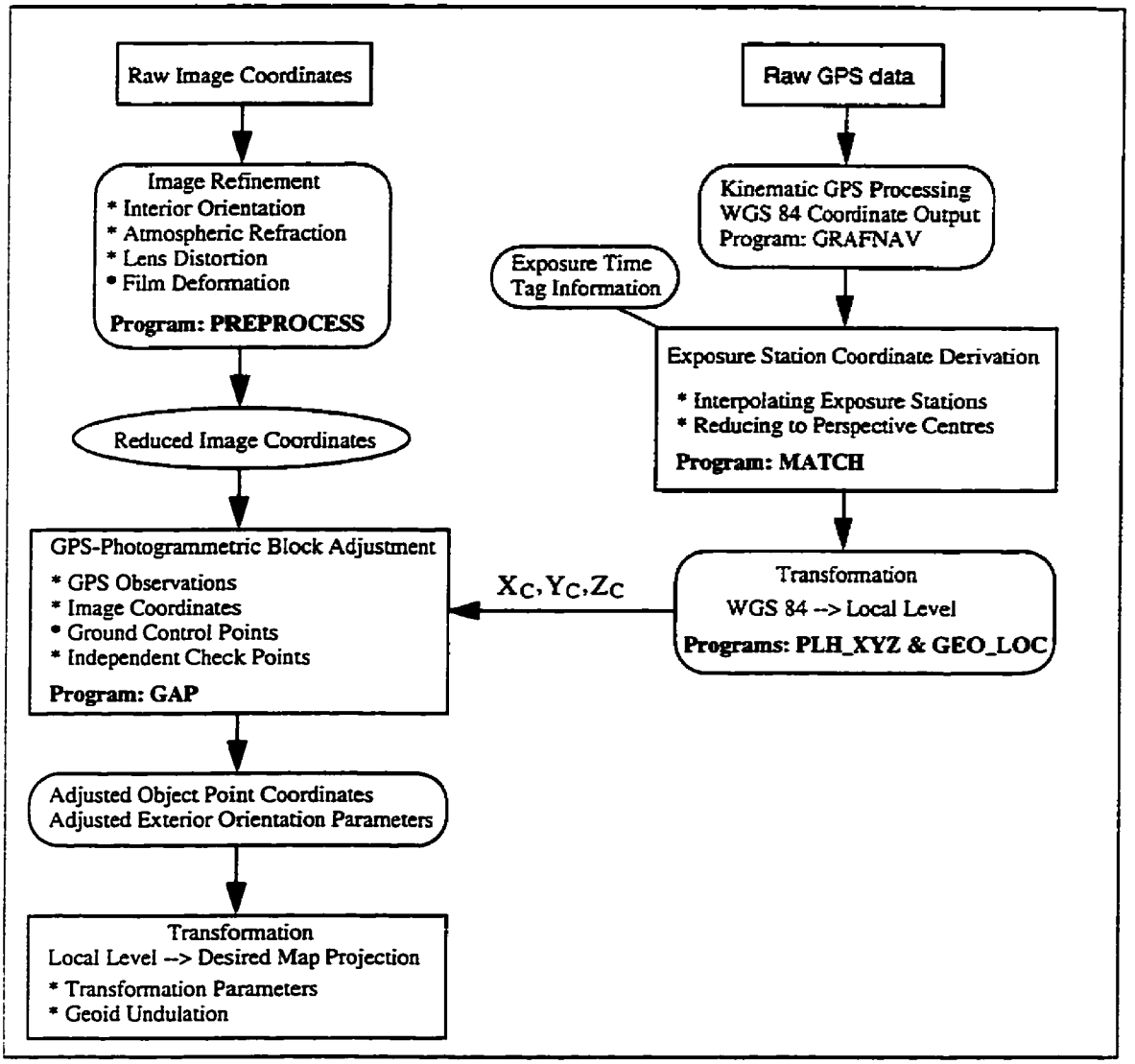

Figure 4. 50. Processing Methodology of GPS-Assisted Aerial Triangulation

4. 4. 1. Methodology

All photogrammetric measurements were carried out on a Wild BC 1 analytical plotter, with point transfer being under taken with a Wild PUG device (Greening et al., 1994). All measured image coordinates were reduced to the fiducial coordinate system,

and corrected for systematic errors such as, principal point displacement, radial lens distortion, film deformation, and atmospheric refraction. Image coordinates were not corrected for earth curvature effects, since the block adjustment was to be executed in a Local Level Cartesian coordinate system (LL). The reduced image coordinates serve as input into the adjustment.

Coordinates of antenna phase centre were obtained from airborne kinematic GPS processing, as described in previous sections (Method 1). All camera exposures were stored as time-tagged events within the GPS data file during the photographic mission. Each instant of exposure was interpolated from the GPS processed data using linear interpolation technique and subsequently reduced to the camera exposure stations knowing the antenna-camera offset and the attitude of the aircraft. The WGS84 coordinates of camera exposure stations were then transformed to the local level Cartesian coordinate system by 3-dimensional, rigorous transformation, before being introduced to the adjustment. The origin of this system was chosen to be in the centre of the project area, such that X_L, Y_L, Z_L coordinate axes were closely oriented with respect to the Northing-Easting-Up system.

The ground control point coordinates were determined using GPS static processing techniques and the baseline vectors were rigorously adjusted through 3-dimensional least squares adjustment software (Greening et al., 1994). These coordinates were also transformed to the LL system from WGS84.

The bundle adjustment was executed in the local level coordinate system. Various configurations of GPS-photogrammetric block adjustment were executed based on the following factors:

* Observational weighting,
* Block geometry,
* Ground control configuration, and
* Self calibration

4. 4. 1. 1. Observational Weighting

The role of observational weighting in GPS-photogrammetric block adjustment has not received adequate attention (Fraser, 1995). This is especially important in the presence of systematic error initiated from GPS and datum related error sources, as well as errors in the camera interior orientation parameters. Three types of observational data are typically present in the GPS-photogrammetric bundle block adjustment, namely, image coordinate observations, GPS exposure station coordinates, and ground control point coordinates. The observational weighting of the image coordinates directly influences to the relative orientation of the block and to block shape in free space, while the weight of GPS camera exposure stations and ground control points relate directly to absolute positions. Relative weighting of observations has a direct impact on the precision of aerial triangulation, especially in the presence of biases. A good example

could be where both GPS and ground control observations have low weights. In this case, the block is allowed to float to fit its best position for an optimal level of triangulation misclosure. The problem here is that the coordinate system is not sufficiently defined, particularly with biases, and block shifts of a significant amount can not be avoided.

Assuming that σ_{GPS} and σ_{GCP} are the positional standard errors of GPS observations and ground control points, and let σ_{XYZ} and σ^{C}_{XYZ} be the standard errors of object point coordinates and exposure station coordinates, respectively, obtained from a fully controlled conventional block adjustment. If $\sigma_{GPS} >> \sigma^{C}_{XYZ}$, the object space datum is defined by the weight matrix of GPS observations (P_{GPS}), and the relative geometry of the block triangulation will be determined by photogrammetric observations. The situation is different when $\sigma_{GPS} \leq \sigma^{C}_{XYZ}$; in this case, the weight matrix of GPS observations, P_{GPS}, serves as a constraint on the relative and absolute orientation of the block. Incorporating ground control points can improve the absolute accuracy of the block depending on the relative contributions of P_{GPS} and P_{GCP} (i.e., the weight matrix of the ground control points) and the presence of systematic errors (Fraser, 1995). For a block with a small number of control points, the effect of ground control points is negligible, unless $\sigma_{GCP} << \sigma_{GPS}$.

Photogrammetric blocks controlled by GPS air stations and no ground control points could have some unfortunate results if interior orientation parameters are

contaminated by systematic errors. For example, a systematic error in focal length will have a direct impact on the Z coordinate of object points.

In order that the ground control points play the dominant role on the absolute orientation of the block, the conventional block adjustment with just control points and very small weights for GPS observations should be carried out.

A favourable procedure found in this study is that the bundle block adjustment can be executed using GPS exposure stations, with appropriate weights through P_{GPS}, and available ground control points with a simultaneous 3D similarity transformation. This transformation accounts for small differences in origin, orientation, or scale between the ground coordinate system and airborne GPS system.

Inclusion of stripwise drift parameters allows for compensation of these systematic errors and, therefore, GPS signal interruption between strips can be tolerated (Fraser, 1995).

4. 4. 1. 2. Block Geometry

Loss of satellite lock, with subsequent cycle slips and difficulties in recovering the GPS ambiguity resolutions, have been viewed as a significant problem and error source for airborne kinematic GPS applications (Fraser, 1995). Error modeling through inclusion of

drift parameters in the block adjustment allows the modeling of the errors introduced by the approximate ambiguity solutions through stripwise shifts and time-dependent linear drift terms (Ackermann and Schade, 1993). These six parameters per strip will destabilize the geometry of the block, and might have some negative impacts on recovery of all unknowns in the adjustment (e.g., singularity of normal matrix). Therefore, cross strips are employed to overcome this problem, making it possible to recover all unknown parameters. It has to be mentioned that the airborne GPS data should be collected in a special way (i.e., locking on new course GPS positions derived from C/A code pseudorange after signal interruption), in order to use drift parameters in a block adjustment.

4. 4. 1. 3. Self Calibration

In order to further improve the accuracy of combined GPS-photogrammetric bundle block adjustment, the self calibration approach was also considered. Self-calibration bundle block adjustments were carried out with and without additional parameters. GAP uses three different techniques to formulate the additional parameters; conventional lens distortion formulas, Brown's formulas, and harmonic functions.

4. 4. 2. Combined GPS-Photogrammetric Block Adjustment Results

Based on the GPS-derived coordinates of the exposure stations, various ground control configurations (Figure 4. 1), and image coordinates of all tie and control points, combined GPS-photogrammetric block adjustments were carried out for different experiments.

The goal is to investigate and analyze various methods for a real GPS-photogrammetric medium scale mapping project. These experiments include various ground control configurations, self-calibration, cross strips, and 3D transformation between GPS and GCP coordinate systems. The characteristics of each experiment are depicted in Table 4.4.

Table 4. 4. Methodologies For Combined GPS-Photogrammetric Block Adjustment

Method	Ground Control Configuration	Self Calibration (Basic Interior Orientation)	Cross Strips	3D Transformation	σ_{GPS} (m)	σ_{GCI} (m)
1	A	No	NO	NO	0.25	0.1
2	B	No	NO	NO	0.25	0.1
3	B	YES	NO	NO	0.25	0.1
4	C	NO	YES	NO	1000.0	0.1
5	C	YES	YES	NO	1000.0	0.1
6	D	NO	YES	NO	0.25	0.1
7	D	YES	YES	NO	0.25	0.1
8	D	YES	YES	YES	0.25	0.1

In order to appreciate the results obtained from these experiments, the second experiment is explained in more detail as an example for other experiments. Configuration B from Figure 4.1, which has 4 ground control points at the corners of the

block, was chosen as the ground control configuration. Neither self-calibration nor cross strips were used for this adjustment. The standard deviation of the GPS derived coordinates of the exposure stations and ground control points were set at 0.25 m and 0.1 m, respectively. These values are converted to weights for these kinds of observations and introduced to the block adjustment. The option for a 3D similarity transformation between GPS and GCP coordinate system was also turned off for this experiment. After assigning the appropriate options, the combine block adjustment was executed using GAP.

Experiments 7 or 8, which include cross strips, are expected to offer better results compared to other experiments. On the other hand, experiment 1, with no ground control and no cross strips, is expected to have the least accurate results.

4.4.2.1. Results Obtained from the Experiments using Real Data

The Root Mean Square Error (RMSE) of the check points for Jackson project is shown in Figure 4. 51 for all scenarios. As shown in this figure, there is a systematic error associated with Z (two times greater than that of X or Y coordinate) when no self-calibration parameters and no cross strips are included. Applying self-calibration (basic interior orientation parameters) and including cross strips removes this systematic error, and implies that fixing the wrong focal length in a bundle block adjustment would have a direct impact on the Z coordinate. Another conclusion is that there is still a need for

vertical control across the block, which can be replaced by cross strips. The common conclusion is that using self-calibration techniques, and including cross strips, improved the accuracy of Z coordinate of the object points. The theoretical precision obtained from inversion of normal matrix was also compatible with the practical precision obtained from check point coordinates (Figure 4. 52).

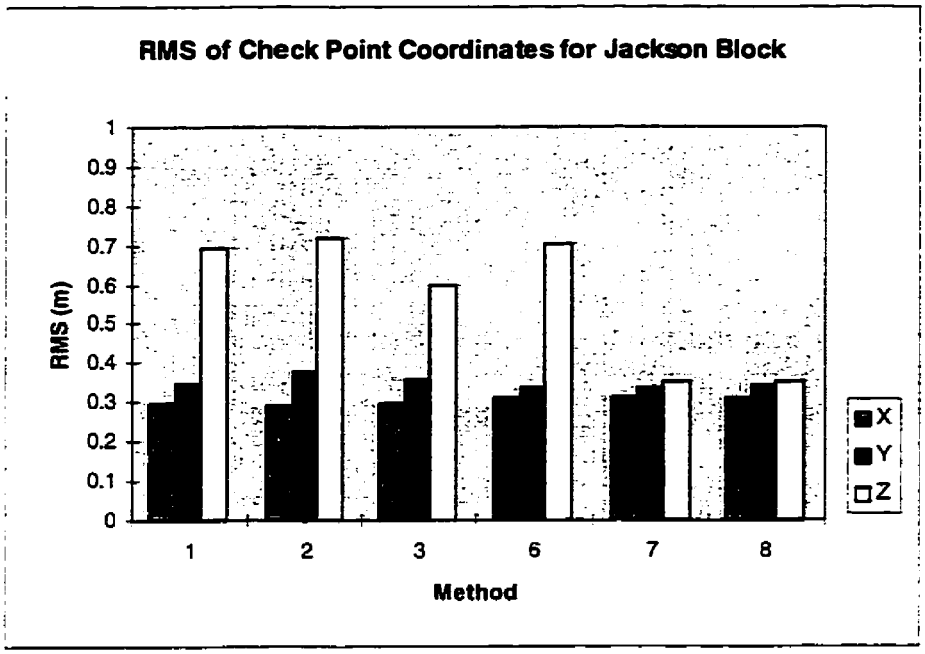

Figure 4. 51. RMSE of All Check Points Obtained from Jackson Block

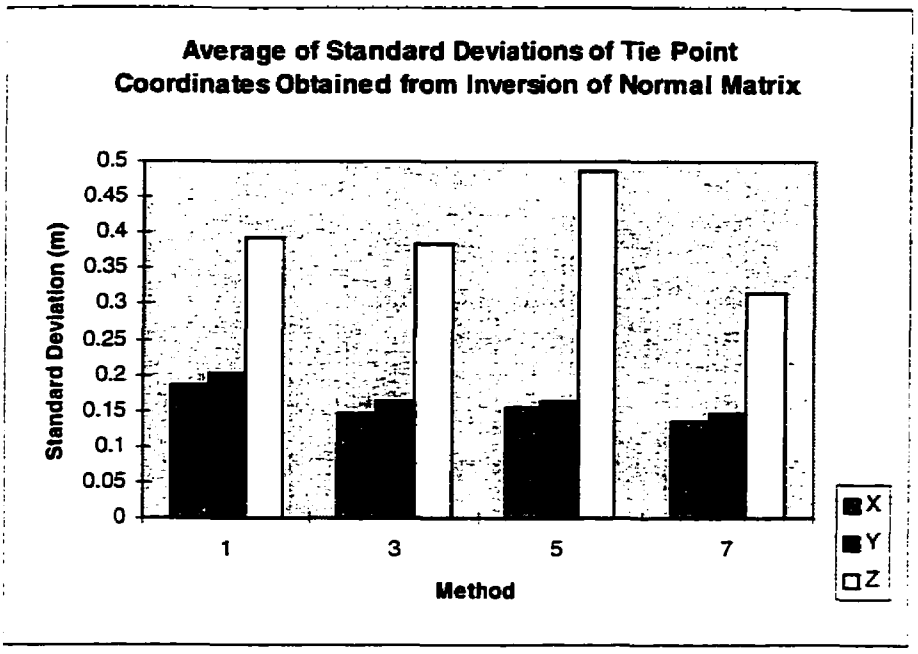

Figure 4. 52. Standard Deviations of All Tie and Pass Points Obtained from Jackson Block

To determine whether incorporating additional self-calibration parameters would improve the results, self-calibration block adjustments were carried out using three models for formulating additional parameters, namely: conventional radial and decentering distortion model (method 7-1), Brown's formulation (method 7-2), and harmonic functions (method 7-3). For this purpose, six control points were used and cross strips were also included in the adjustment. Figure 4. 53 shows the RMSE of check points when additional parameters were applied. It can be seen that the conventional model for additional parameters offered better results (method 7-1) compared to the results obtained from the other two methods, implying that the additional parameters used in Method 7-1 modeled the lens distortion better that those of other two methods. Comparing Figure

4.53 and Figure 4.51 show that an improvement of 30 mm in Z was feasible when applying additional parameters. It is speculated that the reason that applying additional parameters did not improve the results significantly is that the distortion characteristics (both radial and decentering lens distortions) of the camera are low.

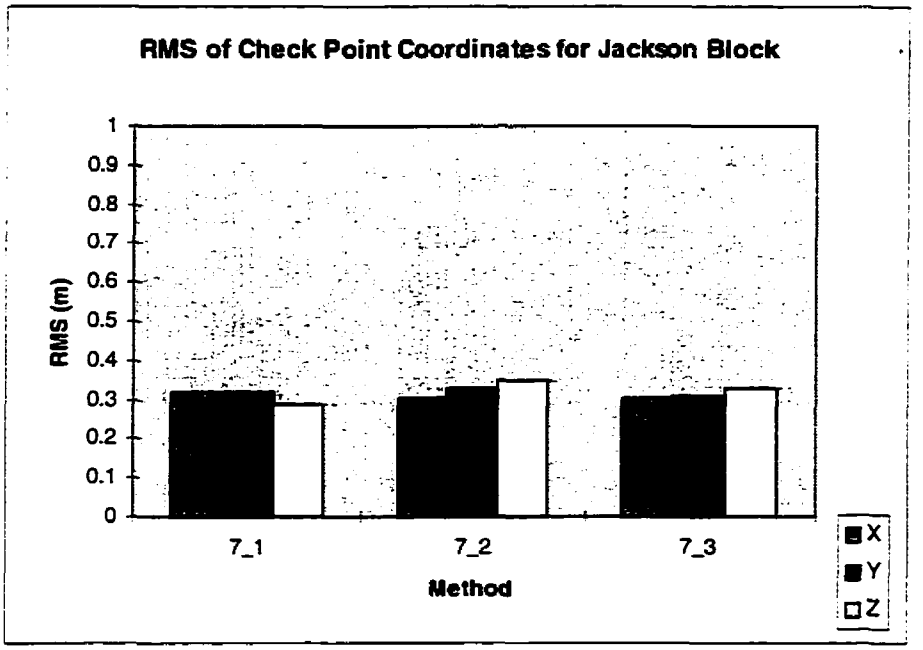

Figure 4.53. RMSE of Check Points (Additional Parameters included in The Adjustment)

To assess the change in focal length from the laboratory calibrated value, and the focal length obtained from self-calibration block adjustment, Figure 4. 54 shows this value for various methods. There is a 50μm difference (1.2 m in Z in the object coordinate system) between the focal length obtained from laboratory and the one obtained from Method 7-1. This implies the difference between the conditions (i.e., temperature, pressure, etc.) of the laboratory calibration and the field calibration.

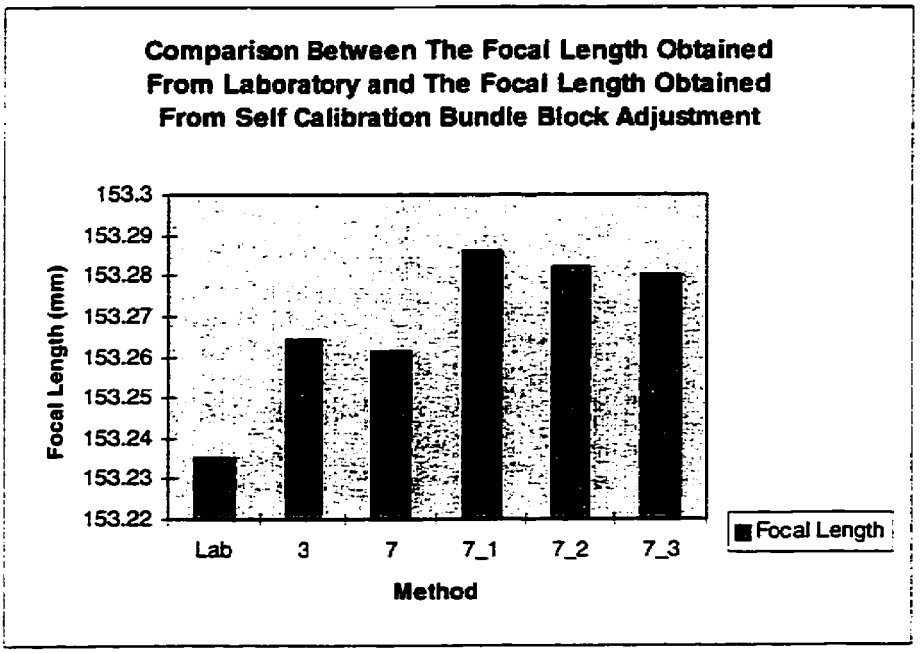

Figure 4. 54. Focal Length Obtained From Various Methods for Jackson Block

In the reliability analysis, redundancy numbers and external reliability factors of image coordinates, GPS observations of exposure stations, and ground control points were extracted using the variance covariance matrix of residuals and weight matrix of observations. Figures 4. 55 - 4. 57 show the redundancy numbers for these three types of observations, and for the various processing methods. Redundancy numbers for both x and y image coordinates obtained from Methods 6, 7, and 8 (GPS-assisted) are marginally better than those obtained from Methods 4 and 5 (conventional block adjustment), confirming that incorporating GPS coordinates of the camera exposure stations into the photogrammetric block improves the reliability of image coordinates. Redundancy numbers for image coordinates obtained from method 2 or 3 (4 ground control points included) and those of Method 1 (no ground control point) are almost the same.

Therefore, including ground control points in the GPS-photogrammetric block has little impact on the reliability of image coordinates. Redundancy numbers of GPS coordinates of the camera exposure stations are the same for all processing methods (Figure 4. 56). This was expected due to the fact that GPS exposure station coordinates were assigned the same precision for all methods. Including cross strips in a GPS photogrammetric block adjustment improves not only the accuracy of the block, but the reliability of the ground control points as well (Figure 4. 57).

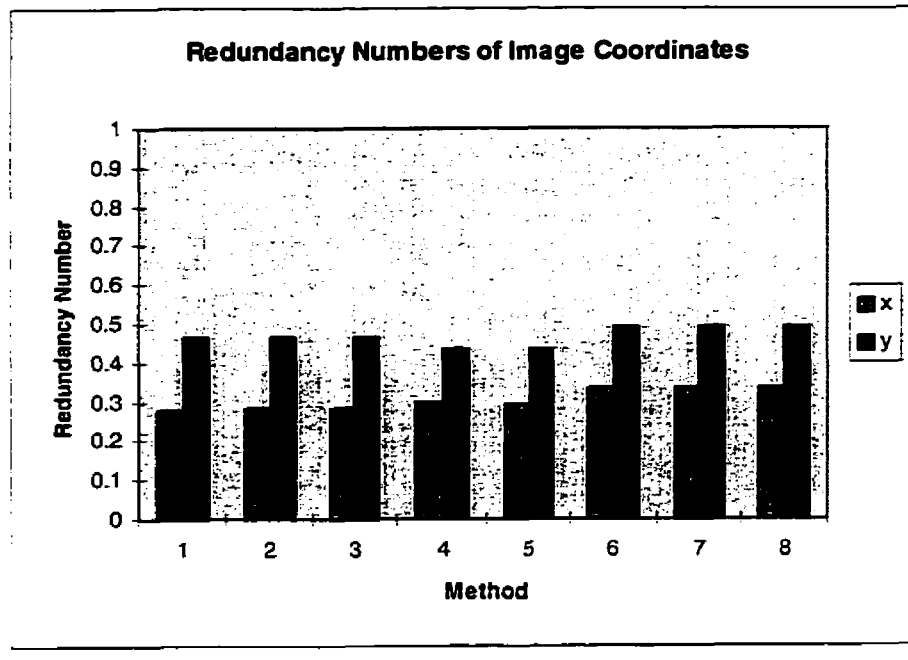

Figure 4. 55. Redundancy Numbers of Image Points Obtained from Jackson Block

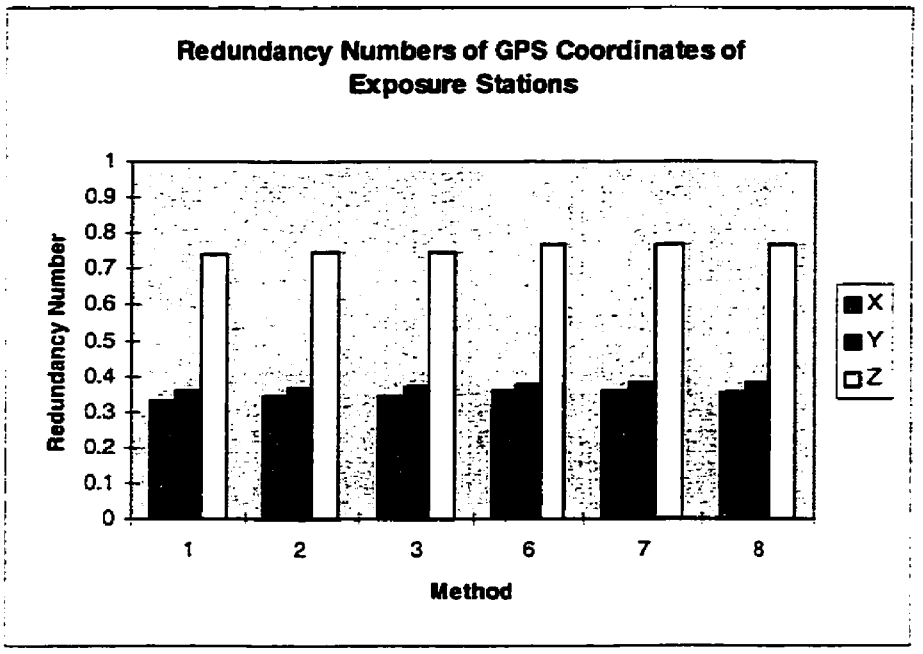

Figure 4. 56. Redundancy Numbers of GPS Coordinates of Camera Exposure Stations Obtained from Jackson Block

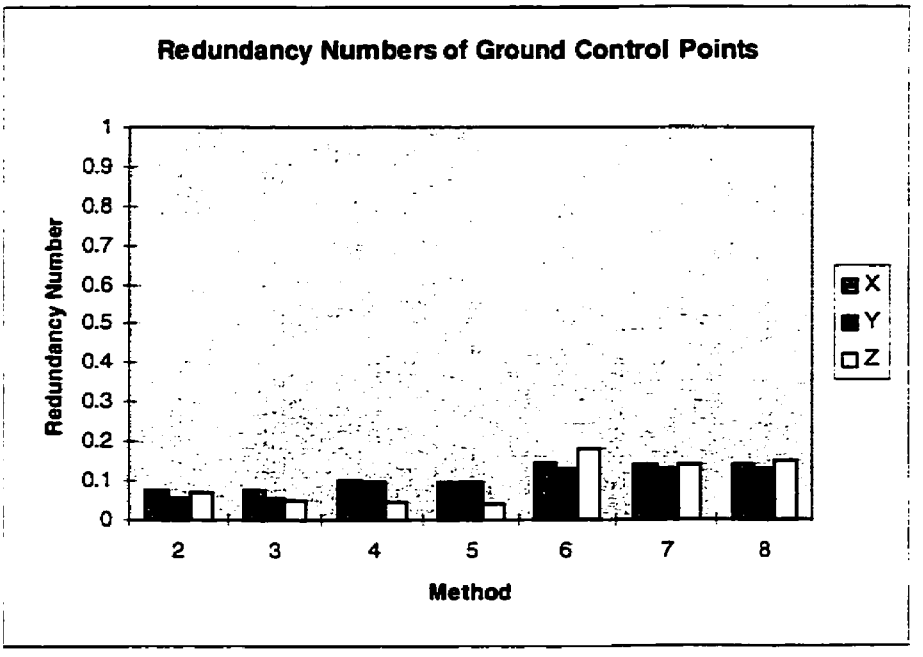

Figure 4. 57. Redundancy Numbers of Coordinates of Ground Control Points Obtained from Jackson Block

The external reliability factors of image coordinates, GPS coordinates of the exposure stations, and ground control points are shown in Figures 4.58 - 4.60. The external reliability factors for x and y image coordinates, Figure 4.58, obtained from all methods are ranked as acceptable and good according to Table 2.2. However, Methods 6, 7, and 8 improved these values by 10%. Figure 4.59 shows the external reliability factors for GPS observation, in which all methods offer comparatively the same results due to the fact that the GPS accuracy was considered the same for all methods.

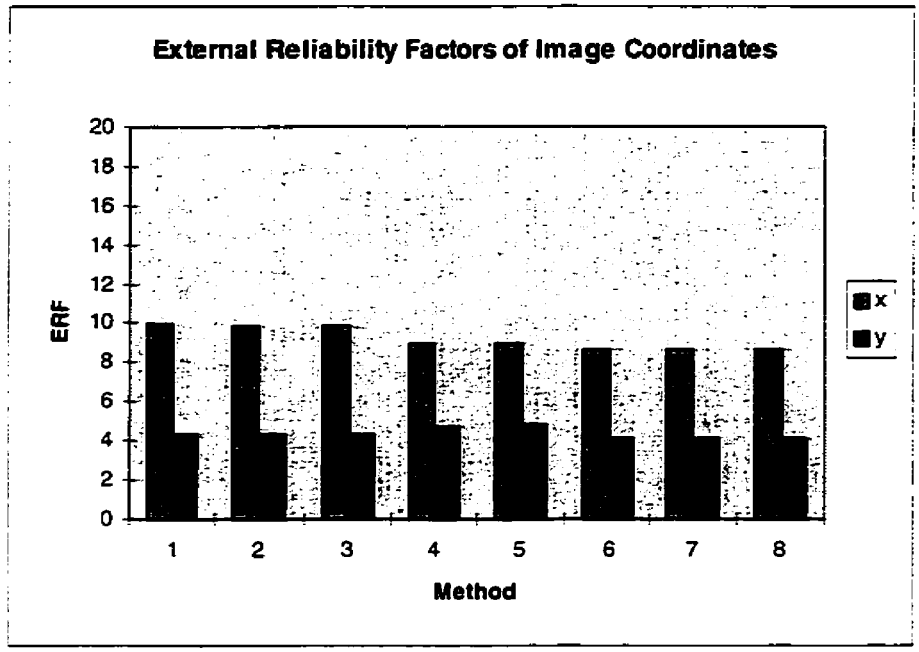

Figure 4. 58. External Reliability Factors of Coordinates of Image Points

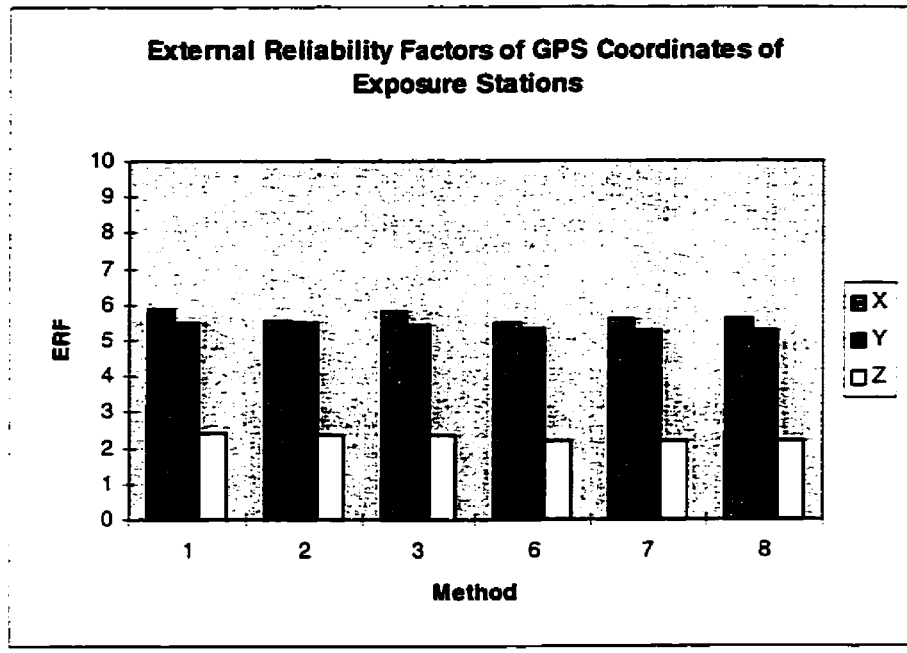

Figure 4. 59. External Reliability Factors of GPS Coordinates of Camera Exposure Stations

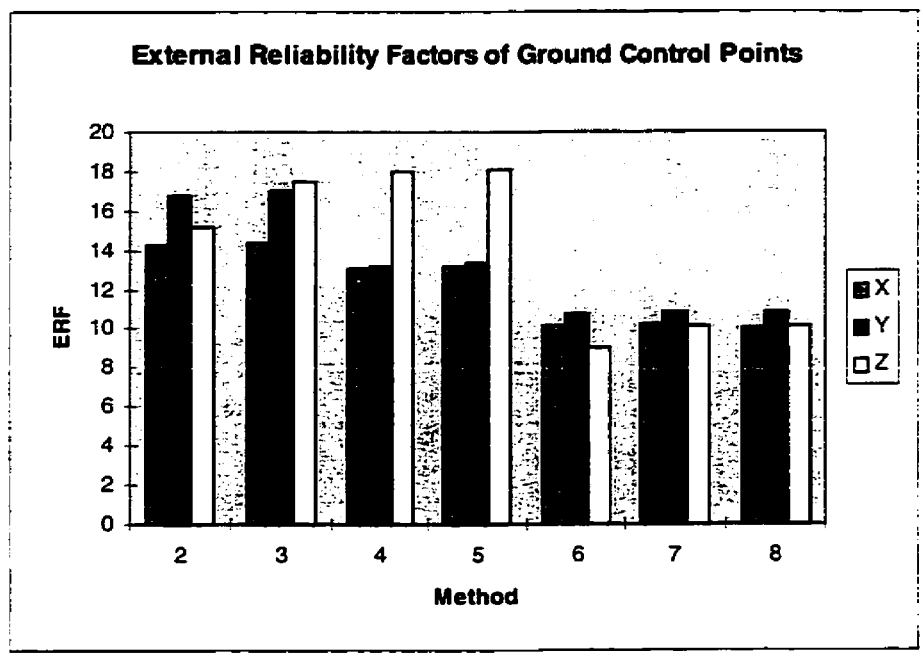

Figure 4. 60 External Reliability Factors of Coordinates of Ground Control Points

CHAPTER 5

NEW APPROACH DEVELOPED FOR SINGLE STRIP AERIAL TRIANGULATION

Previously, ground control points, typically in the form of planimetric points along the perimeter of the block and relatively dense chains of vertical points across the block, were mandatory for relating the image coordinate system to the object coordinate system, and to ensure the geometric stability of the conventional aerial block. The minimum control requirement for absolute orientation of the block is three non-collinear points. For a GPS-photogrammetric block, condition is fulfilled by using GPS observations at the perspective centres as "control points". However, in the case of strip triangulation, the GPS observations of the exposure stations are almost collinear along a strip. The above condition is no longer satisfied and, therefore, the roll angle (i.e., the rotation about the flight line) can not be recovered reliably. This makes the use of ground control points necessary in strip triangulation to solve for all exterior orientation parameters (Alobaida, 1993).

This chapter describes a new technique for GPS controlled strip triangulation using geometric constraints of man-made structures (e.g. high voltage towers and high-rise buildings) located approximately along the flight line. The effects of the accuracies of different GPS measurements were also investigated. Precision and reliability analyses

were performed on both simulated and real data. All results were obtained using the program GAP developed for this study.

5. 1. GPS Controlled Strip Triangulation with Geometric Constraints of Man- Made Structures

The inherent geometry of a block and the common tie points in consecutive strips make it possible to recover all three rotation angles in the combined block adjustment. Unfortunately, this method can not be used for a single strip, since the GPS coordinates of the exposure stations can not adequately recover the roll angle of the aircraft. As a consequence, control introduced by airborne-GPS leaves an ill-conditioned, if not singular, system of normal equations. However, ground control points have traditionally been used along the flight line to overcome this problem.

A new technique for GPS controlled strip triangulation was developed based on geometric constraints derived from man-made structures (e.g. high voltage towers, high rise buildings) located along the flight line (Figure 5.1). The principle of this technique is based on 2D (X, Y) coordinate difference observations (i.e., the horizontal coordinate differences between the top and the bottom of any vertical structure). The approach is based on the assumption of verticality of man-made structures (i.e., top and bottom of the structure should have the same horizontal coordinates).

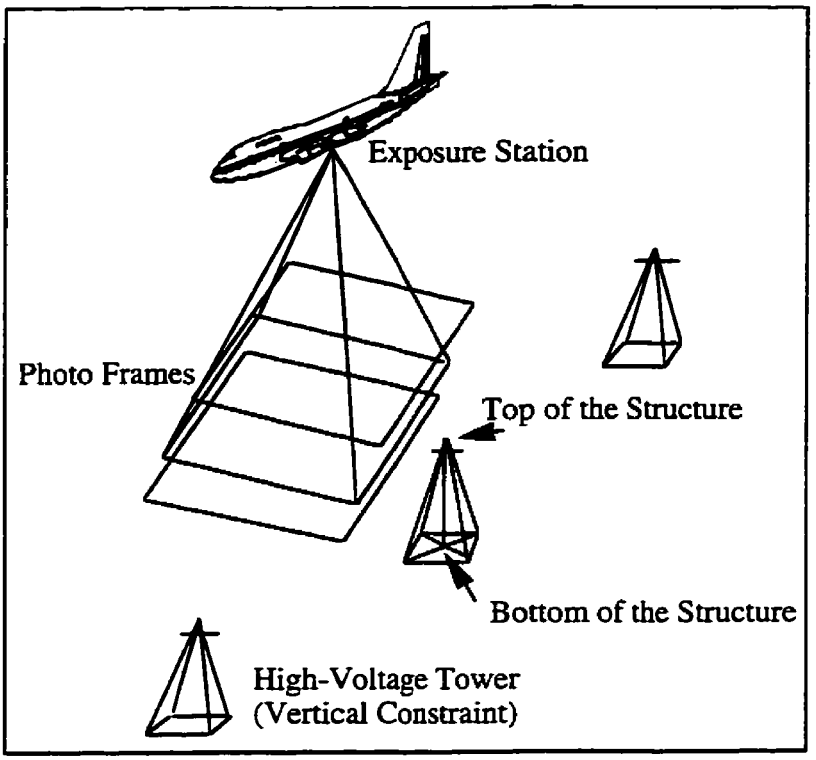

Figure 5. 1 Vertical Constraint in A Single Strip Triangulation

The observation equations for these constraints, with appropriate weights, are introduced into the combined strip adjustment. The constraint observation equation for any vertical structure is written as:

$$\begin{bmatrix} X_j \\ Y_j \end{bmatrix} - \begin{bmatrix} X_i \\ Y_{ij} \end{bmatrix} = \begin{bmatrix} 0 \\ 0 \end{bmatrix}; \quad P_{\Delta X,\Delta Y} = \begin{bmatrix} 1.0/\sigma^2_{\Delta X} & 0 \\ 0 & 1.0/\sigma^2_{\Delta Y} \end{bmatrix} \qquad 5.1$$

where

(X_j, Y_j) are the horizontal coordinates of the top of the structure,

(X_i, Y_i) are the horizontal coordinates of the bottom of the structure,

$(\sigma^2_{\Delta X}, \sigma^2_{\Delta Y})$ are the variances of the coordinate differences,

$P_{\Delta X,\Delta Y}$ is the weight matrix of the coordinate differences.

The weights for these equations should be appropriately chosen to account for possible small deviations from verticality. Notably, the absolute ground coordinates of the structure are not required, since only the coordinate differences of the top and the bottom of the structure are introduced, and the points on the structure are treated as horizontal pass points. The concept is to use a number of towers along the flight line, to allow recovery of the roll angle of the aircraft and, hence, minimize the number of ground control points in strip triangulation.

5. 2. Methodology for Simulated Data

Many experiments were conducted to evaluate the performance of the new model. One single strip of 50 photographs was simulated. The interior and exterior orientation parameters were predefined. The image coordinates of all object points (pass points and tower points) were computed using the known exterior orientation of each photograph. Table 5. 1 lists the information concerning this simulated strip.

Table 5. 1. Simulated Strip

Strip Information	
Number of Photos	50
Photo Scale	1:5000
Focal Length	152 mm
Terrain Elevation Difference	150 m
Average Flying Height	900 m
Forward Overlap	60%
Photograph Format	23 cm x 23 cm
Accuracy of Image Coordinates	5 μm
Accuracy of Ground Control Points	0.1 m
Accuracy of GPS	0.25-1.0 m
Tower Height	15 m
Number of Towers	50
Number of Pass points per Photo	15

The behavior of the new model was studied using various GPS accuracies at the perspective centres. The performance of the technique was evaluated using the standard deviations of the coordinates of pass points obtained from their variance-covariance matrix, and comparing the adjusted coordinates with "true" simulated coordinates. The following methods of strip adjustment were carried out:

1 - GPS-photogrammetric strip adjustment with 2 ground control points and without tower points,

2 - GPS-photogrammetric strip adjustment with no ground control points and with tower points,

3 - Full control strip adjustment (no GPS data)

5.2.1. Results with Simulated Data

Figure 5. 2 shows the root mean square error (RMSE) of X, Y, and Z coordinates of all pass points for scenario without tower points and Figure 5. 3 shows the RMS of X, Y, and Z coordinates of all pass points with the inclusion of tower points. The RMS of X, Y, and Z coordinates of pass points for the full ground control adjustment are 45, 57, and 197 mm, respectively.

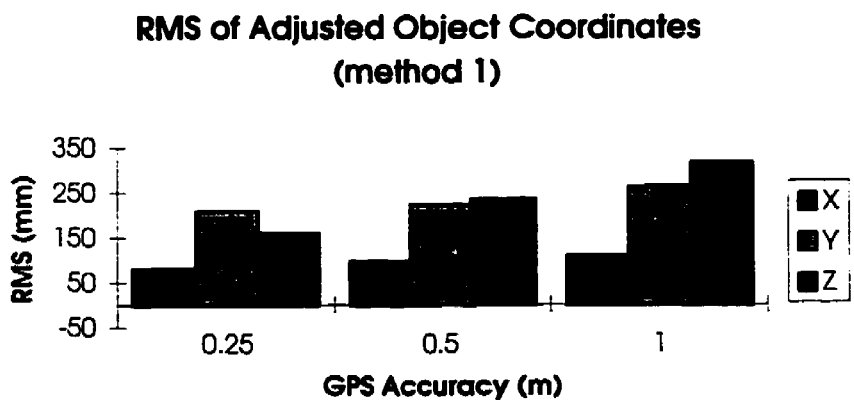

Figure 5. 2. RMS of X, Y, and Z Coordinates of All Object Points (method 1)

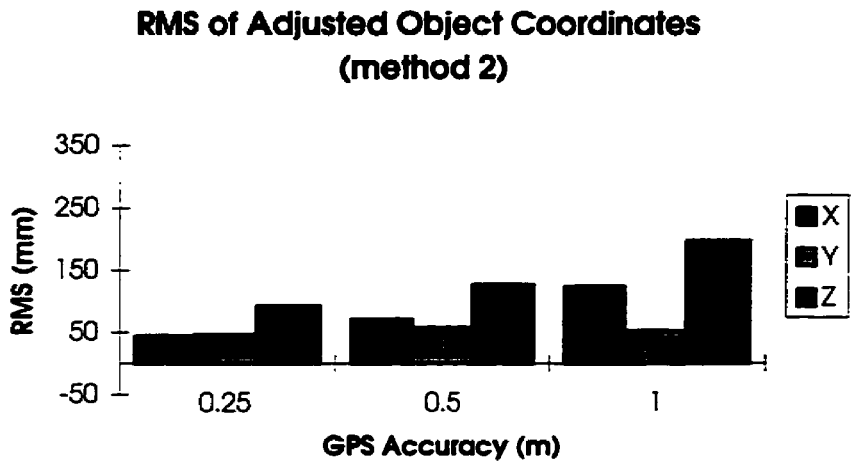

Figure 5. 3. RMS of X, Y, and Z Coordinates of All Object Points (method 2)

Figures 5. 2 and 5. 3 show that if GPS can provide accuracy at the level of 0.25 to 0.5 m for camera exposure stations coordinates, the RMS values for all object coordinates are better or equal to those obtained from the full ground control version for this scale of photography. These results confirm that constraint information from the tower points can replace the ground control points and eliminates the need for the second strip of photography which has been adapted conventionally to improve the geometry of the strip. To see how this technique recovers the roll angle of the aircraft, Figures 5. 4, 5. 5, and 5. 6 show the adjusted roll angle of each photo obtained from the 3 methods (σ_{GPS}=0.25 m). As seen in these figures, the adjusted roll angle recovered from method 2 (tower points included) is almost the same as that obtained from method 3 (full ground control version).

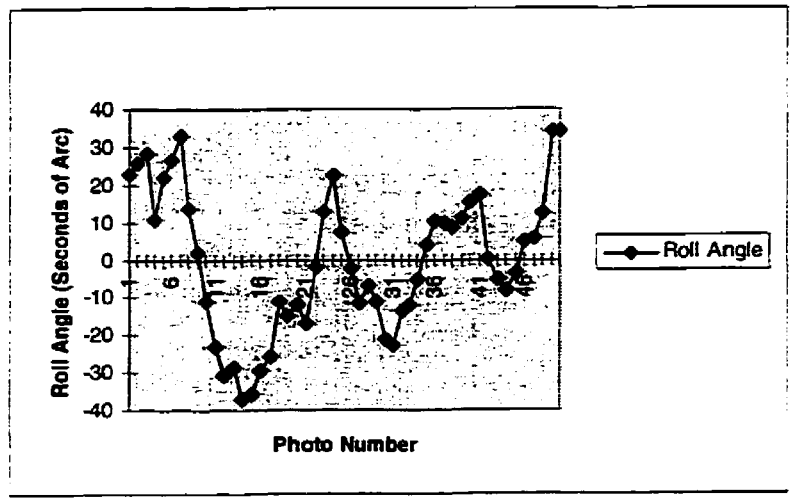

Figure 5. 4. Adjusted Roll Angle from Method 1

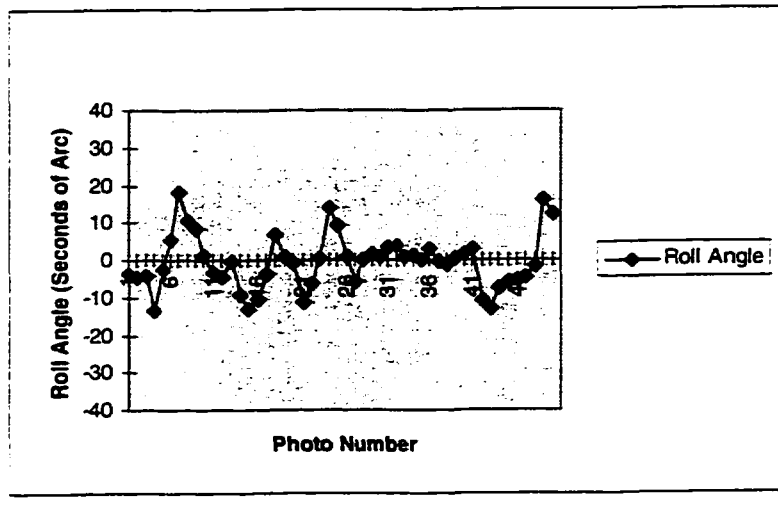

Figure 5. 5. Adjusted Roll Angle from Method 2

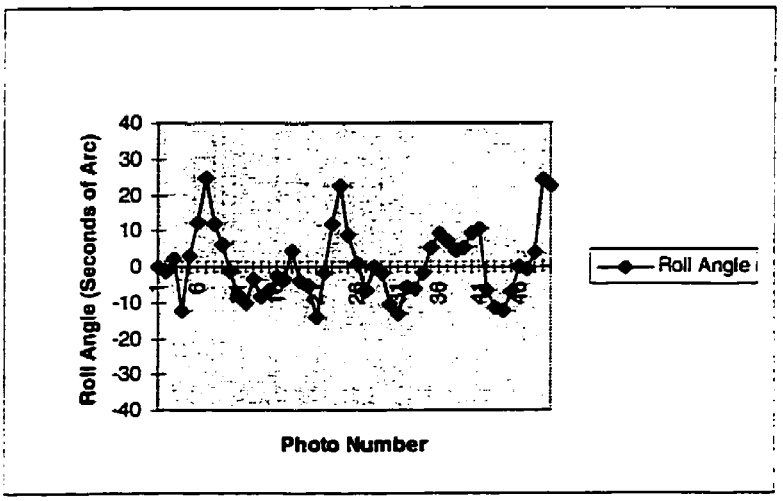

Figure 5. 6. Adjusted Roll Angle from Method 3

In the reliability analysis, redundancy numbers, internal reliability factors, and external reliability factors were computed for various observations (image coordinates, GPS coordinates of exposure stations). Table 5. 2 and 5. 3 show the reliability measures for image coordinates and GPS coordinates of exposure stations for the various methods.

Table 5. 2. Reliability Measures for Image Coordinates Obtained from Simulated Strip

Method	1		2		3	
Reliability Measure	x	y	x	y	x	y
r_i	0.28	0.11	0.34	0.54	0.23	0.39
$\delta_{0,i}$	8.34	12.52	8.41	5.73	9.96	6.61
$\bar{\delta}_{0,i}$	7.21	11.85	7.11	3.93	8.98	5.21

Table 5. 3. Reliability Measures for GPS Derived Coordinates of Exposure Stations Obtained from Simulated Strip

Method / Reliability Measure	1			2			3		
	X	Y	Z	X	Y	Z	X	Y	Z
r_i	0.74	0.80	0.84	0.74	0.85	0.82	N/A		
$\delta_{0,i}$	4.65	4.47	4.36	4.66	4.34	4.42	N/A		
$\bar{\delta}_{0,i}$	2.36	1.98	1.72	2.37	1.67	1.85	N/A		

These values are rated as good ($0.5 < r_i$, $\bar{\delta}_{0,i} < 4.0$), acceptable ($0.1 \le r_i < 0.5$, $4.0 \le \bar{\delta}_{0,i} < 10.0$), bad ($0.04 \le r_i < 0.1$, $10.0 \le \bar{\delta}_{0,i} < 20.0$), and not acceptable ($r_i < 0.04$, $20.0 \le \bar{\delta}_{0,i}$)(Förstner, 1985). The best values for the reliability measures have been obtained from method 2 which implies that including tower points in the GPS controlled strip triangulation improves the reliability of both image coordinates, especially the y-coordinates in this case.

5. 2. 2. Minimum Number Of Tower Structures Required For A GPS Single Strip Triangulation

In order to find out the minimum number of towers which are needed to serve as constraint, GPS single strip adjustments were carried out for the different number of tower structures. Table 5. 4 shows the RMSE of the check points for the X, Y, and Z

coordinates. This table shows that if there is one tower every five photos (i.e., 11 towers), then the same results can be expected as those obtained from the case that there is one tower per photo.

Table 5. 4. RMSE of Check Points for Various Number of Towers

Number Of Towers	X (m)	Y (m)	Z (m)
2	0.049	0.203	0.111
3	0.049	0.173	0.104
4	0.042	0.096	0.092
5	0.041	0.085	0.090
6	0.040	0.056	0.091
11	0.043	0.048	0.088
50	0.042	0.044	0.090

5. 2. 3. Height of the Tower Structures

Various trials of GPS single strip adjustments were executed based on different heights for the tower structures. It was found that the taller the structure, the better the accuracy of the adjustment, as intuitively expected. Table 5. 5 shows the RMSE of the check points for various trials. It can be concluded from this table that for a typical large scale mapping project if imagery can provide towers with heights in the range of 2% to

7% of flying height, then the GPS single strip adjustment with constrained tower structures can offer the required accuracy.

Table 5. 5. RMSE of Check Points for Various Heights of Towers

Height Of Tower (m)	X (m)	Y (m)	Z (m)
15	0.044	0.046	0.092
30	0.031	0.030	0.091
45	0.019	0.025	0.087
60	0.019	0.024	0.087

5. 3. Methodology for Real Data

Encouraging results from the simulated data convinced the author to apply this new technique on a real data. Trans Alta Ltd. of Calgary, AB conducted a corridor mapping project in 1992, in an area east of Edmonton, Alberta, Canada. The information for this project is shown in Table 5. 6. A fully-controlled conventional block adjustment was executed to estimate the camera exposure stations and simulate airborne GPS data, due to the fact airborne GPS data were not available. Image coordinates of all control and pass points were provided by Trans Alta Ltd., while the image coordinates of tower points were measured using a Wild AC1 available at the Department of Geomatics Engineering.

Table 5. 6. Project Parameters

Strip Information	
Purpose of Photography: Corridor Mapping, East of Edmonton, Canada	
Number of Photos	22
Number of Strips	2
Photo Scale	1:10,000
Focal Length	153.692 mm
Average Terrain Elevation Difference	50 m
Average Flying Height	1500 m
Forward Overlap	60%
Photograph Format	23 cm x 23 cm
Precision of Image Coordinates	5 μm
Precision of Ground Control Points	0.2 m
Precision of simulated GPS	0.25-1.0 m
Number of Ground Control Points	14
Number of Check Points	9
Tower Height	40 m
Number of Towers	29
Number of Pass points per Photo	20

Three scenarios were selected from the geometric configurations of control and tower points as:

1 - Photogrammetric strip adjustment with two ground control points,

2 - GPS-photogrammetric strip adjustment with tower points and no control points,

3 - GPS-photogrammetric block adjustment used as a reference.

5.3.1. Results with Real Data

Figures 5. 7 and 5. 8 show the RMS values for check points obtained from methods 1 and 2, while Figure 5. 9 shows the same value for Method 3 (block of two strips). By comparing these three figures, it can be concluded that best results were achieved using Method 2, in which the tower points were included in the bundle strip adjustment. It is interesting to note that the RMS values of Z coordinate of check points obtained from Method 2 is similar to that of the X and Y coordinates.

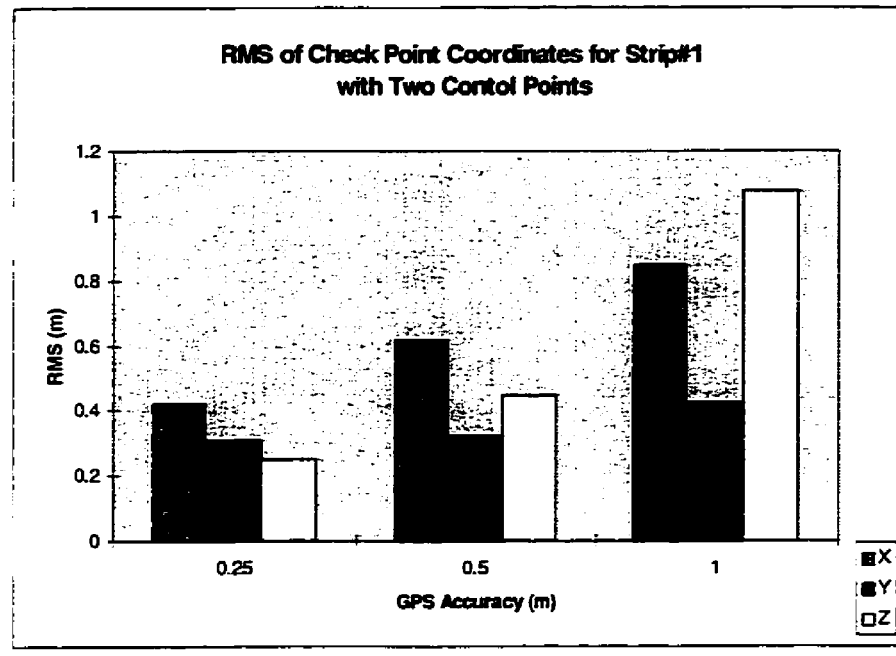

Figure 5. 7. RMS of Check Points Obtained from Method 1

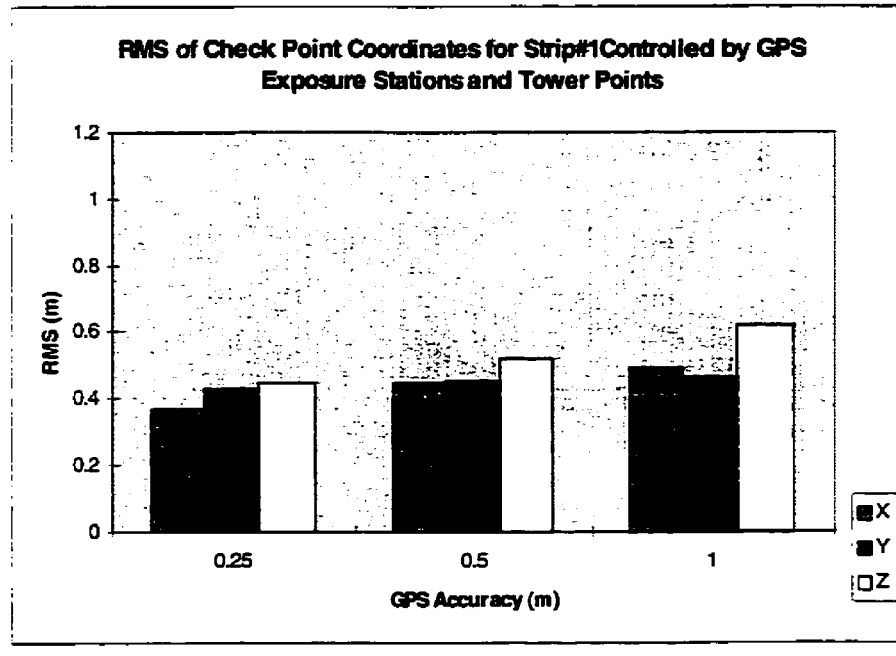

Figure 5. 8. RMS of Check Points Obtained from Method 2

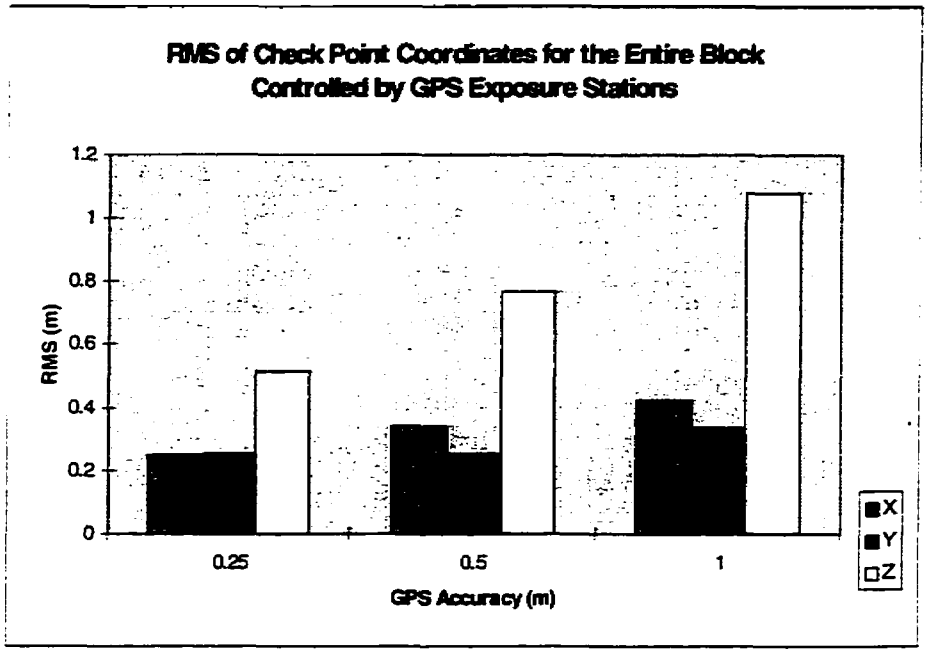

Figure 5. 9. RMS of Check Points Obtained from Method 3

Table 5. 7 and 5. 8 show the reliability measures for image coordinates and GPS coordinates of exposure stations for the various methods obtained from real data. Including the tower points in a single strip adjustment increases the reliability of the strip (Tables 5. 7 and 5. 8).

Table 5. 7. Reliability Measures for Image Coordinates Obtained from Real Data

Method	1		2		3	
Reliability Measure	x	y	x	y	x	y
r_i	0.13	0.43	0.22	0.51	0.13	0.43
$\delta_{0,i}$	14.51	6.18	12.08	5.70	14.20	6.23
$\bar{\delta}_{0,i}$	13.97	4.68	11.26	4.00	13.64	6.23

Table 5.8. Reliability Measures for GPS Derived Coordinates of Exposure Stations Obtained from Real Data

Method / Reliability Measure	1			2			3		
	X	Y	Z	X	Y	Z	X	Y	Z
r_i	0.71	0.64	0.77	0.74	0.69	0.76	N/A		
$\delta_{0,i}$	4.78	5.03	4.58	4.66	4.84	4.62	N/A		
$\bar{\delta}_{0,i}$	2.60	3.03	2.19	2.36	2.68	2.28	N/A		

The results obtained from both simulated and real data show that if kinematic GPS can provide decimetre-level accuracy for the camera exposure stations, then the strip adjustment can be carried out without any ground control points as long as the datum transformation is known. Normally, two or three strips of photography are taken to recover the roll angle of the aircraft and to increase the geometry of a single strip. This new technique for single strip adjustment eliminates the need for multiple strips of photography and reduces significantly both the time and the cost of the mapping project.

CHAPTER 6

SUMMARY, CONCLUSIONS, AND RECOMMENDATIONS

6. 1. Summary

A thorough analysis of GPS assisted aerial triangulation was carried out in this research. This analysis examined both the precision and the reliability of the combined GPS-photogrammetric blocks. Real data were used for the medium scale mapping, while for the large scale mapping, data were simulated.

A new technique for the single strip aerial triangulation was developed in this study. This technique takes advantage of geometric constraints of man-made structures to strengthen the geometry of the single strip. This was demonstrated using simulated and real data for a single strip.

A comprehensive software package, GAP (General Adjustment Program) was developed to integrate GPS, geodetic, and photogrammetric observations in a single unified least squares adjustment. It can be used to adjust a geodetic network, a photogrammetric block, or a combined geodetic-photogrammetric block. It can also incorporate GPS positions of the camera exposure stations into the block adjustment. Due to the huge number of unknowns for a large block of photography, the "KING" reordering scheme was adopted to minimize the bandwidth of the normal equations and reduce the memory and CPU requirements. GAP can be used to carry out both precision and reliability analyses.

6. 2. Conclusions

Based on the results obtained from real data for a medium scale mapping (1:10,000), the following conclusions can be drawn:

- Although using a dual frequency receivers like the one used in this study (Trimble 4000 SSE) can take advantage of a linear combination of L1 and L2 observations to eliminate the effects of the ionospheric errors, and to resolve the ambiguities quicker and more reliable, the results obtained from L1 carrier phase data did not deteriorate significantly as compared to the L1/L2 results (Figures 4.40 and 4.41).

- Accurate and reliable results in kinematic airborne GPS applications depend on the number of satellites being tracked, satellite geometry, the flight strip length, the stability of the signal reception in the individual strips, the inclination of the aircraft in the turning loops, and the consistency of the weather conditions.

- It is important to appropriately weight the various observations in the combined GPS-photogrammetric block adjustment in the presence of the systematic errors initiated from GPS and datum related errors, as well as errors in the interior orientation parameters of the camera.

- GPS-photogrammetric block is allowed to float to fit its position if low weights are assigned to both GPS observations and ground control points. However, the problem arises that the coordinate system is not sufficiently defined. GPS-photogrammetric block adjustments with no ground control points may have some unfortunate results if the interior orientation parameters are contaminated by systematic errors.

- In order to account for the differences between the ground control coordinate system and the GPS coordinate system, and to compensate for any systematic errors introduced from the interior orientation, self-calibration bundle block adjustment was carried out with appropriate weights for the GPS observations and available ground control points, and a simultaneous 3D similarity transformation between the two coordinate systems.

- The best results for medium scale mapping were obtained by solving for the additional parameters in a self calibration block adjustment, and including 4 ground control points at the corners of the block (Methods 7 or 8, Figure 4.51).

Based on the results obtained using simulated data for a typical large scale mapping project, (1:2,000), the following conclusions can be drawn:

- Due to the high accuracy needed for this type of mapping (less than 0.1 m), GPS coordinates of the exposure station should be determined with centimetre accuracy. The GPS data rate has to be selected as high as possible (1 or 0.5 Hz) to minimize the exposure station interpolation error. A dual frequency GPS receiver can take advantage of "widelane" observable for an accurate and reliable recovery of integer ambiguities. An advanced "On The Fly" ambiguity resolution technique helps to recover the ambiguities correctly.

- The accuracy of the adjusted object point coordinates obtained from GPS-photogrammetric block adjustment are better than those obtained from the conventional block adjustment, provided that the accuracy of the GPS coordinates of the exposure stations are better than 0.1 m (Figures 4.2 - 4.4).

- The adjusted object point coordinates are more precise than GPS coordinates of the exposure stations implying that the accuracy of point determination can be at centimetre level while the camera station accuracy is at decimetre level (Figures 4.2 - 4.4).

- From both the accuracy and reliability points of view, the best scenario for a GPS-photogrammetric block is to have a 60% sidelap, plus cross strips, to improve the geometry of the block (Figures 4.14 - 4.16 and Figures 4.20 and 4.21).

- Based on Figures 4.11 - 4.13, the flight strategy of extra strips and photographs is recommended due to the fact that the precision is worse both at the corners and edges of the block, especially for a block with no ground control points.

- The distribution of the precision of the object point coordinates in the interior part of the GPS-photogrammetric block is homogeneous both in planimetry and height (Figures 4.14 - 4.16). Conventional blocks normally include a dense distribution of the ground control points to reach such homogeneity of precision.

- The reliability of the image coordinates does not depend heavily on the ground control points in a GPS-photogrammetric block (Figures 4.20 and 4.21). Therefore, ground control points are not required in a GPS assisted aerial triangulation from the reliability point of view. The average reliability of the image coordinates obtained from a GPS-photogrammetric block adjustment is better than that of the conventional block adjustment.

- The replacement of the ground control points with GPS observations of the exposure stations can thoroughly avoid the poor reliability of the ground control points in a conventional block adjustment (i.e., configuration F, Figures 4.25 - 4.27).

- From the external reliability point of view, GPS-photogrammetric blocks offer more reliable results as compared to the conventional blocks (Configuration D, E, or F, Figures 4.28 - 4.29).

An important part of this dissertation was the development of a new technique for a single strip aerial triangulation. This technique is based on the geometric constraints of vertical man-made structures. Based on the results obtained from both simulated and real data, the following conclusions can be made:

- If the coordinates of the exposure stations can be provided by GPS with the accuracy at the range of 0.2 m to 0.5 m, then the results of the GPS single strip bundle adjustment are better or equal to those obtained from the full ground control strip adjustment (Figure 5.3).

- The roll angle of the camera can be recovered reliably using the tower structures in a GPS single strip aerial triangulation (Figure 5.5).

- Based on Table 5.2, including the tower points in a GPS controlled strip adjustment improves the reliability of both image coordinates, especially the y coordinates of the image points.

- The best results, using real data, were achieved from the method in which the tower structures were included in the strip adjustment when compared to the results from

the GPS-photogrammetric bundle block adjustment with two parallel strips (Figures 5.8 and 5.9).

- If imagery can provide tower structures with heights in the range of 2% to 7% of the flying height, the GPS single strip adjustment with constrained tower points can offer the required accuracy for a typical large scale mapping according to Table 5.5. The greater the number of tower points, the better the accuracy of the strip adjustment. However, the minimum number of tower points is 1 in every 5 photos.

- This new technique eliminates the need for multiple strips of photograph and has a positive impact on both the time and the cost of the mapping project.

6. 3. Recommendations

The following recommendations are proposed for the future studies:

- Although the implementation of the new technique for a single strip aerial triangulation was performed on real data, the airborne GPS data was simulated using "inverse photogrammetry" technique (projecting from the ground and tie points to the exposure stations). It is recommended that this new technique be examined using the actual airborne GPS data collected in a photogrammetric flight mission.

- As mentioned in Chapter 1, the best scenario in mapping projects is the direct acquisition of the exterior orientation parameters to accuracy sufficient that the aerial triangulation can be neglected. GPS multi-antenna approach in an airborne applications offers 10 arc minute accuracy, which is far from what is required. The main errors for attitude determination using GPS come from multipath and incorrect integer ambiguities. Therefore, more research needs to be done to reduce these errors.

An alternative is to use an integrated GPS-INS to fully measure all parameters of the exterior orientation. The high cost of INS is a factor to be considered.

- Overparametrization is a problem with using 6 linear shift and drift parameters per strip in a GPS-photogrammetric block adjustment. Singularity of the normal equation occurs when adding these additional unknown parameters to the regular unknown parameters. Cross strips or chains of vertical points across the block offers remedy to this problem, which directly affect the cost and the time of the mapping project. Another solution is to introduce GPS data recorded during the photo flight mission directly into the combined block adjustment without weakening the block by additional shift and drift parameters. With this method, one correction for every tracked satellite is required. If no cycle slip has been detected for some satellites, then, these satellites are connecting the flight strips and cross strips are not needed. Preliminary results for this method as obtained by Jacobsen (1996) are promising. However, more research needs to be done in this area to exploit the effectiveness of this integrated approach.

REFERENCES

Abdullah, Q. A. (1997), *Control Requirements for Single Strip Block Airborne GPS Triangulation*, Proceedings of ASPRS/ACSM, Annual Convention and Exposition, Seattle, Washington, Vol. 2, pp. 220-237.

Abidin, H (1991), *New Strategy For On The Fly Ambiguity Resolution*, Proceedings of ION-GPS 91, The Institute of Navigation, Alexandria, VA, pp. 875-886.

Ackermann, F.E. (1966), *On the Theoretical Accuracy of Planimetric Block Triangulation*, *Photogrammetria*, Vol. 21, pp. 145-170.

Ackermann, F.E. (1974), *Accuracy of the Statoscope Data: Results from OPEEPE test Oberschwaben*, ISP Symposium, Commission III, Stuttgart, Germany.

Ackermann, F.E. (1975), *Results of Recent Test in Aerial Triangulation*, **Photogrammetric Engineering and Remote Sensing**, Vol. 41, No. 1, pp. 91-99.

Ackermann, F.E. (1984), *Utilization of Navigation Data for Aerial Triangulation*, Commission III, , **International Congress for Photogrammetry and Remote Sensing,** Rio de Janeiro.

Ackermann, F.E. (1992), *Operational Rules and Accuracy Models for GPS Aerial Triangulation*, **International Archives of Photogrammetry and Remote Sensing**, Washington D.C., pp. 691-700.

Ackermann, F.E. (1994), *On the Status and Accuracy Performance of GPS Photogrammetry*, **Proceedings of Mapping and Remote Sensing Tools for the 21st Century**, Washington D.C., August 26-29, pp 80-90.

Ackermann, F.E. and H. Schade (1993), *Application of GPS for Aerial Triangulation*, **Photogrammetric Engineering and Remote Sensing**, Vol. 59, No. 11, pp.1625-1632.

Alobaida, A., (1993), *Design and Simulation of a Real-Time Mapping Satellite for the Kingdom of Saudi Arabia*, Ph.D. Dissertation, Department of Geodetic Science and Surveying, The Ohio State University.

Baarda, W., 1968, *A Testing Procedure for Use in Geodetic Networks*, Netherlands Geodetic Commission, Publications on Geodesy, New Series, Vol. 2, No. 5, Delft, Netherlands.

Black, H.D. (1978), *An Easily Implemented Algorithm for Tropospheric Range Correction*, **Journal of Geophysical Research**, 38(B4), pp. 1825-1828.

Blais, J.A.R. (1976), *SPACE-M; Spatial Photogrammetric Adjustment for Control Extension using Independent Models*, Commission III, **International Congress for Photogrammetry and Remote Sensing** , Helsinki, Finland.

Blais, J.A.R. and M.A. Chapman (1984), *The Use of Auxiliary Airborne Sensor Data in SPACE-M Photogrammetric Block Adjustment*, **The Canadian Surveyor**, Vol. 38, No. 1, pp. 3-14.

Brown, D.C. (1966), *Decentering Distortion of Lenses*, **Photogrammetric Engineering**, Vol. 32, No.3, pp. 444-462.

Brown, D.C. (1976), *The Bundle Adjustment: Progress and Prospects*, **XIIIth International Congress for photogrammetry and Remote Sensing**, Helsinki, Finland.

Brown, D.C. (1979), *Establishment of Photogrammetric Control by Satellite Doppler Positioning*, **Proceedings of the International Symposium on Current Trends in the Development, Execution, and Use of Aerial Triangulation**, Brisbane, Queensland.

Burman H., and K. Tolegård (1994), Empirical Results of GPS Supported Block Triangulation, OEEPE Publication.

Cannon, M.E. (1987), *Kinematic Positioning Using GPS Pseudorange and Carrier Phase Observations*, **M. Sc. Thesis**, Department of Geomatics Engineering, University of Calgary, Calgary.

Cannon, M.E. (1990), *High Accuracy GPS Semi-Kinematic Positioning: Modeling and Results*, **Navigation,** Vol. 37, No.1, pp. 53-64.

Cannon, M.E. (1991), *Airborne GPS/INS with an Application to Aerotriangulation*, **Ph.D. Dissertation,** Department of Geomatics Engineering, University of Calgary, Calgary.

Chapman, M.A. (1994), *Lecture Notes on Digital Stereo Image Processing*, Department of Geomatics Engineering, University of Calgary, Calgary.

Colomina, I. (1993), *A Note on the Analytics of Aerial Triangulation with GPS Aerial Control*, **Photogrammetric Engineering and Remote Sensing**, Vol 59, No. 11, pp. 1619-1624.

Combs, J. E., J. W. Crabtree, J. Kim, and M. E. Lafferty (1980), *Planning and Executing the Photogrammetric Project*, Chapter VII, Manual of Photogrammetry, 4th Edition, pp. 367-412.

Corten, F.L. (1960), *Survey Navigation and Determination of Camera Orientation Elements*, **Photogrammetria**, Vol 15., pp. 251-281.

Corten, F.L. and F.J. Heimes (1976), *Integrated Flight and Navigation System*, Commission I, **International Congress for Photogrammetry and Remote Sensing,** Helsinki, Finland.

Curry, S. and K. Schuckman (1993), *Practical Considerations for the Use of Airborne GPS for Photogrammetry*, **Photogrammetric Engineering and Remote Sensing**, Vol 59, No. 11, pp.1611-1617.

Chen. D., (1994), Development of A Fast Ambiguity Search Filtering (FASF) Method For GPS Carrier Phase Ambiguity Resolution, Ph.D. Dissertation, UCGE Report No. 20071, Department of Geomatics Engineering, University of Calgary.

Ebadi, H. and M.A. Chapman (1995), *An Experience on GPS Assisted Aerotriangulation*, **Proceedings of the 7th International Conference on Geomatics**, June 13-15, Ottawa.

Ebner, H. (1972), *Theoretical Accuracy Models for Block Triangulation*, Bildmessung Und Luftbildesen, Vol 40, pp. 214-221.

Ebner, H. (1976), *Self Calibrating Block Adjustment*, Invited Paper of Commission III, ISP Congress, Helsinki, Finland.

El Hakim, S.F. (1979), *Potentials and Limitations of Photogrammetry for Precision Surveying*, **Ph.D. Dissertation,** Department of Geodesy and Geomatics Engineering, University of New Brunswick, Fredericton.

Erickson, C., (1992), *Investigations of C/A Code and Carrier Measurements and Techniques for Rapid Static GPS Surveys*, M.Sc. Thesis, UCGE Report No. 20044, Department of Geomatics Engineering, University of Calgary.

Faig, W. (1976), *Independent Model Triangulation with Auxiliary Vertical Control*, Commission III, **International Congress for Photogrammetry and Remote Sensing**, Helsinki, Finland.

Faig, W. (1979), *Canadian Experiences in the Adjustment of Large Photogrammetric Blocks with Auxiliary Vertical Control*, **Proceedings of the International Symposium on Current Trends in Aerial Triangulation,** Brisbane, Queensland.

Faig, W. (1985), *Lecture Notes on Aerial Triangulation and Digital Mapping*, **Monograph 10**, School of Surveying, The University of New South Wales, Kensington, N.S.W., Australia.

Faig, W. and T.Y. Shih (1989), *Should One Consider Combining Kinematic GPS with Aerial Photogrammetry?*, **Photogrammetric Engineering and Remote Sensing**, Vol. 55, No. 12, pp. 1723-1725.

Förstner, W. (1985), *The Reliability of Block Triangulation*, **Photogrammetric Engineering and Remote Sensing,** Vol. 51, pp. 1137-1149.

Fraser, C. S. (1995), *Observational Weighting Considerations in GPS Aerial Triangulation*, **Photogrammetric Record**, 15(86), pp. 263-275.

Frieβ, P. (1987), *The NAVSTAR Global Positioning System for Aerial Photogrammetry*, **Proceedings of the 41st photogrammetric week at Stuttgart University**, Stuttgart, Germany.
Frieβ, P. (1991), *GPS Supported Aerial Triangulation, Empirical Results*, **Proceedings of the 2nd International Workshop on High Precision Navigation**, Dummler, Verlag, Bonn, Germany, pp. 7-18.

Frieβ, P. (1992), *Experience with GPS Supported Aerial Triangulation*, **Proceedings of ISPRS**, Commission I, Vol. 29, Part B1, Washington D.C., pp. 299-305.

Gelb, A. (1974), *Applied Optimal Estimation*, **The MIT Press,** Cambridge, Mass, U.S.A.

George, A. and J. Liu, (1995), *Computer Solution Of Sparse Linear Systems*, Publication of The Computer Science Department, University Of Waterloo, Canada.

Georgiadou, Y. and A. Kleusberg (1989), *Multipath Effects in Static and Kinematic GPS Positioning*, **Proceedings of IAG International Symposium 102 on Global Positioning System: An Overview**, Springer Verlag, New York, pp. 82-89.

Georgiadou, Y. and A. Kleusberg (1991), *Algorithms and Results of Kinematic GPS Positioning*, **CICM Journal ACSGC**, Vol. 45, No. 4, pp. 569-579

Greening, W. J. T, B. A. Chaplin, D. G. Sutherland, and D. E. DesRoche (1994), *Commercial Applications of GPS-Assisted Photogrammetry*, Proceedings of the Fourth GPS/GIS Conference, Washington, D.C., pp. 391-402.

Grün, A. (1978), *Experience with Self Calibrating Bundle Adjustment*, ASP Annual Meeting, Washington D.C.

Habib, A. and K. Novak (1994), *GPS Controlled Aerial Triangulation of Single Flight Lines*, **Proceedings of ASPRS/ACSM**, Annual Convention and Exposition, Reno, Nevada, Vol. 1, pp. 225-235.

Hanson, R.H., (1978), *A Posteriori Error Propagation*, **Proceedings Of The Second International Symposium On Problems Related To The Redefinition Of North American Geodetic Networks**, Washington, D.C., National Geodetic Information Centre, NOAA, pp. 427-445.

Hatch, R. (1990), *Instantaneous Ambiguity Resolution*, **Proceedings of the FIG Symposium on Kinematic Systems in Geodesy, Surveying, and Remote Sensing**, Symposium 107, Banff, Alberta, pp. 295-307.

Hofmann-Wellenhof, B., H. Lichtenegger, and J. Collins, (1992), *GPS: Theory and Practice*, Second Edition, Springer-Verlag Wien, New York, N.Y.

Hopefield, H.S. (1969), *Two-quadratic Tropospheric Refractivity Profile for Correcting Satellite Data*, **Journal of Geophysical Research**, 74(I8), pp. 4487-4499.

Jacobsen, K. (1996), *A New Approach of Combined Block Adjustment Using GPS-Satellite Constellation*, **Proceedings of the International Congress on Photogrammetry and Remote Sensing**, Commission III, Vienna, Austria, Vol. XXXI, Part B3, pp. 355-359

Jennings, A., (1977), *Matrix Computation For Engineers And Scientists*, John-Wiley & Sons, New York, N.Y.

King, J.P., (1970), *An Automatic Reordering Scheme For Simultaneous Equations Derived From Network Systems*, International Journal For Numerical Methods in Engineering, Vol. 2, pp. 523-533.

Klobuchar, J. (1983), *Ionospheric Effect on Earth-Space Propagation*, **Report No. ERP-866**, Airforce Geophysics Laboratory, Hanscom, AFB, Mass.

Krabill, W.B., Martin, C.F., and R.N. Swift (1989), *Applying Kinematic GPS to Airborne Laser Remote Sensing*, **Proceedings of the 2nd International Technical Meeting for ION-GPS**, Colorado Springs, U.S.A., pp. 39-43.

Krakiwsky, E .J. (1990), *The Method of Least Squares: A Synthesis of Advances*, UCGE Report No. 10003, Department of Geomatics Engineering, University of Calgary.

Lachapelle, G. (1991), *GPS Observables and Error Sources for Kinematic Positioning*, **Proceedings of IAG International Symposium 107 on Kinematic Systems in Geodesy, Surveying, and Remote Sensing**, Springer Verlag, New York, September 10-13, pp. 17-26.

Lachapelle, G., Cannon, M.E., and G. Lu (1992), *High Precision GPS Navigation with Emphasis on Carrier Phase Ambiguity Resolution*, **Marine Geodesy**, Vol. 15, pp. 253-269.

Lachapelle, G., Cannon, M.E., and H. Schade (1993), *An Accuracy Analysis of Airborne Kinematic Attitude Determination with the NAVSTAR Global Positioning System*, **SPN**, pp. 90-95.

Lachapelle, G. (1993), *Lecture Notes on NAVSTAR GPS; Theory and Applications*, Department of Geomatics Engineering, University of Calgary, Calgary.

Lapine, L., (1991), *Analytical Calibration of the Airborne Photogrammetric System Using A Priori Knowledge of the Exposure Station Obtained from Global Positioning System Technique*, Ph.D. Dissertation, Department of Geodetic Science and Surveying, The Ohio State University, Publication No. 9111738, Ann Arbor, MI 48109

Li, D. and S. Jie (1989), *Quality Analysis of Bundle Block Adjustment with Navigation Data*, **Photogrammetric Engineering and Remote Sensing**, Vol. 55, No. 12, pp. 1743-1746.

Liu, C., (1993), Precise GPS Positioning in The Marine Environment, M.Sc. Thesis, UCGE Report No. 20055, Department of Geomatics Engineering, University of Calgary.

Lucas, J.R. (1987), *Aerotriangulation without ground control*, **Photogrammetric Engineering and Remote Sensing**, Vol. 53, No. 3, pp. 311-314.

Martin, E.H. (1980), *GPS User Equipment Error Models*, **Global Positioning System**, Vol. 1, Institute of Navigation, Washington D.C., pp. 109-118.

Milbert, D.G., (1984), *Heart Of Gold: Computer Routines For Large, Sparse, Least Squares Computations*, NOAA Technical Memorandum NOS NGS-39.

Miliken, R.J. and Zoller, C.J. (1990), *Principle of Operation of NAVSTAR GPS and System Characteristics*, **Global Positioning System**, Volume I, Institute of Navigation, Washington D.C., pp. 3-14.

Molenaar, M. (1984), *The Connection of Aerotriangulation Blocks and Ground Control Reconsidered*, Commission III, ISPRS Congress, Rio de Janeiro, pp. 721-736.

Moniwa, H. (1977), *Analytical Photogrammetric System with Self Calibration and its Applications*, **Ph.D. Dissertation**, Department of Geodesy and Geomatics Engineering, University of New Brunswick, Fredericton.

Remondi, B. (1984), *Using the Global Positioning System (GPS) Phase Observable for Relative Geodesy: Modeling, Processing, and Results*, CSR-84-3, Centre for Space Research, The University of Texas, Austin.

Saastamoinen, J. (1973), *Contributions to the Theory of Atmospheric Refraction*, **Bulletin Geodesique**, Vol. 105-107, pp. 279-298, 283-297, 13-34.

Schut, G.H. (1968), *Formation of Strips from Independent Models*, **Photogrammetric Engineering**, Vol 34., No. 7., pp. 690-695.

Salmenpera, H., Anderson, J.M., and A. Savolainen (1974), Efficiency of The Extended Mathematical Model In Bundle Adjustment, Bildmessung Und Luftbildwesen, Vol. 6.

Schwarz, K.P., Cannon, M.E., and R.V.C Wong (1989), *A Comparison of GPS Kinematic Models for the Determination of Positions and Velocity along a Trajectory*, **Manuscripta Geodetica**, Springer Verlag, Vol. 14, pp. 345-353.

Schwarz, K.P., Chapman, M.A., Cannon, M.E., and P. Gong (1993), *An Integrated INS/GPS Approach to the Georeferencing of Remotely Sensed Data*, **Photogrammetric Engineering and Remote Sensing**, Vol. 55, No. 12, pp. 1667-1674.

Shi, J. (1994), High Accuracy Airborne Differential GPS Positioning Using A Multi-Receiver Configuration, M.Sc. Thesis, UCGE Report No. 20061, Department of Geomatics Engineering, University of Calgary.

Vaníček, P., E. J. Krakiwsky, M. R. Craymer, Y. Gao, and P. S. Ong, 1991, Robustness Analysis, Technical Report No. 156, Department of Geodesy and Geomatics Engineering, University of New Brunswick, Canada.

Waypoint Consulting Inc.(1994), Reference Manual for GRAFNAV.

Wells, D.E., N. Beck, D., Delikaraoglou, A. Kleusberg, E.J. Krakiwsky, G. Lachapelle, R.B. Langley, M. Nakiboglou, K.P. Schwarz, J.M. Tranquilla, and P. Vanicek (1986), *Guide to GPS Positioning*, Canadian GPS Associates, Fredericton.

Zarzycki, J.M. (1972), *The Use of Auxiliary Data in Aerial Triangulation*, Commission III, ISPRS Congress, Ottawa.

APPENDIX A

CONCEPTS AND MODELS OF GPS KINEMATIC POSITIONING

Global Positioning System (GPS) concepts and the mathematical models used in kinematic positioning are outlined in this appendix. The basic concept of Global Positioning System , GPS observables, and their associated mathematical models are described. The various errors affecting GPS positioning and the remedies to reduce or eliminate them are also explained.

A. 1. Global Positioning System (GPS)

GPS is a satellite-based radio positioning system developed by the U.S. Department of Defense (DOD) for accurate positioning and navigation. Radio signals are used from a constellation of earth-orbiting satellites to determine the 3D position of a receiver. The system consists of 21 satellites and three spare satellites orbiting approximately 20,000 km above the earth's surface in six orbital planes, having a period of 12 hours. GPS is an all-weather positioning system providing 24 hour world-wide coverage with at least four satellites in view at any time (Miliken et al., 1990 and Wells et al., 1986). The system has been fully operational since 1993.

GPS has three main components; the satellite system, the control system, and the users. The control system is operated by the U.S. Air Force for the Joint Program Office (JPO) of the DOD. The system consists of five monitoring stations distributed around the world. The role of these stations is to monitor the health of the satellites. These tracking stations receive signals from the satellites and transmit the collected data to the master

station where new ephemerides are computed and the navigation messages are prepared for uploading to the satellites.

A. 1. 1. User Segment

Users are the third component of GPS. Civilian users wish to determine their positions using GPS signals. There are mainly three observables which have been implemented in most GPS receivers:

- Pseudorange
- Carrier beat phase
- The rate of phase change

Both position and velocity of a moving platform can be calculated by measuring signals from different GPS satellites (Wells et al., 1986).

A. 2. GPS Signals

The GPS signals are transmitted autonomously from all GPS satellites on two carrier frequencies; L1 frequency at 1575.42 MHz and L2 frequency at 1227.60 MHz. C/A code of 1.023 MHz is modulated on the L1 carrier and P code of 10.23 MHz is modulated on both L1 and L2 carriers. A satellite message containing the satellites' ephemeris is also modulated on both carriers. A summary of the signal components is given in Table A.1.

Table A. 1. GPS Signal Components (from Erickson, 1992)

Carrier	Frequency	Wavelength	Modulation	Frequency	Chip length
L1	1575.42 MHz	19 cm	C/A code	1.023 MHz	293 m
			P code	10.23 MHz	29.3 m
			Message	50 MHz	
L2	1227.60 MHz	24 cm	P code	10.23 MHz	29.3 m
			Message	50 MHz	

There are two types of receivers; Single Frequency (receiving only L1 signal) and Dual Frequency (receiving both L1 and L2 signals). Most C/A code receivers correlate the incoming signal from a satellite with a replica of the code generated in the receiver. The dual frequency receivers provide access to P code data through code correlation resulting in a full L2 wavelength of 24 cm. Due to a high absolute accuracy available using P codes, Selective Availability (SA) is turned on to deteriorate the positioning accuracy.

The type of data that a receiver collects has a direct impact on both achievable accuracy and its price. The C/A code receivers are the least expensive receivers on the market which determine real time positions with horizontal accuracy of 100 m and vertical accuracy of 156 m (Lachapelle, 1993). P code receivers provide accuracies at the level of 25 m (horizontal) and 30 m (vertical) in real time mode. Access to P code is limited to U.S. and NATO military users.

Receivers which compute their positions based on carrier phase observations are more accurate because of the much finer resolution of the 19 cm and 24 cm carrier

wavelengths. The most sophisticated and expensive receivers are dual frequency P code receivers that provide accuracy ranging from a part per million to a few part per billion. Between theses two extreme cases, one can find a wide range of receivers which meet the users' accuracy requirements.

A. 3. GPS Observables

A pseudorange (code observation) is the difference between the transmission time at the satellite and the reception time at the receiver (Erickson, 1992). Pseudorange between the satellite and the receiver is obtained by scaling it using the speed of light. The observation equation for a pseudorange is given as (Wells et al., 1986);

$$p = \rho + c(dt - dT) + d_\rho + d_{ion} + d_{trop} + \varepsilon_p \qquad \text{A.1}$$

where

p is the observed pseudorange,

ρ is the unknown satellite-receiver range,

c is the speed of light,

dt is the satellite clock error,

dT is the receiver clock error,

d_ρ is the orbital error,

d_{ion} is the ionospheric error,

d_{trop} is the tropospheric error,

ε_p is the code measurement noise and multipath.

The code measurement noise, ε_p, is a function of the code receiver noise, ε_{prx}, and multipath, ε_{mult}, (Lachapelle, 1991).

The satellite-receiver range, ρ, has the form of:

$$\rho = \sqrt{(X^s - X_r) + (Y^s - Y_r) + (Z^s - Z_r)} \qquad \text{A.2}$$

where

(X^s, Y^s, Z^s) are satellite coordinates computed using broadcast ephemeris,

(X_r, Y_r, Z_r) are the unknown receiver coordinates.

For single point positioning, the number of unknowns are four (X_r, Y_r, Z_r, dT), therefore, a minimum of four satellites are required to solve for a solution at a single epoch.

The carrier phase observation is a measure of the misalignment between an incoming signal and replica of it generated by the receiver oscillator when a satellite is locked on. If a continuous lock is assumed, this measurement is a sum of the initial phase misalignment at epoch t_0 and the number of integer cycles from epoch t_0 to the current epoch t. The measured carrier phase can be written as (Erickson, 1992):

$$\Phi_{measured} = \text{fraction}(\Phi) + \text{integer}(\Phi, t_0, t) \qquad \text{A.3}$$

Carrier phase measurements are converted from cycles to units of lengths by their wavelengths. An ambiguity term (the unknown number of integer cycles between the satellite and receiver at starting epoch t_0) should be added to carrier phase measurement in order to represent a satellite-receiver range. The carrier phase observation equation is written as (Lachapelle, 1993):

$$\Phi = \rho + c(dt - dT) + \lambda N + d_\rho - d_{ion} + d_{trop} + \varepsilon_\Phi \qquad \text{A.4}$$

where

Φ is the observed carrier phase,

ρ is the unknown satellite-receiver range,

c is the speed of light,

dt is the satellite clock error,

dT is the receiver clock error,

λ is the carrier wavelength,

N is the unknown integer cycle ambiguity,

d_ρ is the orbital error,

d_{ion} is the ionospheric error,

d_{trop} is the tropospheric error,

ε_Φ is the carrier phase measurement noise and multipath.

The differences between pseudorange and carrier phase observation equations are the addition of ambiguity term, λN, for carrier phase observations and the reversal of signs for the ionospheric correction term d_{ion} due to the phase advance, while code is delayed.

Doppler frequency is the third fundamental GPS observation which is the first derivative of the carrier phase with respect to time. The Doppler frequency is measured on the pseudorange. The observation equation for GPS Doppler frequency can be written as (Liu, 1993):

$$\dot{\Phi} = \dot{\rho} + c(\dot{dt} - \dot{dT}) + \dot{d}_\rho - \dot{d}_{ion} + \dot{d}_{trop} + \varepsilon_{\dot{\Phi}} \qquad \text{A.5}$$

where (-) denotes a time derivative. As seen in the above equation, this measurement is not a function of the carrier phase ambiguity, therefore, it is free from cycle slips and can be used to determine the receiver velocity.

A. 4. GPS Error Sources

The GPS errors consist of orbital errors, satellite and receiver clock errors, tropospheric and ionospheric delays, receiver noise, and multipath. They are explained in the following sections.

A. 4. 1 Orbital Error

Orbital error initiates from the uncertainties of the predicted ephemerides and Selective Availability (SA). An estimation of the broadcast ephemerides error is about 20 m. If post-mission ephemerides are used, then the precise orbits are accurate to 1 m. SA is implemented by both satellite clock dithering and degrading satellite orbital information to prevent unauthorized real-time use of full GPS position and velocity accuracy.

A. 4. 2. Satellite and Receiver Clock Errors

The satellite clock error is defined as the difference between satellite clock time and true GPS time. The functional relationship between these two times is given as (Wells et al., 1986):

$$\Delta t_{sv} = a_0 + a_1(t - t_0) + a_2(t - t_0)^2 \qquad \text{A.6}$$

where

Δt_{sv} is the difference between satellite clock and GPS time,

t is the measurement transmission time,

t_0 is the reference time,

a_0 is the satellite clock time offset,

a_1 is the frequency offset,

a_2 is the frequency drift.

GPS satellites use atomic clocks which maintain a highly accurate GPS time. However, the accuracy is deteriorated by SA. Single differencing between two receivers removes the satellite clock error.

Receiver clock error is defined as the offset of the receiver clock time with respect to GPS time. Geodetic receivers are generally synchronized with GPS time before observation sessions but this synchronization accuracy is at the millisecond level. The receiver clock may also drift after synchronization. The receiver clock error depends on receiver hardware and can be estimated as an unknown parameter or eliminated by differencing from one receiver to two satellites.

A. 4. 3. Tropospheric and Ionospheric Delays

The tropospheric delay is caused by the refractions of a GPS signal in the lower atmosphere (the layer from the earth surface to approximately 60 km). The magnitude of this delay is influenced by a number of parameters such as the temperature, humidity, pressure, and the type of the terrain below the signal path. A number of studies have been performed to create tropospheric models (Hopefield, 1969, Saastamoinen, 1973, Black, 1978). A thorough analysis of these models can be found in (Hofmann et al., 1992).

The ionospheric layer is roughly from 50 to 1000 km above the earth surface. GPS signals traveling through the ionosphere are affected by both refraction and dispersion. The refractive group index of the ionosphere is greater than 1, meaning that the group velocity of radio waves is less than the speed of light in vacuum. The refractive phase index of ionosphere is less than 1, therefore, the phase velocity of radio waves is greater than the speed of light in vacuum. This causes an advance on the measured carrier phase and delay on the measured pseudorange. The ionospheric delay is directly determined by the Total Electron Content (TEC) along the propagation path (Klobuchar, 1983). The ionospheric error may range from 5 m (at night, the satellite at the zenith) to 150 m (at midday and the satellite at low elevation)(Wells et al. 1986).

Ionospheric effect can be assessed by taking dual frequency measurements and using the dispersive nature of the ionosphere. The techniques based on dual frequency correction can remove most of the ionospheric error. However, during high solar activity cycle and mid afternoons this technique may not be adequate for certain applications (Well et al., 1986). Another way to reduce ionospheric effect is to use differencing observations from one satellite between two stations due to the spatial correlation between the stations. The third method is to apply the broadcast model for reducing the ionospheric error (Klobuchar, 1983).

A. 4. 4. Receiver Noise

Receiver measurement noise includes the thermal noise intercepted by the antenna or generated by the internal components of the receiver (Martin, 1980). It is affected by signal to noise density, the tracking bandwidth, and code tracking mechanization parameters. The noise levels for C/A code pseudorange is 1m, for P code pseudorange is

10 cm and for carrier phase is 5 mm. The new narrow co
achieve 10 cm accuracy for C/A code pseudorange.

A. 4. 5 Multipath

Multipath is the phenomena where the reception o
and surfaces in the environment around the antenna (Liu,
can reach up to one chip length of the PRN codes (e.g. 2
for P code) while carrier phase multipath is less than 25%
(e.g. 5 cm for L1)(Georgiadou and Kleusberg, 1989). In
multipath error signatures are generally randomized due to
(Shi, 1994).

A. 5. Differential GPS

In order to achieve high accuracy for geodetic pos
carrier phase observations techniques are used to elimina
sources.

A. 5. 1 Single Differencing

The observation equations for pseudorange, carrier
contain bias terms such as satellite and receiver clo
atmospheric effects. Many of these errors are spatially co
the receivers tracking simultaneous satellites. Some errors
atmospheric, and satellite clock errors) and some errors a
clock error). Single differencing (between satellites or t

differencing (between receivers and between satellites) of GPS observations can be applied to eliminate or effectively reduce the common errors. The single " between receivers" and " between satellites" differences are shown in Figures A.1 and A.2.

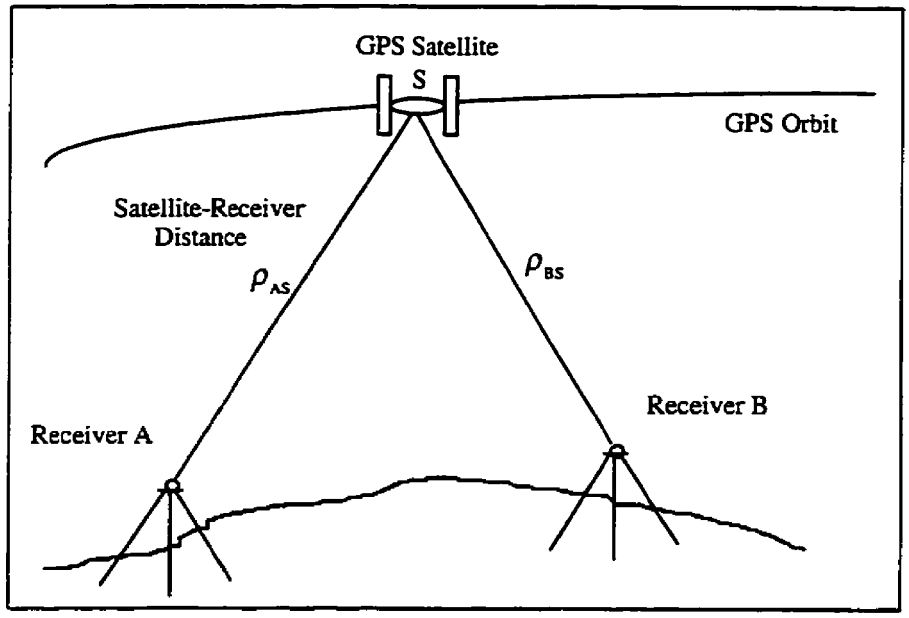

Figure A.1. Single Differencing Between Receivers

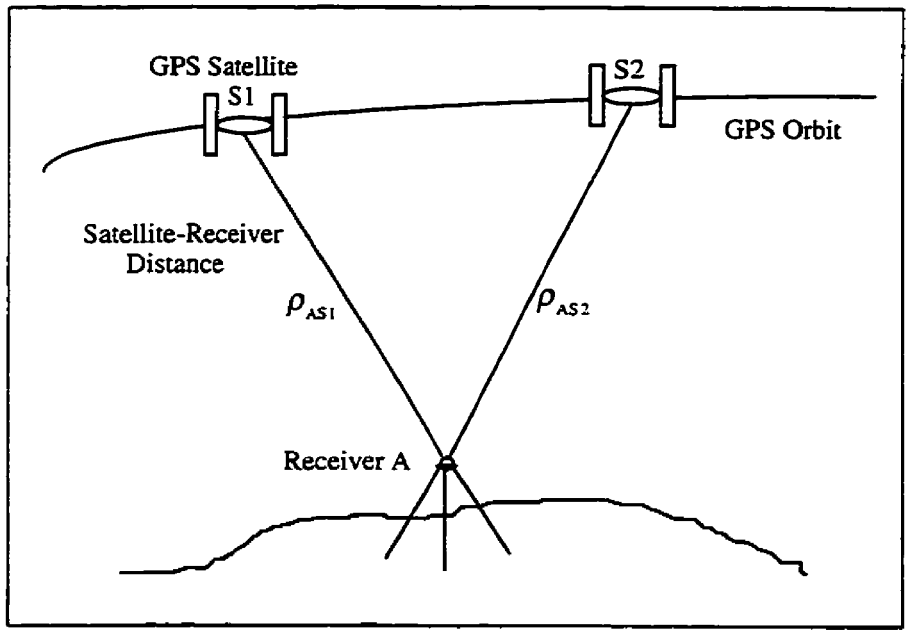

Figure A.2. Single Differencing Between Satellites

A. 5. 2. Double Differencing

This technique is based on taking difference between receivers and between satellites (Figure A.3).

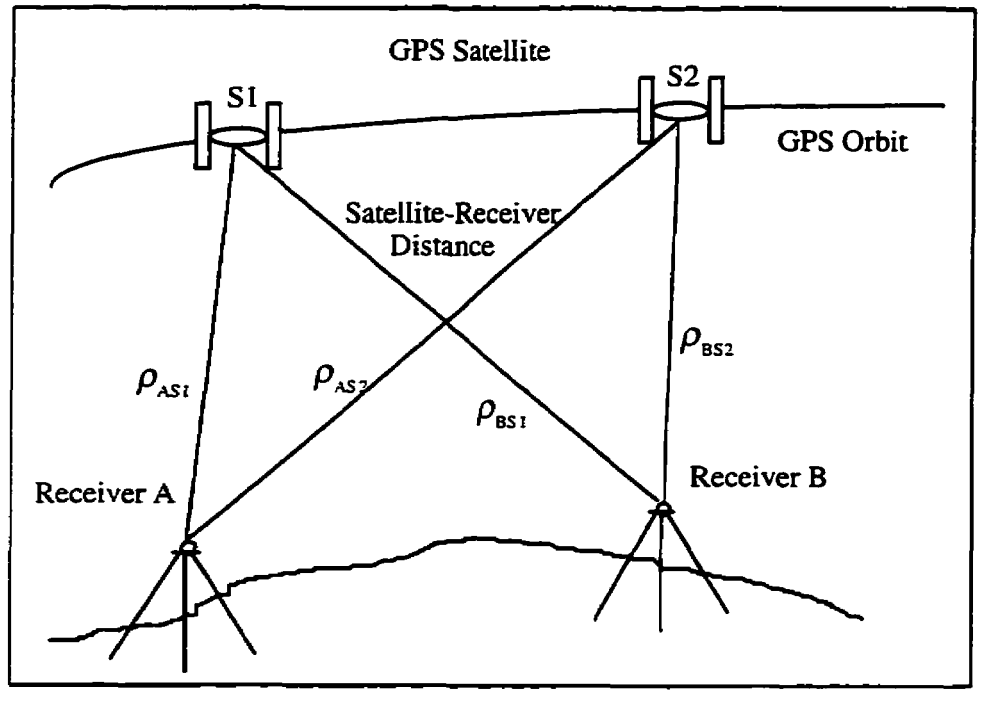

Figure A.3. Double Differencing

Double difference observation equations are written as(Lachapelle, 1993):

$$\nabla\Delta p = \nabla\Delta\rho + \nabla\Delta d_\rho + \nabla\Delta d_{ion} + \nabla\Delta d_{trop} + \nabla\Delta\varepsilon_p \quad \text{A.13}$$

$$\nabla\Delta\Phi = \nabla\Delta\rho + \nabla\Delta d_\rho + \lambda\nabla\Delta N - \nabla\Delta d_{ion} + \nabla\Delta d_{trop} + \nabla\Delta\varepsilon_\Phi \quad \text{A.14}$$

$$\nabla\Delta\dot{\Phi} = \nabla\Delta\dot{\rho} + \nabla\Delta\dot{d}_\rho - \nabla\Delta\dot{d}_{ion} + \nabla\Delta\dot{d}_{trop} + \nabla\Delta\dot{\varepsilon}_\Phi \quad \text{A.15}$$

where $\nabla\Delta$ denotes the double difference operator between two stations and two satellites.

The advantage of using this observable is that both the receiver and satellite clock errors have been canceled out, while the disadvantage is increased noise. This method also allows to optimally exploit the integer nature of carrier phase ambiguity. Double differencing GPS positioning is considered as the best processing method (Cannon, 1987,1991, Remondi,1984). This observable still contains the double difference ambiguity term which has to be resolved before the beginning of the kinematic mission and then fixed in kinematic surveys. In airborne kinematic positioning, cycle slips may often occur in carrier phase observation due to aircraft dynamics (e.g. turning) and multipath effects. Therefore, it is mandatory to resolve ambiguity on the fly for precise GPS positioning.

A. 6. Algorithms for Kinematic GPS

There are mainly two algorithms being used in kinematic GPS; Kalman filtering and least squares (Schwarz et al., 1989, Cannon, 1987,1991, Georgiadou and Kleusberg, 1991). Under certain conditions, one algorithm is equivalent to the other one in terms of computational aspects. It is important to know about the features of the algorithms and their relationships in kinematic GPS.

A. 6. 1 Kalman Filter Algorithm

Assuming the system model and measurement model have the form of:

$$X_k = \Phi_{k,k-1} X_{k-1} + W_{k,k-1} \qquad \text{A.16}$$

$$l_k = A_k X_k + \varepsilon_k \qquad \text{A.17}$$

for the update equations:

$$\hat{X}_k(+) = \hat{X}_k(-) + K_k\{l_k - A_k\hat{X}_k(-)\} \quad \text{A.18}$$

$$C_k^X(+) = \{I - K_k A_k\} C_k^X(-) \quad \text{A.19}$$

$$K_k = C_k^X(-) A_k^T \{A_k C_k^X(-) A_k^T + C_l^{-1}\}^{-1} \quad \text{A.20}$$

and for the prediction equations:

$$\hat{X}_k(-) = \Phi_{k,k-1}\hat{X}_{k-1}(+) \quad \text{A.21}$$

$$C_k^X(-) = \Phi_{k,k-1} C_{k-1}^X(+) \Phi_{k,k-1}^T + C_{k,k-1}^W \quad \text{A.22}$$

where

X is the state vector,

Φ is the transition matrix,

I is the identity matrix,

W is the system process noise vector,

A is the design matrix,

ε is the measurement noise,

k is the epoch number,

C^W is the covariance matrix of W,

K is the Kalman gain matrix,

C_l is the covariance matrix of l,

C^X is the covariance matrix of X,

(-) is a predicted quantity,

(+) is an updated quantity,

(^) is an estimated quantity.

Different definitions of the transition matrix, Φ, and the covariance of the system process noise, C^W, can be used based on the choice of the state space model for kinematic GPS (Schwarz et al., 1989). The covariance matrix of the system process noise, C^W, is given as (Shi, 1994):

$$C^W = \int_0^{\Delta t} \Phi(z) Q(z) \Phi^T(z) dz \qquad \text{A.23}$$

where Q is the spectral density matrix. The state space model is affected by parameters such as, the system dynamics, state vector, and the assumption on the process behavior of the system (Gelb, 1974, Schwarz et al., 1989). The state space model plays an important role in improving the interpolation accuracy when the data rate is low. Schwarz et al. (1989) have shown that with a 3 seconds data rate, positioning accuracy improves when using a constant velocity model and velocity accuracy improves when using a constant acceleration model.

The Kalman filter can be implemented with different kinematic GPS models and different measurements (Shi, 1994). The process noise is also fully used in the filter by considering the spectral density matrix, Q, which allows the system to adjust the contribution to the estimates from the observables at the measurement epoch versus a contribution before the epoch.

The Kalman filter is usually employed in kinematic GPS applications where the remote receiver is installed on a moving platform and the reference receiver is set up on the ground station.

A. 6. 2. Least Squares Algorithm

The least squares algorithm for kinematic GPS does not use dynamic information (Georgiadou and Kleusberg, 1991). In this algorithm, no assumption is made on the remote motion and no system process noise is considered. If a priori information about

unknown parameter is used, the approach is called sequential least squares but if only observables at the measurement epoch are used, it is called the least squares approach.

If the measurement model is considered as:

$$l_k = A_{k-1} X_{k-1} + \varepsilon_{k-1} \qquad \text{A.24}$$

then the equation for the estimated vector and its covariance matrix in the sequential least squares approach are given as (Krakiwsky, 1990):

$$\hat{X}_k(-) = \hat{X}_{k-1}(+) + \Delta X \qquad \text{A.25}$$

$$C_k^X(-) = C_{k-1}^X + C^{\Delta X} \qquad \text{A.26}$$

$$\hat{X}_k = \hat{X}_k(-) + \left[A_k^T C_l^{-1} A_k + \{C_k^X\}^{-1}\right]^{-1} A_k^T C_l^{-1} \left[l_k - A_k \hat{X}_k(-)\right] \qquad \text{A.27}$$

$$C_k^X = \left[A_k^T C_l^{-1} A_k + \{C_k^X(-)\}^{-1}\right]^{-1} \qquad \text{A.28}$$

where

ΔX is the increment vector over two successive epochs,

$C^{\Delta X}$ is the covariance matrix of ΔX,

(-) is for an estimate based on data collected before epoch k.

The equations for least squares approach are written as:

$$\hat{X}_k = \left[A_k^T C_l^{-1} A_k\right]^{-1} A_k^T C_l^{-1} l_k \qquad \text{A.29}$$

$$C_k^X = \left[A_k^T C_l^{-1} A_k\right]^{-1} \qquad \text{A.30}$$

In the least squares approach, the discrete position of the remote station is computed by using observations at one epoch, without any need of the process noise

information or dynamic assumption. Therefore, the positioning solutions in successive epochs are independent. This approach can be applied to the case when the reference receiver is used either in static or in kinematic mode and a high data rate is used. Shi (1994) found that with a 2 Hz or even 1 Hz data rate, the position of an aircraft (with the speed of 80 m per second) from the Kalman filter algorithm (with a constant velocity model) are identical to those from the least squares approach. The Kalman filter algorithm can be mathematically transformed to the least squares approaches. The mathematical proofs can be found in (Shi,1994).

The advantage of using Kalman filter is that it has a general form of the equations which allows the implementation of different kinematic GPS models and measurements. In addition to this, because of its flexibility, it can meet the needs of a practical application in different dynamic environments.

APPENDIX B

Mathematical Models for Aerial Triangulation

B.1 Case # 1

* Observed photo coordinates,

* Known object space coordinates, and

* Unknown exterior orientation elements.

The observation equation is given as:

$$W_P = A_{EO}\,\delta_{EO} \tag{B.1}$$

$$W_P = \left(-F_x, -F_y\right)^T \tag{B.2}$$

$$A_{EO} = \begin{bmatrix} \frac{\partial F_x}{\partial X_o} & \frac{\partial F_x}{\partial Y_o} & \frac{\partial F_x}{\partial Z_o} & \frac{\partial F_x}{\partial \omega} & \frac{\partial F_x}{\partial \Phi} & \frac{\partial F_x}{\partial \kappa} \\ \frac{\partial F_y}{\partial X_o} & \frac{\partial F_y}{\partial Y_o} & \frac{\partial F_y}{\partial Z_o} & \frac{\partial F_y}{\partial \omega} & \frac{\partial F_y}{\partial \Phi} & \frac{\partial F_y}{\partial \kappa} \end{bmatrix} \tag{B.3}$$

$$\delta_{EO} = \left(dX_o, dY_o, dZ_o, d\omega, d\Phi, d\kappa\right)^T \tag{B.4}$$

where

W_P is the misclosure vector,

A_{EO} is the design matrix (exterior orientation parameters), and

δ_{EO} is the correction vector of exterior orientation parameters,

The correction vector, δ_{EO}, is determined using the least squares approach as:

$$\delta_{EO} = \left(A_{EO}^T P_P A_{EO}\right)^{-1} A_{EO}^T P_P W_P \tag{B.5}$$

$$P_P = C_{L(P)}^{-1} \tag{B.6}$$

where

P_P is the weight matrix of image coordinates, and

$C_{l,(P)}$ is the covariance matrix of image coordinates

The covariance matrix of image coordinates for one image point is defined as:

$$C_{l,(P)} = \begin{bmatrix} \sigma_x^2 & \sigma_{x,y} \\ \sigma_{x,y} & \sigma_y^2 \end{bmatrix} \qquad \text{B.7}$$

Due to non-linearity of the model, an iterative solution method should be exercised until the corrections to the unknown parameters become insignificant. The final exterior orientation parameters can be computed as:

$$X_{EO}^{n} = X_{EO}^{0} + \sum_{i=1}^{n-1} \delta_{EO}^{i} \qquad \text{B.8}$$

where X_{EO}^{n} is the vector of exterior orientation in the nth iteration.

B.2 Case # 2

* Observed photo coordinates,
* Unknown object space coordinates, and
* Unknown exterior orientation elements.

The observation equation is written as:

$$W_P = \overline{A\delta} \qquad \text{B.9}$$

or

$$W_P = \begin{pmatrix} A_{EO} & A_S \end{pmatrix} \begin{pmatrix} \delta_{EO} \\ \delta_S \end{pmatrix} \qquad \text{B.10}$$

where

A_S is the design matrix (object space coordinates), and

δ_S is the correction vector of object space coordinates,

$$A_S = \begin{bmatrix} \frac{\partial F_x}{\partial X_i} & \frac{\partial F_x}{\partial Y_i} & \frac{\partial F_x}{\partial Z_i} \\ \frac{\partial F_y}{\partial X_i} & \frac{\partial F_y}{\partial Y_i} & \frac{\partial F_y}{\partial Z_i} \end{bmatrix} \quad \text{B.11}$$

$$\delta_S = (dX_i, dY_i, dZ_i)^T \quad \text{B.12}$$

The correction vector, $\bar{\delta}$, is given as:

$$\begin{pmatrix} \delta_{EO} \\ \delta_S \end{pmatrix} = \left(\begin{bmatrix} A_{EO}^T \\ A_S^T \end{bmatrix} P_P [A_{EO} \quad A_S] \right)^{-1} \begin{bmatrix} A_{EO}^T \\ A_S^T \end{bmatrix} P_P W_P \quad \text{B.13}$$

or

$$\begin{pmatrix} \delta_{EO} \\ \delta_S \end{pmatrix} = \begin{pmatrix} A_{EO}^T P_P A_{EO} & A_{EO}^T P_P A_S \\ A_S^T P_P A_{EO} & A_S^T P_P A_S \end{pmatrix}^{-1} \begin{pmatrix} A_{EO}^T P_P W_P \\ A_S^T P_P W_P \end{pmatrix} \quad \text{B.14}$$

B.3 Case # 3

* Observed photo coordinates,

* Observed object space coordinates,

* Unknown object space coordinates, and

* Unknown exterior orientation elements.

The observation equations for observed object space coordinates are written as:

$$f(X_i) = X_i^{observed} - X_i^{unknown} = 0 \quad \text{B.15}$$

$$f(Y_i) = Y_i^{observed} - Y_i^{unknown} = 0 \quad \text{B.16}$$

$$f(Z_i) = Z_i^{observed} - Z_i^{unknown} = 0 \quad \text{B.17}$$

The observation equations in matrix form can be shown as:

$$\begin{pmatrix} A_{EO} & A_S \\ 0 & -I \end{pmatrix} \begin{pmatrix} \delta_{EO} \\ \delta_S \end{pmatrix} = \begin{pmatrix} W_P \\ W_S \end{pmatrix} \quad \text{B.18}$$

The correction vector, $\overline{\delta}$, is defined as:

$$\begin{pmatrix}\delta_{EO}\\ \delta_S\end{pmatrix}=\begin{pmatrix}A_{EO}^T P_P A_{EO} & A_{EO}^T P_P A_S\\ A_S^T P_P A_{EO} & A_S^T P_P A_S+P_S\end{pmatrix}^{-1}\begin{pmatrix}A_{EO}^T P_P W_P\\ A_S^T P_P W_P - P_S W_S\end{pmatrix} \qquad \text{B.19}$$

where

P_S is the weight matrix of object point coordinates, and

W_S is the misclosure vector of object point coordinates.

B.4 Case # 4

* Observed photo coordinates,

* Observed object space coordinates,

* Unknown object space coordinates,

* Observed exterior orientation elements, and

* Unknown exterior orientation elements.

The equations for the observed exterior orientation parameters can be written as:

$$g(X_o) = X_o^{observed} - X_o^{unknown} = 0 \qquad \text{B.20}$$

$$g(Y_o) = Y_o^{observed} - Y_o^{unknown} = 0 \qquad \text{B.21}$$

$$g(Z_o) = Z_o^{observed} - Z_o^{unknown} = 0 \qquad \text{B.22}$$

$$g(\omega) = \omega^{observed} - \omega^{unknown} = 0 \qquad \text{B.23}$$

$$g(\Phi) = \Phi^{observed} - \Phi^{unknown} = 0 \qquad \text{B.24}$$

$$g(\kappa) = \kappa^{observed} - \kappa^{unknown} = 0 \qquad \text{B.25}$$

The observation equations in matrix form can be given as:

$$\begin{pmatrix} A_{EO} & A_S \\ 0 & -I \\ -I & 0 \end{pmatrix} \begin{pmatrix} \delta_{EO} \\ \delta_S \end{pmatrix} = \begin{pmatrix} W_P \\ W_S \\ W_{EO} \end{pmatrix} \qquad \text{B.26}$$

The correction vector is determined as:

$$\begin{pmatrix} \delta_{EO} \\ \delta_S \end{pmatrix} = \begin{pmatrix} A_{EO}^T P_P A_{EO} + P_{EO} & A_{EO}^T P_P A_S \\ A_S^T P_P A_{EO} & A_S^T P_P A_S + P_S \end{pmatrix}^{-1} \begin{pmatrix} A_{EO}^T P_P W_P - P_{EO} W_{EO} \\ A_S^T P_P W_P - P_S W_S \end{pmatrix} \qquad \text{B.27}$$

where

P_{EO} is the weight matrix of exterior orientation parameters, and

W_{EO} is the misclosure vector of exterior orientation parameters.

B.5 Case # 5

* Observed photo coordinates,

* Observed object space coordinates,

* Unknown object space coordinates,

* Observed exterior orientation elements,

* Unknown exterior orientation elements, and

* Observed geodetic measurements (e.g., distances).

Observation equation for slope distance is written as:

$$f = d_{ij} - \sqrt{(X_j - X_i)^2 + (Y_j - Y_i)^2 + (Z_j - Z_i)^2} = 0 \qquad \text{B.28}$$

where

d_{ij} . is the observed distance between point i and point j,

(X_j, Y_j, Z_j) are the unknown object coordinates of point j, and

(X_i, Y_i, Z_i) are the unknown object coordinates of point i.

The observation equations are given as:

$$\begin{pmatrix} A_{EO} & A_S \\ 0 & -I \\ -I & 0 \\ 0 & A_G \end{pmatrix} \begin{pmatrix} \delta_{EO} \\ \delta_S \end{pmatrix} = \begin{pmatrix} W_P \\ W_S \\ W_{EO} \\ W_G \end{pmatrix} \qquad \text{B.29}$$

where

A_G is the design matrix of geodetic observations between points i and j,

$$A_G = \begin{bmatrix} \frac{\partial f}{\partial X_j} & \frac{\partial f}{\partial Y_j} & \frac{\partial f}{\partial Z_j} & \frac{\partial f}{\partial X_i} & \frac{\partial f}{\partial Y_i} & \frac{\partial f}{\partial Z_i} \end{bmatrix} \qquad \text{B.30}$$

and W_G is the misclosure vector of geodetic observation. The correction vector, $\bar{\delta}$, is given as:

$$\bar{\delta} = \begin{pmatrix} \delta_{EO} \\ \delta_S \end{pmatrix} = \begin{pmatrix} A_{EO}^T P_P A_{EO} + P_{EO} & A_{EO}^T P_P A_S \\ A_S^T P_P A_{EO} & A_S^T P_P A_S + P_S + A_G^T P_G A_G \end{pmatrix}^{-1} \times \begin{pmatrix} A_{EO}^T P_P W_P - P_{EO} W_{EO} \\ A_S^T P_P W_P - P_S W_S - A_G^T P_G W_G \end{pmatrix} \qquad \text{B.31}$$

where P_G is the weight matrix of geodetic observations.

APPENDIX C

GRAFNAV

GRAFNAV software, developed by Waypoint Consulting Inc., (1994), was utilized to process the GPS data. This software is a Window and menu based and allows informatic switch from static to kinematic data processing. The Quick Static ambiguity resolution method can be applied to resolve the ambiguities for medium and short baselines (e.g., <7 km) in 5 to 15 minutes, depending on availability of L2 carrier phase data, the length of baseline, and satellite geometry. A fixed static solution can be used for medium length baselines (7-15 km). A float static solution is available for long and/or noisy baselines. "On The Fly" ambiguity resolution allows the user to start up in kinematic mode and/or fix otherwise unrecoverable cycle slips. The software accepts data in .GPB format which is a binary GPS format. Utilities are available to convert from other formats to this format, enabling the software to process data collected with a multitude of receivers.

Differential processing determines a three dimensional baseline between two stations. There are three types of static solutions supported by GRAFNAV; float solution, fixed solution, and quick static solution. Kinematic processing is usually started with a static survey or from a known point. All GPS computations are carried out in differential mode (double difference) meaning that the pseudorange, carrier phase, and doppler values

are subtracted twice. The first subtraction removes the range/phase/doppler value of the baseline, while the second subtraction removes these values from the master station.

C . 1. Overview of Various Processing Modes in GRAFNAV

Static processing is the default mode, however the program can switch automatically from static to kinematic by inspecting a flag in the binary data.

C . 1. 1. Float Static Solution

Positions and velocities (X, Y, Z, Vx, Vy, Vz) and ambiguities (number of satellites - 1) are computed in this mode. During static processing mode, the program goes into a "learning" mode, and positions and ambiguities are solved simultaneously. Any deviation of the position over time is an indication of the accuracy. The ambiguities are not fixed to integer values. For a good data set with long observation time (e.g., >30 minutes), the ambiguities will converge to integer values which is an indication of stability in the data. Carrier phase RMS is also an indication of a clean data set when it is less than 0.05 m. Accuracy of 5 ppm (parts per millions) can be expected using this solution for baselines with 45 minutes of observation time.

C . 1. 2. Fixed Static Solution

In the first step, the optimal observation time span is found by scanning the static data section, and selecting the longest interval without any cycle slips or loss of satellites on the selected satellites. The next step is to determine a fairly good approximate position of the remote station with one pass of the float solution. The float solution is assumed to be accurate enough for subsequent processing (± 20 cm). An ambiguity search technique is initiated next ± 1.5 cycles around the float solution, assuming that the ambiguities must be integer values. These intersections are then tested on the data by applying a sequential technique. The result is an averaged solution using the fixed ambiguities and an RMS value which shows how well this intersection fits the data. It is recommended that this solution be used for baselines smaller than 15 km or for time spans more than 15 minutes.

The fixed solution uses a phase trend cycle slip method to detect and correct cycle slips. This method fits a polynomial through a few epochs of phase measurements to detect slips. The accuracy of fixed static solution is approximately 2 ppm provided that at least 30 minutes of data are collected.

C . 1. 3. Quick Static Solution

This method commences with a float solution, which performs a single pass to determine an initial starting position, about which the search cube is centred. In the

second pass, the quick static takes over, and determines a search cube at the beginning and the end of the time span. The method uses a cosine function test. Acceptable intersections are tested at the second epoch at the end of the quick static period. An RMS is computed and used to sort the intersections and extract optimal values. A third pass is carried out to finally find the best solution. The size of the search cube depends on the accuracy of the solution from the first pass, therefore, narrow correlator receivers or P-code receivers offer more accurate solution after 10 minutes than C/A code receivers. This method requires a minimum of 5 minutes of observation time. It is advised that quick static techniques be used on baselines shorter than 7 km.

The third pass tests ambiguity values using the positions of the best intersections. This method is independent of cycle slips, because of using position other than ambiguities. During this pass, the ambiguities should be stable if they are correct. The accuracy of this method is about 5 ppm of the baseline length..

C . 2. GPS Kinematic Processing using GRAFNAV

The processing techniques are the same as the float static solution. The only difference is that the program is not in a "learning" mode. Position (X, Y, Z), velocity (Vx, Vy, Vz) and ambiguities (N-1) are computed. When a cycle slip is detected, the ambiguities become unknown and their variances are increased. In this case, the ambiguity of the relevant satellite becomes unstable, and may cycle around for a few

epochs. The ambiguity unknowns may also be adjusted to compensate for multipath or ionosphere. The following techniques can be used to start the kinematic GPS survey:

a - starting from a known control point,

b - initializing with static or quick static solution,

c - "On The Fly" kinematic ambiguity resolution which requires 5 or more satellites.

C . 2. 1. On The Fly Ambiguity Resolution

"On The Fly" (OTF) kinematic ambiguity resolution searches the ambiguities and evaluates relative quality of each intersection (RMS). This technique can be used in kinematic mode because it examines ambiguities instead of positions. OTF uses many minutes of kinematic and static data following a serious loss of lock. OTF is only applied if the program is started in kinematic mode or a serious loss of lock occurs (i.e., the receiver is tracking less than four satellites).

OTF searches the data following the loss of lock. A suitable time span is chosen in such a way that it maximizes the number of satellites, maximizes the length of the time span, and minimizes the time between the loss of lock and the start of the OTF. The search cube is defined based on whether the receiver has precise pseudorange available. An instantaneous C/A code position may not fall within this cube size. Due to the fact

that OTF uses many seconds of data following the loss of lock, a more precise position is derived. It is very beneficial to OTF if L2 phase measurements are also available.

Unreliable results may be obtained if the RMS value is more than 0.05 cycles and the reliability value is less than 1.5. This can happen due to the following:

* poor initial approximate,

* the long distance between master and remote stations,

* unavailability of L2 carrier phase data,

* Large ionospheric or multipath error, and

* poor geometry or not enough satellites.

TEST TARGET (QA-3)

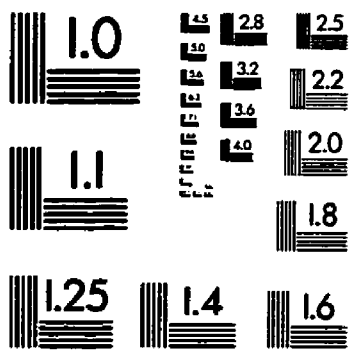

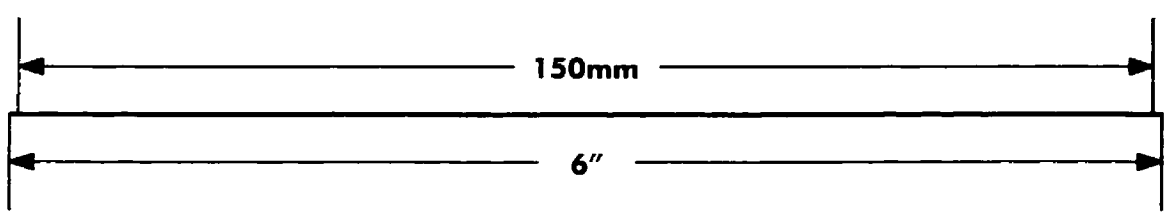

APPLIED IMAGE, Inc
1653 East Main Street
Rochester, NY 14609 USA
Phone: 716/482-0300
Fax: 716/288-5989